SCRUTINIZING THE ROLE OF AMBIPOLAR UNITS IN THE DONOR-ACCEPTOR

FRAMEWORK

A Dissertation
Submitted to the Graduate Faculty
of the
North Dakota State University
of Agriculture and Applied Science

By

Trent Eugene Anderson

In Partial Fulfillment of the Requirements
for the Degree of
DOCTOR OF PHILOSOPHY

Major Program:
Chemistry

November 2020

Fargo, North Dakota

North Dakota State University
Graduate School

Title

SCRUTINIZING THE ROLE OF AMIBIPOLAR UNITS IN THE
DONOR-ACCEPTOR FRAMEWORK

By

Trent Eugene Anderson

The Supervisory Committee certifies that this ***disquisition*** complies with North Dakota

State University's regulations and meets the accepted standards for the degree of

DOCTOR OF PHILOSOPHY

SUPERVISORY COMMITTEE:

Dr. Seth C. Rasmussen

Chair

Dr. Kenton R. Rodgers

Dr. John Hershberger

Dr. Warren Christensen

Approved:

12/10/2020	Dr. Gregory Cook
Date	Department Chair

ABSTRACT

Conjugated polymers (CPs) are a class of materials that contradict what is commonly considered when people hear the terms plastics and electronics. While these two phrases are generally considered exclusive, CPs combine the optical and electronic properties of inorganic materials and the flexibility and processability of traditional organic polymers and plastics. Research into CPs has resulted in an improved understanding of these compounds, leading to its application in the form of organic photovoltaics, organic light-emitting diodes, sensors, electrochromics, and field effects transistors. During this time, a number of models were developed for designing these polymers with desired characteristics, with the donor-acceptor framework becoming the most widely used model. This model utilizes electron-rich donor units and electron-deficient acceptor units that generate a material with a reduced energy difference between its frontier orbitals.

Thieno[3,4-*b*]pyrazine (TP) based compounds are compounds used by the Rasmussen group and have distinct characteristics that has deemed it necessary to give it a new classification of an ambipolar unit within the donor-acceptor framework. TP has been previously classified as an acceptor unit within the donor-acceptor framework, but it has been shown to behave as both an acceptor and a donor simultaneously. In an effort to understand how the ambipolar unit behaves when paired with donor and acceptor units, a family of dimers was generated to determine the role of the ambipolar unit. Based on the findings from the dimer family, polymers of an alternating TP unit and different acceptors were generated to form a new family of acceptor-ambipolar polymers that also have desirable electronic characteristics with respect to the band gap and energy levels. This work provides a new insight on evaluating monomer units

within the donor-acceptor framework as well as establishing a viable alternative for polymer design using ambipolar units.

perspective on the things I was struggling with. Your prayers were greatly appreciated, and I rejoice in the fact that we worship a God that hears and answers prayers.

It would be amiss to not recognize the two doctors that saved my life while I was a graduate student. Dr. Erik Fetner and Dr. Ross Meidinger treated me during the five most difficult months of my life. Your care for my well-being and overwhelming commitment to finding a diagnosis, allowed me to live a somewhat normal life when there were times that I did not expect that to be an option.

My high school chemistry and physics teacher Dave Dulas had a huge impact on me studying chemistry for my undergraduate years and pursuing a PhD as well. Your willingness to stay after school and prepare lectures over content that you were not going to test on really helped foster my interest in chemistry.

I would like to thank my committee members for guiding and challenging me during graduate school. The guidance from my advisor Dr. Seth Rasmussen helped me to grow and develop as a researcher during graduate school. You took a huge risk in having a physical chemistry do some very sensitive synthetic chemistry, but it all worked out in the end.

TABLE OF CONTENTS

ix

LIST OF TABLES

LIST OF FIGURES

LIST OF SCHEMES

LIST OF APPENDIX TABLES

LIST OF APPENDIX FIGURES

CHAPTER 1. INTRODUCTION

Conjugated Polymers

A conjugated compound is a chemical species that has overlapping *p*-orbitals that allow for π-electron delocalization along the conjugated path. These *p*-orbitals can be present in the form of double bonds or can come from the non-bonded electrons within the plane of the π-system, as shown in Figure 1.1. This conjugation can propagate either down a chain or through a cyclic system, such as benzene or an aromatic heterocycle. Conjugated systems can form the basis for chromophores, which absorb light and cause a compound to be colored.
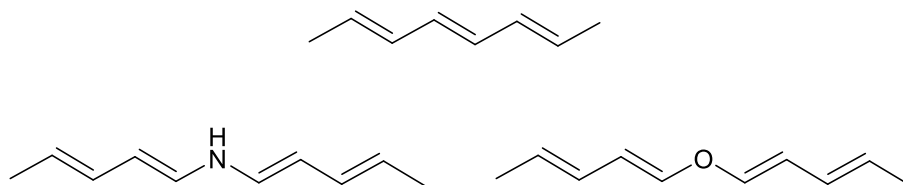
Figure 1.1. Conjugation of a simple alkene and conjugation being continued through the heteroatoms of nitrogen and oxygen.

A polymer (or macromolecule) is a compound that consists of a large number of repeating base units originating from a small molecule precursor, referred to as a monomer. Polymers are essential to everyday life such that their uses as plastics go unnoticed. Polyethylene ($[C_2H_4]_n$) is the simplest and most common organic polymer and is used for packaging and bottles.[1] Polypropylene ($[CH(CH_3)CH_2]_n$) is used in carpeting, containers, and is commonly found in electronic and laboratory equipment.[2] Polyethylene and polypropylene have a global market of 80 million tons and 55 million tons, respectively.[1,3] Their thermal and electrical insulating properties, as well as their malleability, make them ideal for electronic coatings and a wide range of applications. These polymers consist primarily, if not entirely, of single bonds along the backbone of the polymer, meaning there is not substantial *p*-orbital overlap that would result in a conjugated system.

The combination of the characteristics of a polymer and a conjugated material would result in a material with desirable electronic properties and is flexible and easily processable. Conjugated polymers (CPs) are exactly that, being a class of polymer materials with extended *p*-orbital overlap along the backbone.[4] The overlap along the backbone is essential to allow for the delocalization of π-electrons, as shown in Figure 1.2, which results in CPs being able to efficiently conduct charge, thus exhibiting semiconducting and optical properties similar to those of inorganic semiconductors. While neutral conjugated polymers are less efficient at transferring charge, and thus only semiconducting, its doped state may more effectively transfer charge. Conjugated polymers can either be oxidized or reduced to generate "doped" forms, commonly called conductive polymers.
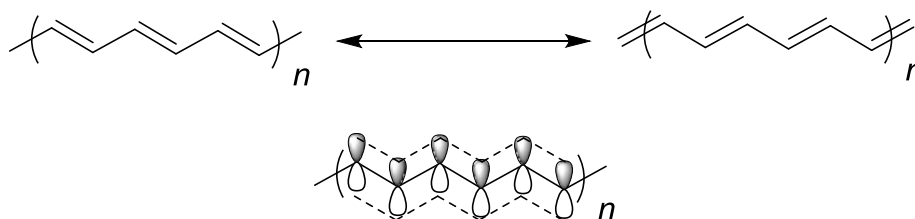
Figure 1.2. Resonance structures of polyacetylene showing the overlap of the *p*-orbitals which allow for the π-electron delocalization.

While nonconjugated polymers are insulators, the electron delocalization present in CPs allows for the polymers to have characteristics desirable for electronic devices while still being able to maintain mechanical flexibility, ease of processing, and low density.[5,6] These CPs can be used in organic photovoltaics (OPVs),[5, 7-9] organic light emitting diodes (OLEDs),[4, 10-17] electrochromics,[18-22] sensors,[23-28] and organic field effect transistors (OFETs).[12, 29-38]

History of Conjugated Polymers

The history and evolution of conducting and conjugated polymers is convoluted. This confusion can be somewhat contributed to the wording of the Nobel Prize in Chemistry in 2000.

Alan Heeger, Alan MacDiarmid, and Hideki Shirakawa were awarded the Nobel Prize "for the discovery and development of electrically conductive polymers."[39-41] While their work on the development of electrically conductive polymers is undeniable, crediting them with discovering conducting polymers is misleading.

The first reported conjugated polymer dates back to 1834.[40,41] F. Ferdinand Runge treated either aniline nitrate with copper oxide in hydrochloric acid, generating $CuCl_2$, or aniline hydrochloride with copper oxide in nitric acid, generating $Cu(NO_3)_2$, to produce polyaniline. The resulting product was described as a "green-black material." Numerous additional studies followed on the production of polyanilines via oxidative methods, but the electronic properties of polyaniline were not characterized until the 1960s. It was at this time that Rene Buvet and Marcel Jozefowicz generated high quality oxidized polyaniline and pressed pellets of the materials were found to have conductivities ranging from 10^{-9} S cm^{-1} to 100 S cm^{-1}.[40,42]

Polypyrrole is another example of one of the earlier conjugated polymers. The first report of polypyrrole was by Angelo Angeli in 1915.[40,43] He used multiple oxidizing agents to produce what he called "pyrrole black." Through his studies, he was even able to conclude that the pyrrole unit remained intact within the pyrrole black. Riccardo Ciusa did additional work with the polymerization of pyrrole while trying to generate a type of pyrrole "graphite" in 1921.[40,43] Ciusa was thermal polymerizing tetraiodopyrrole and produced a black material that appeared similar to graphite, although the resistivity was not reported. Donald Weiss would then expand upon Ciusa's work nearly 40 years later. Weiss repeated Ciusa's synthesis with minor adjustments to the methodology.[40,43] The adjustments that Weiss made resulted in a material that's composition did not agree with Ciusa's due to adsorbed oxygen and water. The material also contained "adsorbed molecular iodine." The iodine and oxygen content helped facilitate the

oxidation of the polymer and are key to its resulting electronic characteristics.[43] The conductivity of the polypyrrole pellets was found to be the highest of any non-pyrolyzed organic polymer at the time. He also found that the removal of the adsorbed iodine resulted in a significant increase in the resistance of the material.

The history of polyacetylene is especially important to the progress of conducting polymers because its study led to the awarding of the 2000 Nobel Prize. In the mid-1950s Giulio Natta applied catalytic methods he had previously used on α-olefins and diolefins to successfully polymerize acetylenes.[39,40] This work was originally presented in three forms (patent, meeting synopsis, and paper) with indication that the work would continue, but there were no subsequent publications by Natta on polyacetylene. However, this did not stop others from continuing research on polyacetylene. Sakuji Ikeda was working on polyacetylene at the Tokyo Institute of Technology when Hideki Shirakawa joined his lab. In 1967, Shirakawa was working with Hyung Chick Pyun, a visiting researcher from Korea, and through the accidental use of excessive catalyst they were able to generate a silvery, plastic polyacetylene film at the air-solvent interface.[39-41]

While Alan MacDiarmid was visiting the Tokyo Institute of Technology he met Shirakawa, who showed MacDiarmid the silvery polyacetylene film and this generated enough interest from MacDiarmid that he asked Shirakawa to join him at University of Pennsylvania to continue work on polyacetylene.[39-41] Shirakawa joined MacDiarmid and Alen Heeger at University of Pennsylvania in 1976. The initial work was focused on improving the purity of the polyacetylene films in hopes that this would result in an increase in its conductivity. However, the contrary was shown to be true. The conductivity of the *trans*-polyacetylene was measured by four-point probe while bromine vapors were passed over the film and within the first ten minutes

the conductivity changed from 10^{-5} S cm^{-1} to 0.5 S cm^{-1}.[44] Iodine treatment resulted in an even higher conductivity, reaching 38 S cm^{-1} with *trans*-polyacetylene and 500 S cm^{-1} when treating *cis*-polyacetylene.[45] It was also shown that it was possible to dope the polyacetylene films with sodium which resulted in conductivities of 8 S cm^{-1}.[46]

The work of MacDiarmid, Heeger, and Shirakawa demonstrated that doped polyacetylene was an organic polymer that was capable of conductivities in the metallic regime and this resulted in a huge increase in interest conductive polymers, leading to a steady increase in publications. There are two important factors to consider as to why their work stood out so much more than the work before them. The work on polyacetylene was broadly published in international journals, making it more available to be read by the scientific community. In contrast, the work done by Weiss was only published in Australian journals and most of the work by Buvet and Jozefowicz was limited to French literature.[41] This greatly limited the reach of their work. Additionally, polyacetylene generated the first silvery, metallic-looking plastic films, which may have been more captivating to look at than the bulk of previous conducting polymers that were dark powders that had been pressed into pellets for conductivity measurements.[41] Eventually, this fundamental progression led to an interest in commercial applications and continued research developed more technologically applicable materials.

Band Gap

The interaction between the *p*-orbitals of conjugated species is likely the most impactful characteristic of CPs. Based on Huckel's molecular orbital theory, when the highest occupied molecular orbital (HOMO) and lowest unoccupied molecular orbital (LUMO) of reactants are similar in energy it is possible for them to mix and hybridize, generating new energy levels in the product.[47] The HOMO energy levels of the individual units interact in such a way that the new

HOMO is destabilized and is at a higher energy level than either of the original HOMOs and an additional energy level is generated that is more stable than either of the original HOMOs. The LUMOs interact in a similar manner, resulting in a LUMO that is more stable than either of the isolated LUMOs and an additional energy level that is more unstable than both of the original LUMOs. Orbital hybridization occurs between all of the orbitals of similar energy, resulting in a large increase in the number of energy levels, as well as an increase in their density. This orbital hybridization continues many times for a polymer unit, limited only by the extent of electron delocalization. The conjugated polymer eventually develops a band-like structure in the solid state due to the density of energy levels caused by the hybridization of energy levels, as well as additional solid state interactions, such as π-π interaction between polymers. The valence band is the band of energy levels that the electrons are occupying whereas the conduction band is the band of energy levels that electrons can be excited to. Once in the conduction band, the electrons can travel freely and create an electric current. The energy difference between the valence band and the conduction band is the band gap (E_g). It is worth noting that the top of the valence band can be viewed as the HOMO and the bottom of the conduction band can be viewed as the LUMO. This relationship allows insightful electronic information to be determined about the polymer. Figure 1.3 is a representation of the increase of the energy levels and reduction of the HOMO-LUMO gap as there is an increase in orbital hybridization, as well as the eventual formation of the valence and conduction bands.
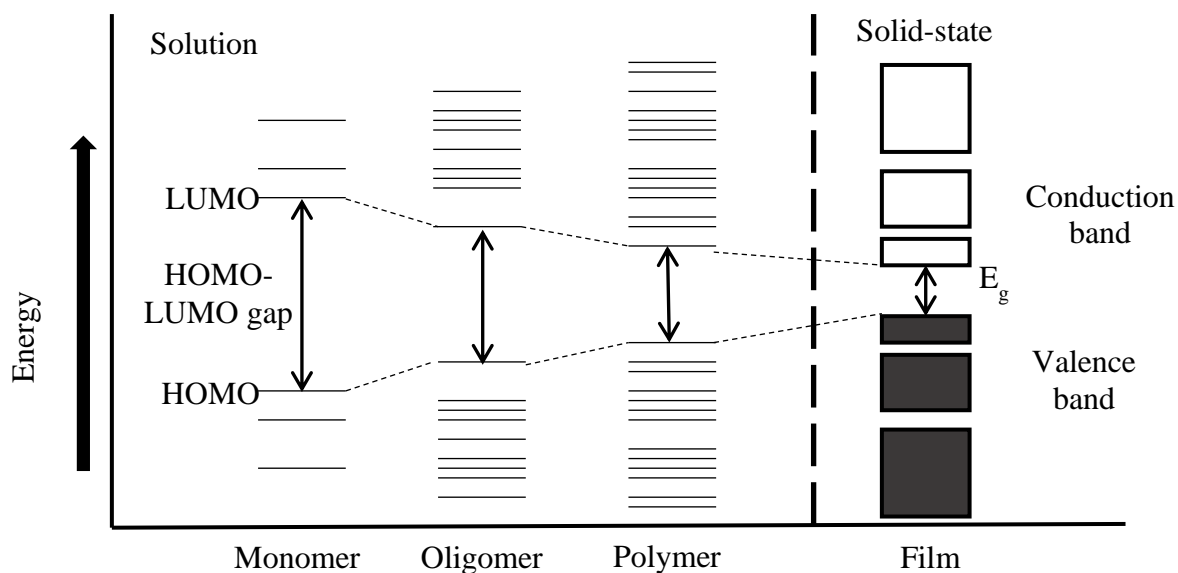
Figure 1.3. Energy level diagram illustrating the interaction of molecular orbitals and band formation in a conjugated system.

The E_g is the primary determining factor in a number of the electronic and optical characteristics of a material. Based on the E_g, materials can be subdivided into three general groups: insulator, metal, and semiconductor.[48] If a material has an E_g greater than 3 eV, it is considered an insulator and will be a poor electron conductor. However, if a material has an E_g of 0 eV it is considered a metal and will be a good conductor of electrons. A material that has an E_g between that of a metal and an insulator (0-3 eV) is considered a semiconductor. However, the values referenced here are not absolute, but merely rough guidelines, and the values given will vary depending on the source and the field of study. Figure 1.4 shows the E_g of the some of the common conjugated polymers.

In 1998, Pomerantz proposed that any CP with an E_g below 1.5 eV would be described as a low band gap material. It was claimed to have been done arbitrarily, but was also justified because polyacetylene was not considered a low E_g material and it has an E_g of 1.5 eV.[49] Since then, a large number of low E_g CPs have been reported.[6,49-52] However, throughout the literature, materials with an E_g of 2.0 eV or less are often described as a low band gap material because

7

polythiophene has an E_g of approximately 2.0 eV.[52,53] With the threshold at 2.0 eV, the

classification has little meaning because most thiophene-based materials have E_g values around

2.0 eV. In hopes of clarifying this inconsistency within the literature, Rasmussen proposed the

description reduced band gap for materials with an E_g between 2.0 and 1.5 eV, while maintaining

Pomerantz's threshold of 1.5 eV for a low band gap material.[52,53]

| Polyacetylene | Polyphenylene | Polyaniline | Polyphenylene vinylene |
| 1.5 eV | 3.4 eV | 3.6 eV | 2.4 eV |

| Polypyrrole | Polythiophene | Poly(3,4-ethylene dioxythiophene) | Polyisothianapthene |
| 3.0 eV | 2.0 eV | 1.6 eV | 1.0 eV |
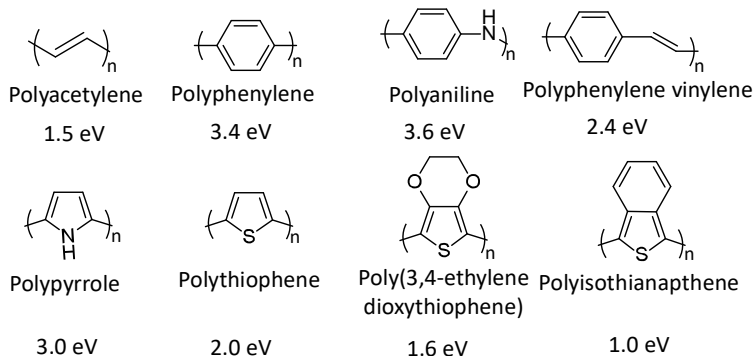
Figure 1.4. Commonly used conjugated polymers and their respective band gaps.[52]

There are two methods that are primarily used to experimentally determine the E_g of a

polymer.[53] The first approach is to measure the absorption spectra of a polymer film and use that

data to determine the E_g (Figure 1.5.A). The data is fit to a Tauc plot, which is a plot of $h\nu$

against $(A\nu \times h\nu)^2$, where h is Plank's constant, ν is the frequency, and A is the absorption at its

respective ν (Figure 1.5.B). The extrapolating the linear portion of the plot to the y-intercept is

corresponds to the optical E_g of the material.
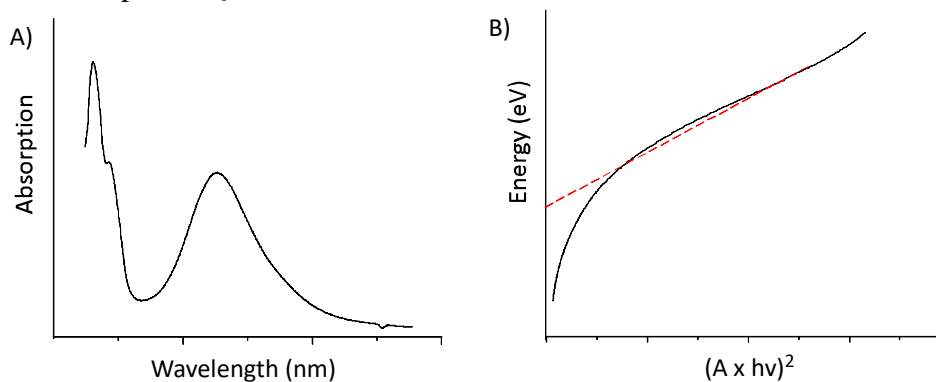
Figure 1.5. Progression of determining optical E_g by Tauc Plot. The raw absorption data (A) is plotted (B) as the energy of absorption vs. the absorption times energy squared $(A \times h\nu)^2$ with the y-intercept of the linear portion of the Tauc plot being the E_g.

The other method for the measurement of the E_g of materials is electrochemistry. This allows for the direct measurement of the first oxidation and the first reduction of the material. These values (reported in eVs) are measured by finding the onset of the oxidation and the reduction potentials via cyclic voltammetry (CV), as shown in Figure 1.6.[51] Ferrocene is commonly used as an internal standard for comparisons of energy levels. If the CV is done of a film and not a solution, the difference between these two energies is an approximation of the E_g. CV still comes with its own limitations. If the onset of oxidation or reduction is outside of the potential window of the solvent or electrolyte, there needs to be a change in the solvent or electrolyte, or CV may not be the best method to determine the HOMO-LUMO gap.
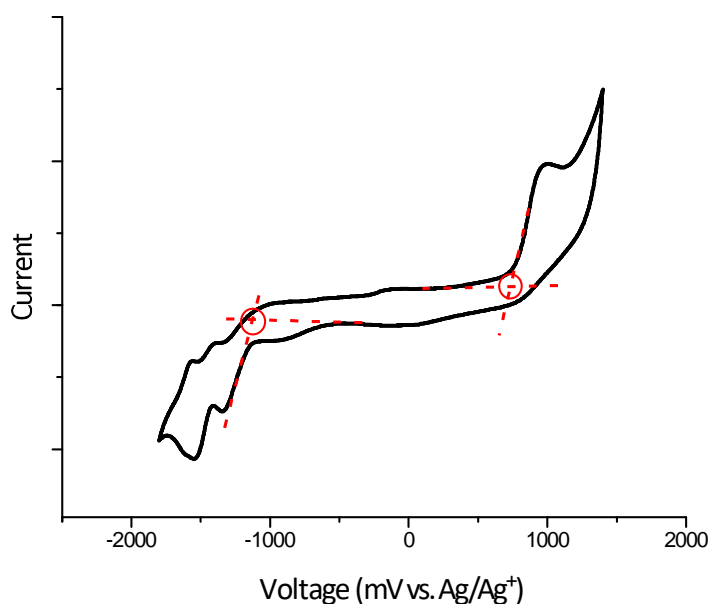
Figure 1.6. Determining electronic band gap by CV.

Structure-Function Relationship of Polymers

Over the many years of research on CPs there are a number of different parameters identified that have a substantial impact on the electronic properties of the polymer. The modification of these parameters allows for the tuning of the energy levels and can be used to explain the characteristics of the resulting polymer. Some of the parameters that affect the

9

conjugation length are bond length alternation, torsion angle, aromatic resonance energy, heteroatom effect, substituents, and intermolecular interactions.[6,54]

The conjugation length is the extent of the π-electron delocalization along the polymer backbone. As was discussed earlier, the more orbitals that are allowed to interact with each other the more unstable the resulting HOMO and the more stable the LUMO, resulting in a reduction in the HOMO-LUMO gap. This reduction in the HOMO-LUMO gap then results in a reduction of the E_g of the eventual polymer film. The conjugation length of a polymer is directly related to its molecular weight because as more units are added to the polymer, the greater number of interactions of the energy levels.[54] This is true until the limit of the conjugation length is reached. For example, polythiophene has a maximum effective conjugation length between 20-30 units.[53]

Bond length alternation is related to the difference in bond length along the conjugated path.[6,54] With aromatic systems that have non-degenerate resonance structures (Figure 1.7), the topic of bond length alternation is often referred to as the extent that the quinoidal resonance form contributes to the ground state of the molecule. The quinoidal and aromatic forms will have different optical and electronic properties. Controlling the contribution of the quinoidal resonance form becomes one of the driving factors in the design of polymers that will be discussed later.

aromatic   quinoidal
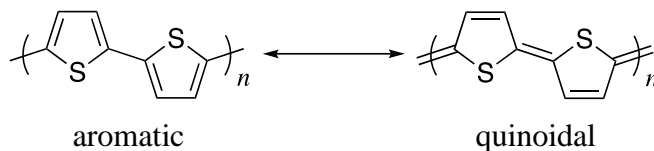
Figure 1.7. Aromatic and quinoidal resonance forms of polythiophene.

The torsion angle is the angle between rings of adjacent units. This is increased by steric hindrance within the molecule. Distortion from planarity reduces the overlap of the *p*-orbitals, resulting in an increase in the band gap of the polymer.[6,54] However, it is not until the torsional

distortion is greater than 40° that there is a substantial impact on the band gap.[55] Some of the methods used to minimize this angle is by using smaller side groups, non-proton carrying atoms, or bridging via covalent bonds or H-bonds.

The aromatic resonance energy deals with the competition between the π-electron confinement within the ring and the delocalization along the backbone.[6,54] One way of evaluating the aromaticity of different rings is by their resonance energy per electron, with a larger resonance energy per electron relating to a ring being more aromatic. The more aromatic the rings, the greater the E_g of the resulting material due to reduced electron delocalization.

The incorporation of heteroatoms in rings can result in changes in the electronic properties of the material.[56,57] Heteroatom inclusion impacts the aromatic resonance of the rings. Depending on how the heteroatom is included it could result in the ring being more electron rich or make the ring more electron deficient. For example, the sulfur in thiophene adds to the electron richness of the ring whereas the nitrogens in a pyrazine ring makes it more electron deficient and increases electron confinement within the pyrazine ring.

One method of modifying the HOMO and LUMO energy levels of molecules is by changing the substituents attached to an aromatic ring. When an electron-donating group is grafted onto a ring the electron density is pushed into the π-system, raising the energy of the corresponding orbitals.[6,54] An electron withdrawing group stabilizes the energy of the corresponding orbitals. This is sometimes simplified to statements that the electron-donating groups will raise the HOMO and electron-withdrawing groups will lower the LUMO, but the addition of these groups will not be able to solely affect just one frontier orbital without also altering the other and the impact will not necessarily be symmetric either. An additional use of substituents is for improving the solubility of the polymers. Solubilizing alkyl sidechains can

increase the molecular weight of the polymer because they allow for a higher degree of polymerization before becoming insoluble and unreactive during the polymerization process.

Intermolecular effects come from how the individual molecules are organized in the condensed phase.[54] One example of these interactions is a reduced torsion angle resulting in improved π-π interaction between two aromatic molecules. It was previously discussed that the addition of alkyl chains increases the solubility of the molecules, but the alkyl chains can also have an impact on the solid-state packing of the polymer and reduce the extent of π-π interaction.

Design Theories for the Production of Low Band Gap Polymers

As more polymers are synthesized and characterized, trends became evident that led to different models for designing new polymers with the specific characteristics, usually focused on the E_g. The two most prominent models for designing low band gap polymers ($E_g < 1.5$ eV) are the use of a fused-ring system that enhances the quinoidal nature of the polymer backbone and the donor-acceptor model, which utilizes an electron-rich unit, the donor, and an electron-poor unit, the acceptor, that are copolymerized in an alternating framework.

Polymers can have enhanced quinoidal characteristics with the careful consideration of aromatic units being fused together in a particular geometry. These systems possess non-degenerate resonance forms, the aromatic and quinoidal, which each have different optical and electronic properties (Figure 1.8). These two resonance forms contribute to the observed ground state to different extents and determine the electronic and optical properties of the resulting material. The aromatic form is usually more stable and represents the ground state structure, but it has a larger E_g than the quinoidal resonance form. In order to increase the quinoidal character along the backbone, it is necessary that the aromatic ring with the smaller resonance energy make up the backbone of the polymer while the second aromatic ring, with the higher resonance

energy, is fused to the first. The difference in resonance energy results in the unit along the

backbone adopting a more quinoidal resonance structure while the second ring is aromatic.

Increased quinoidal content along the backbone has been found to decrease the E_g of the

resulting polymer.[51]
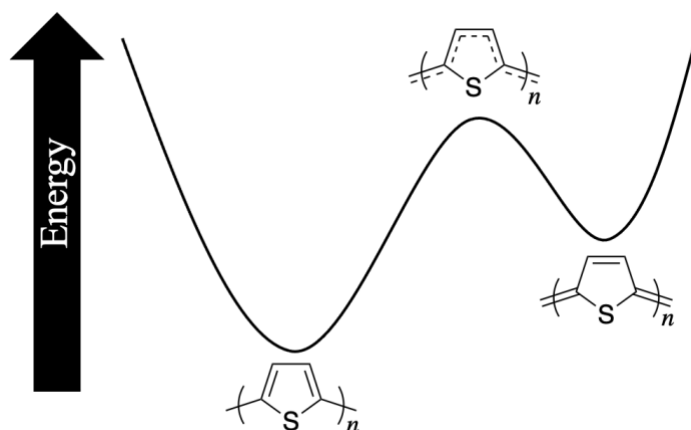
Figure 1.8. Energy of aromatic and quinoidal resonance states of polythiophene.

The donor-acceptor (D-A) model utilizes an alternating electron-rich donor unit and an

electron-poor acceptor unit. It has been proposed that the internal charge transfer between the

donor and acceptor leads to observed low band gaps.[6] The charge transfers results in a large

change in dipole moment as charge density becomes more localized on the acceptor units. The

lower band gaps produced by D-A polymers within the current framework can also be

contributed to possible reduction in bond length alternation. The thought process behind the

current model is that if the donor and acceptor are strong enough, it would result in a new

resonance form consisting of a double bond between the two units, resulting in a decrease in the

bond length alternation, and therefore a decrease in the band gap (Figure 1.9).[58-60]
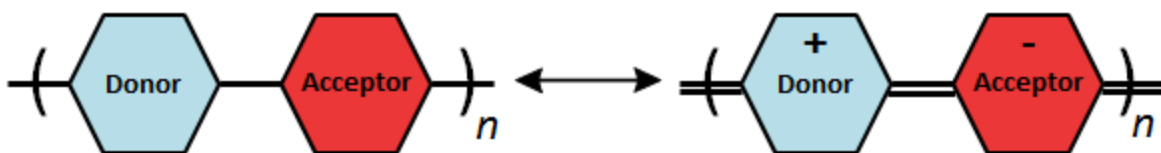
Figure 1.9. The resonance form of the donor-acceptor polymer that has double bonds between the monomer units that is used as an explanation for the reduced E_g for donor-acceptor polymers.

However, the most common explanation consists of the hybridization of the frontier orbitals of the donor and acceptor units (Figure 1.10). The hybridization of the HOMO energy levels results in a new HOMO at an energy level closer to that of the donor's, which is the more unstable of the two HOMOs. The LUMO of the acceptor may also stabilized, depending on the energy matching of the LUMO levels of the two units. This results in a LUMO at or lower in energy than the acceptor, which would be the lower of the LUMOs. If the LUMOs do not have similar enough energies to allow hybridization, the LUMO of the new species will retain a LUMO similar to the more stable of the two species, as shown in Figure 1.10. If the acceptor and donor behave as expected, this results in a lower HOMO-LUMO gap than the donor or acceptor on their own, which effectively results in a smaller E_g once polymerized and in the solid state.
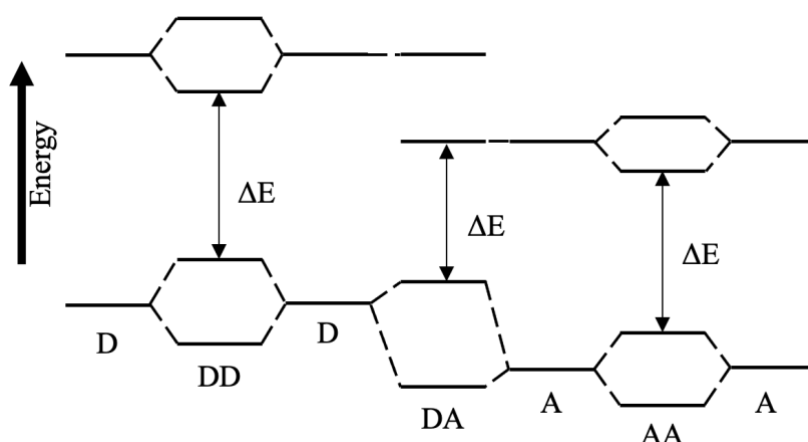
Figure 1.10. Energy scheme for the interaction between a donor unit (D) and an acceptor unit (A) and how the resulting donor-acceptor unit (DA) has a HOMO more closely resembling the donor and a LUMO closely resembling the acceptor and a smaller HOMO-LUMO energy difference (ΔE) than either would obtain independently.

14

Thieno[3,4-*b*]pyrazine

Materials based on thieno[3,4-*b*]pyrazine (TP) have been of great interest to the Rasmussen group for many years.[61,62] One of the driving reasons behind this focus is the success that has been found with generating reduced and low E_g conjugated materials using TP as one of the components.[50-52,63] An additional advantage of TPs is the ability to functionalize the 2- and 3-positions.

The first TP-based compound synthesized was 2,3-diphenylthieno[3,4-*b*]pyrazine, which was reported in 1957 by Motoyama and Imoto.[52] A general synthetic method for TPs was published in 1983 by Outurquin and Paulmier which entails the condensation of 3,4-diaminothiophene with an α-dione to generate to the pyrazine ring (Scheme 1.1). This new method still serves as the basic synthetic method to generate most TPs, although there have been a substantial improvements and optimizations to the synthesis.[64-66]
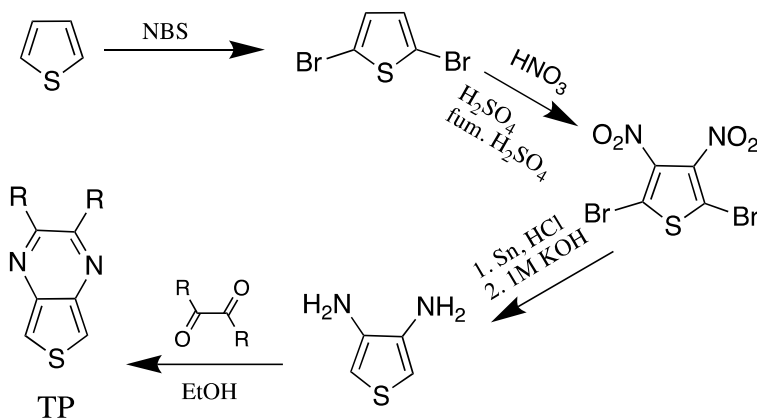
Scheme 1.1. Synthetic pathway for the 1st generation thieno[3,4-*b*]pyrazine.

In order to expand upon the options of substituents on the TP unit it was necessary to develop a method to generate α-diones. Outside of commercially available diones, it was necessary to use symmetric alkynes as a precursor for the α-diones.[67] Marchese was able to develop a method to generate α-diones using oxalyl chloride, Grignard reagents, cuprous

bromide, and lithium bromide.[68] This was later improved by cooling it to -100 °C rather than the procedurally reported -78 °C in order to further reduce the occurrences of homocoupling.[67] This new α-dione synthesis greatly increased the options for diones and thus the options for dialkyl and diaryl substituents on the TP unit.

In 2008, Rasmussen and co-workers synthesized 2,3-dibromothieno[3,4-*b*]pyrazine, which allows for a wide range of TP units that were not previously possible through the conventional TP synthesis.[66] This functionalization through substitution includes alkoxy, cyano, and alkylamino groups which provide more options to tune the electronic and optical properties of the TP unit. The substitution on the pyrazine ring results in a greater impact on the LUMO than the HOMO energies due to the LUMO being localized on the pyrazine ring where the substituents were added while the HOMO is localized on the thiophene ring.

TP has been used in a number of different applications in organic electronic devices. Compounds containing TP have been utilized in organic thin film transistors,[69,70] organic light emitting diodes,[71,72] and OPVs,[52] NIR photodetectors,[73,74] supercapacitors,[75] and anti-corrosion coatings.[52] As stated earlier, the ability of TP to generate low and reduced band gap materials is a desirable characteristic for applications to OPVs.

TP units have been characterized as acceptor units within the donor-acceptor framework for polymer design. The donor characteristics of TP was investigated by the Rasmussen group by generating a family of oligomers containing TP, thiophene, and 3,4-ethylenedioxythiophene (EDOT).[76] Thiophene and EDOT are both electron rich and are classified as donor units. It was found that the TP had a larger contribution to the HOMO and LUMO of the resulting oligomer than either of the two donor units. A new classification of *ambipolar* was proposed for the TP unit due to its dual donor and acceptor nature.

Research Goals

In recent years organic based electronics have come closer and closer to being publicly viable. There are a number of different models that are used for designing different aspects of the electronics, whether it being the framework for synthesizing the polymers or how it is understood that OPVs operate. The primary goal of this research is to investigate some of the oversimplifications in the donor-acceptor framework of polymer design and elucidate additional knowledge in hopes of developing a more thorough understanding of what is actually occurring compared to the model that is used, specifically focusing on the characterization of units as solely donor or acceptor units.

While TP units have been thoroughly characterized by the Rasmussen group, they seem to be a bit of an oddity compared to other molecules used for similar purposes. Within the D-A polymer framework, TP is a substantial contributor to both the HOMO and the LUMO of the resulting polymers, meaning that is simultaneously acting as a strong donor and acceptor. It has been dubbed an ambipolar unit due to this rare property. In order to better understand how TP fits within the D-A framework, a series a dimers were synthesized to understand how TP interacts with other donor and acceptor units. There was also a series of TP based polymers where TP was paired with other acceptor units. The polymers would be classically considered acceptor-acceptor polymer, which would not be expected to generate a low E_g material.

Another aspect of the presented research was the development of a small molecule endcapping group based on the already investigated 2,3-difunctionalized-thieno[3,4-*b*]pyrazine molecules. The functionalized thieno[2,3-*b*]pyrazine would serve as a good endcap unit for small molecule synthesis, which has been a growing field within organic based electronics due to the ability to have consistent molecules and have more control over the electronic characteristics.

With a similar synthetic route being used, this molecule could provide for a wide range of additional small molecules to eventually be synthesized and characterized for electronic applications.

A third, albeit slightly different, research goal was the investigation in the impact that altering the fabrication process of OPVs has on the overall power conversion efficiency (PCE) of the solar cell. The PCE of a solar cell is the ratio of the amount of usable energy generated to the energy put into the solar cell. The project focused on the impact that the solvent temperature has when spin coating a film. This would be a minor change in the fabrication process but could have a substantial impact on the overall efficiency of the solar cell.

References

1.   Piringer, O.G.; Baner, A. L. In *Plastic packaging: interactions with food and pharmaceuticals*, 2nd Ed.; Wiley-VCH, Germany, 2008; p 20.

2.   Bayasi, Z.; Zeng, *J. Materials* **1993**, *90*, 605.

3.   Karget-Kocsis J. In *Polypropylene Structure, blends and Composites: Volume 3 Composites*; Springer Science & Business Media, London, 1995; p 2.

4.   Nyugen, T. P.; Destruel, P. In *Handbook of Luminescence, Display Materials, and Devices*; Inouye, H. S., Rohwer, L. S., Eds; American Scientific Publishers: Sevenson Ranch, CA, 2003; Volume 1; p 5.

5.   Roncali, J. *Chem.Rev.* **1992**, *92*, 711.

6.   Roncali, J. *Chem. Rev.* **1997**, *97*, 173.

7.   Mozer, A. J.; Sariciftci, N. S. In *Handbook of Conducting Polymers: Processing and Applications,* 3rd ed.; Skotheim, T. A., Reynolds, R., Eds.; CRC Press: Boca Raton, FL, 2007; p 10-1.

8.   Brabec, C. J.; Sariciftci, N. S. In *Semiconducting Polymers: Chemistry, Physics, and Engineering*; Hadziioannou, G., van Hutten, P. F., Eds.; Wiley-VCH: Wienheim, 2000; p 515.

9.   Batbella, G.; Melucci, M. In *Handbook of Thiophene-Based Materials: Applications in Organic Electronics and Photonics*; Perepichka, I. F., Perepichka, D. F., Eds.; Wiley: West Sussex, U. K., 2009; Volume 1, p 255.

10.   Friend, R. H.; Greenham, N. C. Electroluminescence in Conjugated Polymers. In *Handbook of Conducting Polymers*, 2nd ed.; Skotheim, T. A., Elsenbaumer, R. L., Reynolds, J. R., Eds.; Marcel Dekker, Inc: New York, 1998; p 823.

11.   Cui, T.; Liu, Y. In *Organic Electronics and Photonics: Electronic Materials and Devices*; Nalwa, H. H., Ed.; American Scientific: Stevenson Ranch, 2008; Volume 1, p 263.

12.   Christian-Pandya, H.;Vaidyanathan, S.; Galvin, M. In *Handbook of Conducting Polymers,* 3rd ed.; Skotheim, T. A., Reynolds, J. R., Eds.; CRC Press: Boca Raton, FL, 2007; Chapter 5.

13.   Grimsdale, A. C.; Chan, K. L.; Martin, R. E.; Jokisz, P. G.; Holmes, A. B. *Chem. Rev.* **2009**, *109*, 897.

14.   Epstein, A. J.; Wang, Y. Z. In *Semiconducting Polymer: Applications, Properties, and Synthesis*; Hsieh, B. R., Wei, Y., Eds.; American Chemical Society: Washington, DC, 1999; p 160.

15.   Murray, M. M.; Holmes, A. B. In *Semiconducting Polymers: Chemistry, Physics, and Engineering*; Hadziioannou, G., van Hutten, P. F., Eds.; Wiley-VCH: Weinheim, 2000; p 1.

16.   Campbell, I. H.; Smith, D. L. In *Semiconducting Polymers: Chemistry, Physics, and Engineering*; Hadziioannou, G., van Hutten, P. F., Eds.; Wiley-VCH: Weinheim, 2000; p 333.

17.   Scott, J. C.; Malliaras, G. G. In *Semiconducting Polymers: Applications, Properties, and Synthesis*; Hadziioannou, G., van Hutten, P. F., Eds.; Wiley-VCH: Weinheim, 2000; p 411.

18.   Thomas, C. A.; Reynolds, J. R. In *Semiconducting Polymers: Applications, Properties, and Synthesis*; Hsieh, B. R., Wei, Y., Eds.; American Chemical Society: Washington, DC, 1999; p 367.

19.   Meng, X. S.; Desjardins, P.; Wang, Z. Y. In *Semiconducting Polymers: Applications, Properties, and Synthesis*; Hsieh, B. R., Wei, Y., Eds.; American Chemical Society: Washington, DC, 1999; p 61.

20.   Invernale, M. A.; Acik, M.; Sotzing, G. A. In *Handbook of Thiophene-Based Materials: Applications in Organic Electronics and Photonics*; Perepichka, I. F., Perepichka, D. F., Eds.; Wiley: West Sussex, U. K., 2009; Volume 1, p 757.

21.   Beaujage, P. M.; Reynolds, R. *Chem Rev.* **2010**, *110*, 268.

22.   Beaujage, P. M.; Amb, C. M.; Reynolds, J. R. *Acc. Chem. Res.* **2010**, *43*, 1396.

23. Guiseppi-Elie, A.; Wallace, G. G.; Matsue, T. In *Handbook of Conducting Polymers*, 2nd ed.; Skothiem, T. A., Elsenbaumer, R. L., Reynolds, J. R., Eds.; Marcel Dekker, Inc.: New York, 1998; p 963.

24. Kossmehl, G.; Engelmann, G. In *Handbook of Oligo- and Polythiophenes*; Fichou, D., Ed.; Wiley-VCH: Weinheim, 1999; p 491.

25. Guiseppi-Elie, A.; Braim, S.; Wilson, A. M. In *Handbook of Conducting Polymers: Processing and Applications*, 3rd ed.; Skotheim, T. A., Reynolds, J. R., Eds.; CRC Press: Boca Raton, FL, 2007; p 12-1.

26. Nilsson, P.; Inganäs, O. In *Handbook of Conducting Polymers: Processing and Applications*, 3rd ed.; Skotheim, T. A., Reynolds, J. R., Eds.; CRC Press: Boca Raton, FL, 2007; p 13-1.

27. MacDiarmid, A. G.; Huang, F.; Fend, J. In *Semiconducting Polymers: Applications, Properties, and Synthesis*; Hsieh, B. R., Wei, Y., Eds.; American Chemical Society: Washington, DC, 1999; p 184.

28. Ho, H.-A.; Leclerc, M. In *Handbook of Thiophene-Based Materials: Applications in Organic Electronics and Photonics*; Perepichka, I. F., Perepichka, D. F., Eds.; Wiley: West Sussex, U. K., 2009; Volume 1, p 813.

29. Katz, H. E.; Dadabalapur, A.; Bao, Z. *Oligo- and Polythiophenes*; Fichous, D., Ed.; Wiley-VCH, Germany, 1999; p 490.

30. Tessler, N.; Veres, J.; Globerman, O.; Rappaport, N.; Preezant, Y.; Roichman, Y.; Solomesch, O.; Talk, S.; Gershman, E.; Alder, M.; Zolotarev, V.; Gorelik, V.; Eichen, Y. In *Handbook of Conducting Polymers: Processing and Applications*, 3rd ed.; Skotheim, T. A., Reynolds, J. R., Eds.; CRC Press: Boca Raton, FL, 2007; p 7-1.

31. Bao, Z. In *Semiconducting Polymers: Applications, Properties, and Synthesis*; Hsieh, B. R., Wei, Y., Eds.; American Chemical Society: Washington, DC, 1999; p 244.

32. Horowitz, G. In *Semiconducting Polymers: Chemistry, Physics, and Engineering*; Hadziioannou, G., van Hutten, P. F., Eds.; Wiley-VCH: Weinheim, 2000; p 463.

33. Otsubo, T.; Takimiya, K. In *Handbook of Thiophene-Based Materials: Applications in Organic Electronics and Photonics*; Perepichka, I. F., Perepichka, D. F., Eds.; Wiley: West Sussex, U. K., 2009; Volume 1, p 321.

34. Hotta, S. In *Handbook of Thiophene-Based Materials*; Perepichka, I. F., Perepichka, D. F., Eds.; Wiley: West Sussex, U. K., 2009; Volume 1, p 477.

35. Fachetti, A. In *Handbook of Thiophene-Based Materials*; Perepichka, I. F., Perepichka, D. F., Eds.; Wiley: West Sussex, U. K., 2009; Volume 1, p 595.

36. McCulloch, I.; Heeney, M. In *Handbook Thiophene-Based Materials*; Perepichka, I. F., Perepichka, D. F., Eds.; Wiley: West Sussex, U. K., 2009; Volume 1, p 647.

37. Dagani, R. *Chem. Eng. News* **2000**, *78*, 4.

38. Dannenberg, E. M.; Paquin, L.; Gwinnell, H. In *Kirk-Othmer Encyclopedia of Chemical Technology*, 4th ed.; Howe-Grant, M., Ed.; John Wiley & Sons: New York, 1992; Volume 4, p 1037.

39. Rasmussen, S. C. *Bull. Hist. Chem.* **2014**, *39*, 64.

40. Rasmussen, S. C. *Substantia* **2017**, *1*, 99.

41. Rasmussen, S. C. In *Handbook of Conducting Polymers*, 4th ed.; Skotheim, T. A., Reynolds, J., Thompson, B. C., Eds.; CRC Press, Boca Raton, FL, 2019, Volume 1, Chapter 1.

42. Rasmussen, S. C. In *100+ Years of Plastics. Leo Baekeland and Beyond*; Strom, E. T., Rasmussen, S. C., Eds.; ACS Symposium Series 1080; American Chemical Society: Washington, DC, 2011; Chapter 10.

43. Rasmussen, S. C. *Bull. Hist. Chem.* **2015**, *40*, 45.

44. Shirakawa, H.; Louis, E. J.; MacDiarmid, A. G.; Chiang, C. K.; Heeger, A. J. *J. Chem. Soc., Chem. Commun.* **1977**, 578.

45. Chiang, C. K.; Park, Y. W.; Heeger, A. J.; Shirakawa, H.; Louis, E. J.; MacDiarmid, A. G. *J. Chem. Phys.* **1978**, *69*, 5098.

46. Chiang, C. K.; Druy, M. A.; Gau, S. C.; Heeger, A. J.; Louis, E. J.; MacDiarmid, A. G.; Park, Y. W.; Shirakawa, H. *J. Am. Chem. Soc.* **1978**, *100*, 1013.

47. Liu, C.; Wang, K.; Gong, X.; Heeger, A. *J. Chem. Soc. Rev.* **2016**, *45*, 4825.

48. Yu, P.Y. and Cardona, M. In *Fundamentals of Semiconductors*, 4th ed.; Yu, P. Y., Cardona, M. Eds.; Graduate Texts in Physics. Springer, Berlin, Heidelberg, 2010, 1.

49. Pomerantz, M. in *Handbook of Conducting Polymer*, 2nd ed.; Skotheim, T. A., Elsenbaummer, R. L., Reynolds, J. R., Eds.; Marcel Dekker, Inc., New York, 1998, Chapter 11.

50. Rasmussen, S. C. and Pomerantz, M. in *Handbook of Conducting Polymers*; Skotheim, T. A., Reynolds, J. R., Eds.; CRC Press, Boca Raton, FL, 2007, Volume 1, Chapter 12.

51. Rasmussen, S. C.; Ogawa, K.; and Rothstein, S. D. in *Handbook of Organic Electronics and Photonics*, 3rd ed.; Nalwa, H. S., Ed.; American Scientific Publishers, Stevenson Ranch, CA, 2008, Volume 1, Chapter 1.

52. Rasmussen, S. C.; Scwiderski, R. L.; Mulholland, M. E. *Chem. Commun.* **2011**, *47*, 11394.

53. Rasmussen, S. C. In *Encyclopedia of Polymeric Nanomaterials*; Kobayashi, S., Mullen, K., Eds.; Springer, Berlin, Heidelberg, 2013; Chapter 57.

54. Kroon, R.; Lenes, M.; Hummelen, J. C.; Blom, P. W. M.; De Boer, B. *Polym. Rev.* **2008**, *48*, 531.

55. Bunz, U. W. F. in *Handbook of Conducting Polymers*, 3rd ed.; Skotheim, T. A., Reynolds, J. R., Eds.; CRC Press: Boca Raton, FL, 2007, Volume 1, Chapter 6.

56. Roncali, J. *Chem. Rev.* **1997**, *97*, 173.

57. Stępień, M.; Gońka, E.; Zyla, M.; Sprutta, N. *Chem. Rev.* **2017**, *117*, 3479.

58. Bundgaard, E.; Krebs, F. *Sol. Energy Mater. Sol. Cells* **2007**, *91*, 954.

59. Chochos, C. L.; Choulis, S. A. *Prog. Polym. Sci.* **2011**, *36*, 1326.

60. van Mullekom, H. A. M.; Vekemans, J. A. J. M.; Havinga, E. E.; Meijer, E. W. *Mat. Sci. Eng. R* **2001**, *32*, 1.

61. Kenning, D. D.; Funfar, M. R.; Rasmussen, S. C. *Polymer Preprints* **2001**, *42*, 506.

62. Kenning, D. D.; Funfar, M. R.; Rasmussen, S. C. *Polymer Preprints* **2001**, *42*, 665.

63. Rasmussen, S. C.; Mulholland, M. E.; Schwiderski, R. L.; Larsen, C. A. *J. Heterocyclic Chem.* **2012**, *49*, 479.

64. Kenning, D. D.; Mitchell, K. A.; Calhoun, T. R.; Funfar, M. R.; Sattler, D. J.; Rasmussen, S. C. *J. Org. Chem.* **2002**, *67*, 9073.

65. Wen, L.; Rasmussen, S. C. *J. Chem. Crystallogra.* **2007**, *37*, 387.

66. Wen, L.; Nietfeld, J. P.; Amb, C. A.; Rasmussen, S. C. *J. Org. Chem.* **2008**, *73*, 8529.

67. Kenning, D. D.; Mitchell, K. A.; Calhoun, T. R.; Funfar, M. R.; Sattler, D. J.; Rasmussen, S. C. *J. Org. Chem.* **2002**, *67*, 9073.

68. Babudri, F.; Fiandanese, V.; Marchese, G.; Punzi, A. *Tetrahedron Lett.* **1995**, *36*, 7305.

69. Lai, M.; Tsai, J.; Chueh, C.; Wang, C.; Chen, W. *Macromol. Chem. Phys.* **2010**, *211*, 2017.

70. Mondal, R.; Miyaki, N.; Becerril, H. A.; Norton, J. E.; Parmer, J.; Mayer, A. C.; Tang, M. L.; Bredas, J.-L.; McGehee, M. D.; Bao, Z. *Chem. Mater.* **2009**, *21*, 3618.

71. Wu, W.; Lee, W.; Chen, W. Macromol. *Chem. Phys.* **2006**, *207*, 1131.

72.   Wu, W.; Liu, C.; Chen, W. *Polymer* **2006**, *47*, 527.

73.   Lu, X.; Zhou, G.; Wang, H.; Feng, Q.; Wang, Z.-S. *Phys. Chem. Chem. Phys.,* **2012,** *14,* 4802.

74.   Chen, E.-C.; Tseng, S.-R.; Chao, Y.-C.; Meng, H.-F.; Wang, C.-F.; Chen, W.-C.; Hsu, C.-S.; Horng, S.-F. *Synth. Met* **2011,** *161,* 1618.

75.   Ju, X.; Kong, L.; Zhao, J.; Bai, G. *Electrochim. Acta* **2017,** *238,* 36.

76.   Wen, L.; Heth, C. L.; Rasmussen, S. C. *Phys. Chem. Chem. Phys.* **2014**, *16*, 7231.

CHAPTER 2. INVESTIGATING THE ROLE OF AMBIPOLAR UNITS IN THE DONOR-ACCEPTOR FRAMEWORK[*]

Introduction

The band gap (E_g) is a critical material parameter that has a large impact on the usefulness and applications of a conjugated polymer. As introduced in Chapter 1, the E_g is the energy difference between the bottom of the conduction band and the top of the valence band of a solid-state material. This determines a number of the electronic and optical properties of the material. The fact that this parameter can be tuned by polymer design is an appealing aspect of organic electronics and allows for materials to be generated for specific applications.[1-3] The most popular approach for generating reduced (E_g=1.5-2.0 eV) or low (E_g<1.5 eV) E_g polymers is the donor-acceptor (D-A) model. This model is based on the concept that pairing an electron-rich species (the donor) and an electron-deficient species (the acceptor) would result in a material with a lower E_g than either unit could generate on their own upon polymerization due to the hybridization of the frontier orbitals which results in a material with HOMO levels similar to that of the donor and LUMO levels similar to the acceptor.[4] As the library of monomers for conjugated materials increases, it allows for even more options for controlling the energy levels of the resulting material.

While the D-A model has proven to be an effective design for the generation of low E_g materials, it does come with a number of issues. The first of which is the over-simplified

---

classification of building blocks/monomers as either being purely donor, acceptor, or spacer units. While this has still resulted in materials with the desired characteristics, the source of those resulting characteristics is simply attributed to the donor and acceptor nature of the monomer units and a further, deeper understanding of underlying structure-function factors are rarely investigated. The result is that the D-A model is used as a catchall explanation for the E_g of a material rather than a further evolving design principle for the generation of low E_g polymers.

Another misconception within the D-A model is the role of spacer units. The spacer unit was first introduced as a unit that would increase the spacing between the donor and acceptor unit that results in the polymer maintaining planarity while the spacer would not have an impact on the electronics of the system.[5] However, this concept of a spacer unit not contributing to the electronics of the resulting material has been shown to be incorrect on multiple accounts.[6-11]

A third issue is not necessarily a shortcoming, but it is a good representation of the propagation of misapplications of analyses that have surrounded the D-A model since its inception. The original context of the D-A model by Havinga was a comparison between an electron rich and electron deficient alternating organic polymer with the inorganic n-i-p-i super lattice structures.[12] Havinga explained that the donor material would modulate the polymer's HOMO while the acceptor material would modulate the polymer's LUMO, thus resulting in a polymer with the desired characteristics of each of the two units. The model proved to be an effective means for designing organic electronics with specific characteristics, namely the tuning of energy levels and adjusting the E_g values. While these problems do not negate the effectiveness of the D-A model, it does bring into question the thoroughness that the model has been investigated. The D-A model has been used as a means of explanation over and over with little rigor in the development and evolution of the model itself.

The thieno[3,4-b]pyrazine (TP, **2.1**, Figure 2.1) based monomers are used for conjugated

materials and have been used to successfully generate a large number of low E_g conjugated

polymers.[13-24] The TP monomer was initially classified as an acceptor unit due to its low-lying

LUMO energy level (-2.0 eV for 2,3-dihexylthieno[3,4-b]pyrazine).[25] While this is a completely

viable reason for its characterization as an acceptor unit, it is an oversimplification of the impact

of the electronic characteristics of TP. The HOMO energy level of TP is more destabilized than

other donors, which would make it an effective donor unit. TP has actually been shown to be a

slightly stronger donor that 3,4-ethylenedioxythiophene (EDOT, **2.2**, Figure 2.1), which is

considered one of the stronger donors applied to conjugated materials.[26] Based on this

characteristic, it would be appropriate to also characterize TP as a donor unit. It is because of the

combination of these characteristics that TP currently serves as an anomaly in the current D-A

model and has been given the new description of an *ambipolar unit*.[8,27-30] The ambipolar unit is

one that is a significant contributor to the HOMO of the new molecule due to its high HOMO,

just as donor units, and a significant contributor to the LUMO of the new molecule due to its low

LUMO, just as acceptor units, simultaneously. In order to understand the impact that ambipolar

units have on tuning the energy levels and affecting the E_g of conjugated materials that they are a

part of, it is necessary to systematically incorporate ambipolar units with other molecules in the

D-A framework.
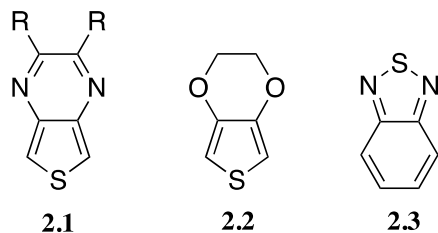
Figure 2.1. Structures of 2,3-difunctionalized thieno[3,4-b]pyrazine (**2.1**), 3,4-
ethylenedioxythiophene (**2.2**), and benzo[c][1,2,5]thiadiazole (**2.3**).

One of the first investigations of these peculiar characteristics of TP was performed by Wen et. al.,[9] who synthesized trimers with varying amounts of TP paired with either thiophene or EDOT. With EDOT being considered one of the stronger donor units and the TP being classified as an acceptor, the D-A model would predict that the mixed oligomer would have a smaller HOMO-LUMO gap. However, it was found that the more TP that was present in the oligomer, the smaller the HOMO-LUMO gap, with the trimer TP_3 having the smallest HOMO-LUMO gap. The TP molecule actually behaved as a better donor than EDOT in the oligomer as shown with the further destabilization of the HOMO as the TP content increases. These findings showed that TP's role in the D-A model was more complicated than that of a traditional acceptor unit.

To expand upon this initial study, Mulholland synthesized copolymers in which TP was paired with a traditional acceptor unit.[31] The first of the polymers was pairing a TP unit with benzo[*c*][1,2,5]thiadiazole (BTD, **2.3**, Figure 2.1) resulting in poly(2,3-didodecylthieno[3,4-*b*]pyrazine-*alt*-benzo[*c*][1,2,5]thiadiazole). The resulting material was described at the time as being an acceptor-acceptor polymer and had an E_g of 1.3 eV, making it a low E_g material. These results served as a basis for two concepts that do not fit within the current paradigm because of the uncertainty of the properties of ambipolar units. The first of which is the role of the TP ambipolar unit within the D-A framework. The second of which is the viability of an ambipolar-acceptor polymer, which will be explored in a future chapter.

In this chapter, the role of **2.1** within the D-A framework will be discussed via the investigation of a family of dimers consisting of the ambipolar TP, the strong donor unit EDOT, and the strong acceptor unit BTD (Figure 2.2). A combination of homo- and hetero-dimers have been synthesized and the electronic and optical properties of the dimers were obtained and analyzed. The molecule design will also provide an avenue to explore the donor-acceptor effects

27

through the contribution of traditional and ambipolar building blocks. Additionally, some

explanations for the effectiveness of D-A molecules are explored. An associated manuscript is

currently in preparation for submission to *Physical Chemistry Chemical Physics*.[32]
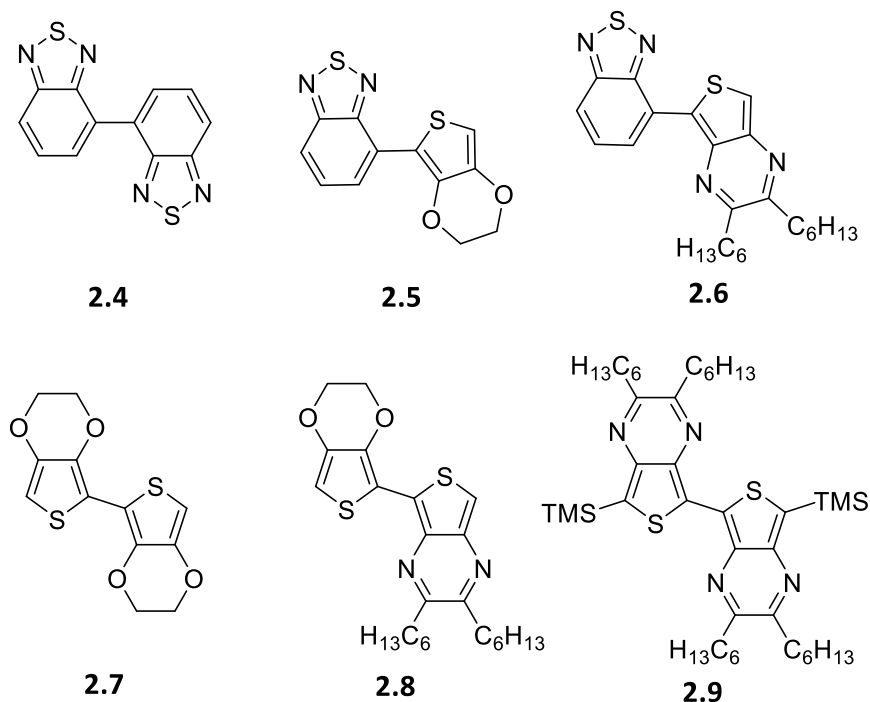
Figure 2.2. The family of dimers are synthesized to understand the role of ambipolar units in the DA framework as well as to probe the donor-acceptor effects through the contributions of traditional and ambipolar building blocks.

Results and Discussion

Synthetic Overview

4-Bromobenzo[c][1,2,5]thiadiazole

While the TP and EDOT functionalized species used in the coupling were prepared and

used *in situ*, it was necessary to isolate the functionalized BTD species prior to the coupling. The

functionalized 4-bromobenzo[*c*][1,2,5]thiadiazole (BTD-Br, **2.10**) was generated by the

bromination of **2.3** via liquid Br_2 in HBr. Initial attempts at the bromination consisted of using a

1:1 ratio of Br_2 to **2.3**, but resulted in primarily 4,7-dibromobenzo[*c*][1,2,5]thiadiazole (BTD-

Br$_2$, **2.11**) with little **2.10** being isolated, likely due to the increased reactivity of BTD-Br (Scheme 2.1). Even reducing the ratio of Br$_2$ did not change the dominant product being **2.11** over **2.10**.

2.3 + Br$_2$ → (no reaction) **2.10**

HBr → **2.3** + **2.10** + **2.11**
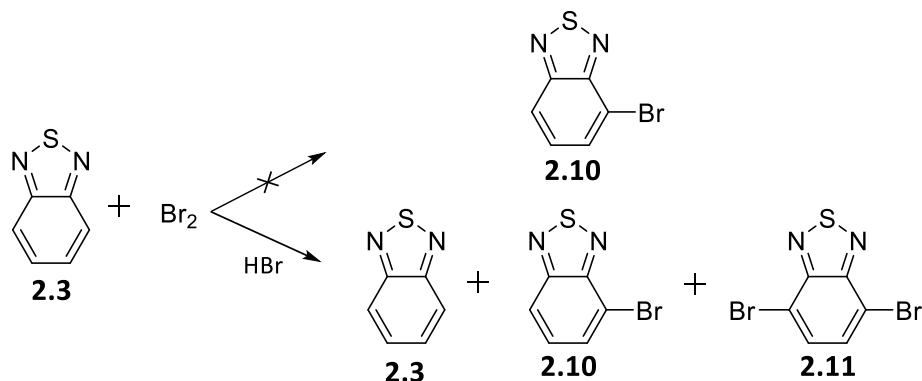
Scheme 2.1. Initial synthesis attempts of brominating **2.3** by Br$_2$ in HBr in hopes of generating **2.10**.

In hopes of recovering **2.10**, different solvents were used as eluents for separation of the mixture by column chromatography while using silica as the stationary phase. The initial solvent mixture used was ethyl acetate and hexane, with the only solvent combination that resulted in any sort of separation on thin layer chromatography plates was a 1:3 ethyl acetate:hexane solvent system. However, the combination resulted in no clear separation upon column chromatography. The second solvent combination was hexane and chloroform, with the best separation on TLC occurring at a 1:1 ratio. Unfortunately, similar results, or rather lack thereof, were obtained using this second solvent combination for column chromatography.

The inefficient means of purification by column chromatography was a clear sign that it was necessary to find an alternative means of isolating **2.10**. Rather than directly synthesizing **2.10** from **2.3**, the focus changed to the easily synthesized dibromo- **2.11** and having that undergo debromination in hopes of obtaining the desired monobromo- **2.10** (Scheme 2.2). The initial debromination attempt was with one equivalence of BuLi at 0 °C in THF and then water

was added as a proton source. The reaction was not successful with only ≈8% of **2.11** being

debrominated, as determined by ^{1}H NMR, and the majority of the isolated material was **2.11**.

The second attempt at debromination was by treating **2.11** with zinc metal in acetic acid at reflux

temperatures. After five hours at reflux, there was no debrominated species, resulting in yet

another path that did not yield a promising means of generating the monobromo species

necessary for the coupling.
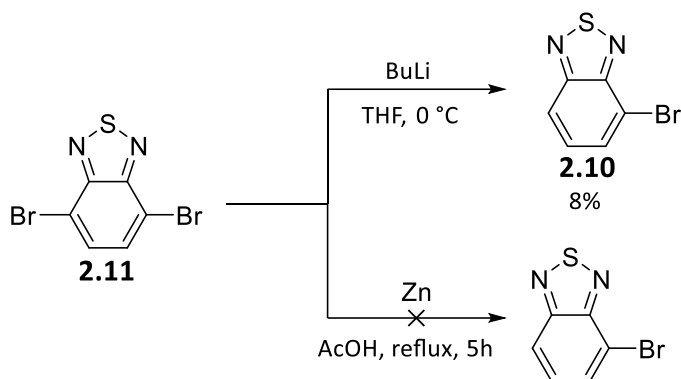
Scheme 2.2. Debromination attempts of **2.11** to generate the desired **2.10**.

Pilgram, et. al. had actually already published a report for the generation of **2.10** (Scheme

2.3).[33] The method used was the bromination of **2.3** in HBr with Br$_2$ at 1:1 mol ratio, but the

reaction was heated at reflux for one hour compared to the three hours that had been practiced up

to this point. However, the means of purification was not column chromatography, as previously

employed. Instead it was necessary to have a two-step purification process to isolate **2.10** from

the mixture also including **2.3** and **2.11**. The first step was steam distillation to collect the

compounds **2.3** and **2.10**. The mixture of **2.3** and **2.10** was then purified by recrystallization,

finally resulting in the successful isolation of **2.10**.
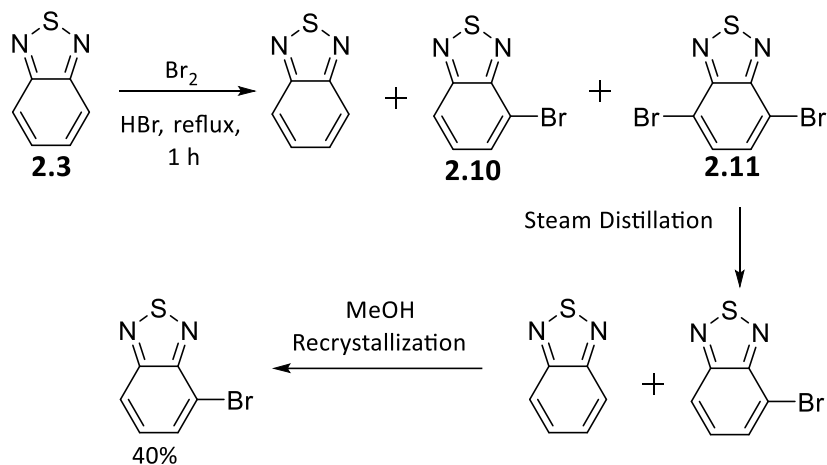
Scheme 2.3. Successful synthetic pathway starting with **2.3** and resulting in the isolation of **2.10**.

4,4'-Bis(benzo[c][1,2,5]thiadiazole)

With **2.10** being isolated, it was now possible to synthesize the dimers containing the

BTD unit. The first dimer synthesized was the homodimer 4,4'-bis(benzo[*c*][1,2,5]thiadiazole)

(**2.4**). The initial synthesis attempt was to generate the dimer by Ullmann coupling, which

required the heating of **2.10** in the presence of copper metal (Scheme 2.4). Despite overnight

heating at reflux, no dimer was obtained. It seemed that a stronger coupling method was required

and Stille coupling appeared to be the most logical option with the functionalization already in

place.
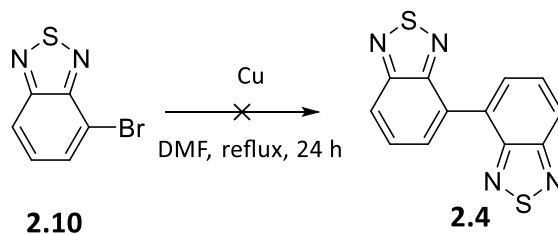
Scheme 2.4. Failed homocoupling of **2.10** to generate **2.4**.

The first attempt at Stille coupling was by sequentially treating **2.3** with butyllithium

(BuLi) and then trimethylstannyl chloride (SnMe₃Cl) (Scheme 2.5). The mixture was then heated

after the addition of **2.10** and a palladium catalyst, although the only isolated materials were the

31

starting materials **2.10** and unreacted **2.3**. This reaction was then repeated, but **2.10** was treated with BuLi and SnMe₃Cl rather than unfunctionalized **2.3**. Neither of these reactions yielded the desired dimer, however the latter did yield a white solid that had physical characteristics different than the starting **2.10**, but its spectra did not match with the previously reported **2.4**.[32]
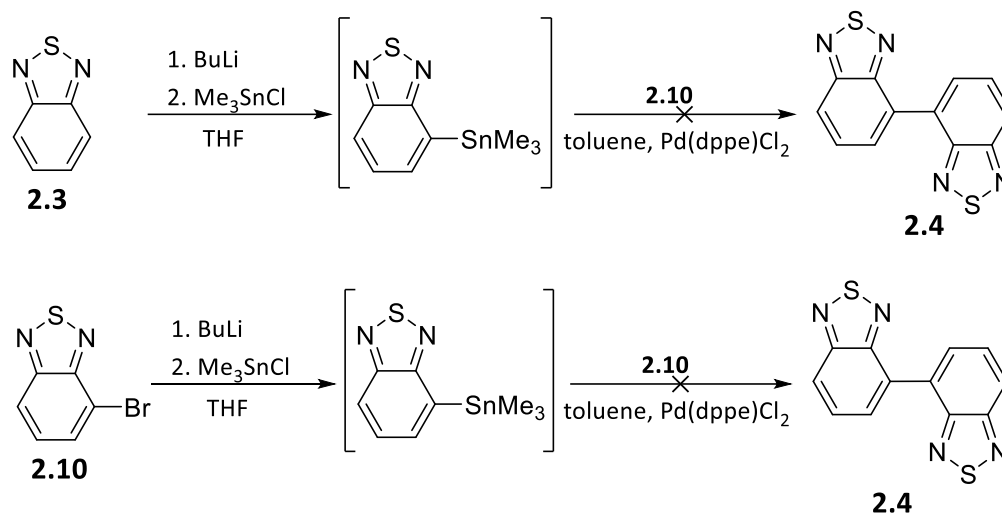
Scheme 2.5. Failed Stille coupling synthetic pathways starting with **2.3** and **2.10** to generate **2.4**.

Evan Culver (another graduate student in the Rasmussen lab) was finally able to successfully synthesize **2.4** that matched the previously reported data.[32] His synthesis consisted of adding zinc powder, dichloro[bis(1,3-diphenylphosphino)propane]nickel(II) (Ni(dppp)Cl₂), and tetrabutylammonium bromide (TBABr) to a round bottom flask, along with THF as a solvent (Scheme 2.6). The molecule **2.10** was then added and the solution was heated at reflux for 6 hours, resulting in a slightly yellow solid after column chromatography.
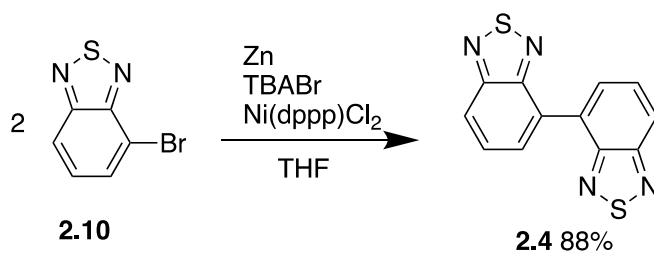
Scheme 2.6. Successful coupling of **2.10** resulting in **2.4**.

2,2'-Bis(3,4-ethylenedioxythiophene)

Unfunctionalized EDOT (**2.2**) was brominated by *N*-bromosuccinimide to generate 2-bromo(3,4-ethylenedioxythiophene) (**2.12**), which was then heated in the presence of copper metal (Scheme 2.7). While three hours of heating at reflux did not generate the desired 2,2'-bis(3,4-ethylenedioxythiophene) (**2.7**), 20 hours at reflux was sufficient to generate the dimer (Scheme 2.7). While this method was able to generate **2.7** that matched with previously reported values, there were larger oligomers that were also generated that could not be adequately separated by column chromatography.
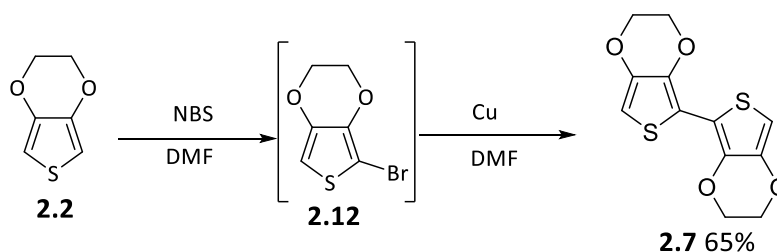
Scheme 2.7. The sequential bromination of **2.2** followed by Ullmann coupling to generate **2.7**.

Evan Culver was able to utilize an alternative synthetic pathway by treating **2.2** with BuLi and then added CuCl$_2$ to generate the desired **2.7** without any of the additional oligomeric species (Scheme 2.8).[32] The NMR matched the previously reported values and there were less oxidation peaks present during the electrochemistry, even further justifying the presence of oligomers in the previous synthetic attempt. The isolated product was purified with a CH$_2$Cl$_2$ column and yielded a white solid.
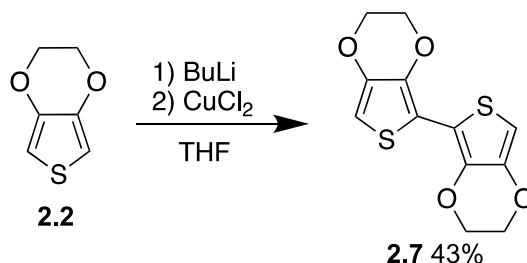
Scheme 2.8. Successful coupling of **2.2** to generate **2.7**.

4-(3,4-Ethylenedioxythiophen-2-yl)benzo[c][1,2,5]thiadiazole and 4-(2,3-dihexylthieno[3,4-

b]pyrazin-5-yl)benzo[c][1,2,5]thiadiazole.

The synthesis of 4-(3,4-ethylenedioxythiophen-2-yl)benzo[*c*][1,2,5]thiadiazole (**2.5**) and

4-(2,3-dihexylthieno[3,4-*b*]pyrazin-5-yl)benzo[*c*][1,2,5]thiadiazole (**2.6**) were synthesized with

similar conditions (Scheme 2.9 and 2.10). With the brominated BTD species **2.10** already being

isolated, it was only necessary to generate the corresponding stannyl species of TP and EDOT to

generate the dimers via Stille coupling. This was accomplished by sequentially treating the

unfunctionalized monomers with BuLi and SnMe₃Cl. The Stille coupling then only required the

Pd catalyst source in addition to **2.10** in order to generate the two dimers in high yields.
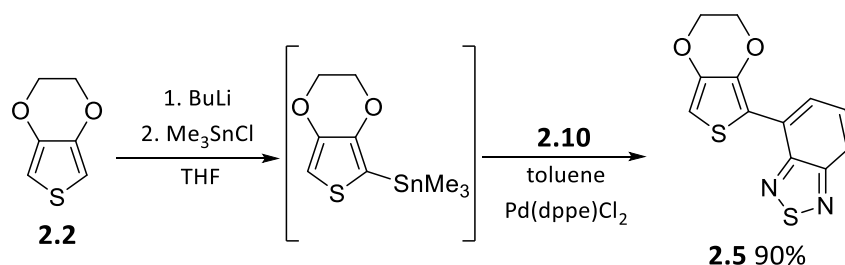
Scheme 2.9. The synthetic pathway to couple **2.2** and **2.10** via Stille coupling to generate **2.5**.
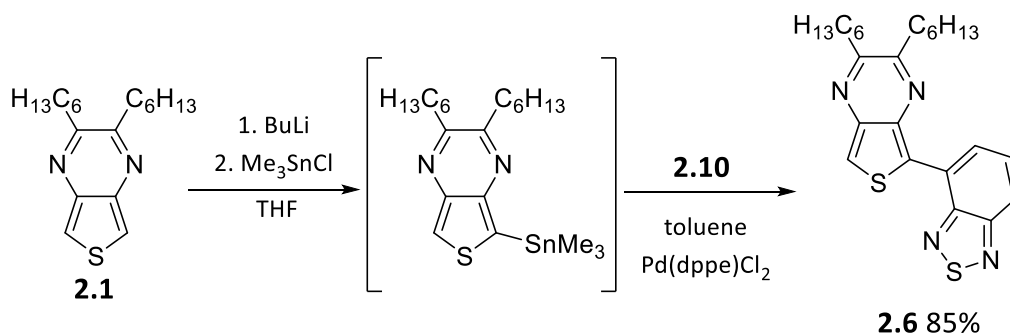
Scheme 2.10. The synthetic pathway to couple **2.1** and **2.10** via Stille coupling to generate **2.6**.

While the **2.5** dimer remained stable for multiple months when left in the freezer, the

same could not be said about the **2.6** dimer. When the compound was revisited after a few

months in the freezer, additional peaks were present on the ^{1}H NMR that were not in the original

sample. What likely occurred was the coupling of the TP unit of the dimer to another TP unit on an additional dimer, resulting in a larger oligomer. This coupling was likely caused by the thiophene of the TP being oxidized by oxygen present, resulting in the new tetramer compound. An appropriate eluent could not be determined to separate the dimer from the larger oligomer by column chromatography.

5-(3,4-Ethylenedioxythiophen-2-yl)-2,3-dihexylthieno[3,4-b]pyrazine

The most sensitive of the dimers synthesized proved to be 5-(3,4-ethylenedioxythiophen-2-yl)-2,3-dihexylthieno[3,4-*b*]pyrazine (**2.8**). Initial conditions consisted of the generation of a stannyl-EDOT species followed by the addition of isolated 5-bromo-2,3-dihexylthieno[3,4-*b*]pyrazine and a palladium catalyst, shown in Scheme 2.11. This unfortunately did not result in the generation of the dimer. To ensure that there was not a purity issue with the TP species the process was repeated, but with the functionalization and the coupling performed the same day. However, this still showed no sign of the generation of the dimer.
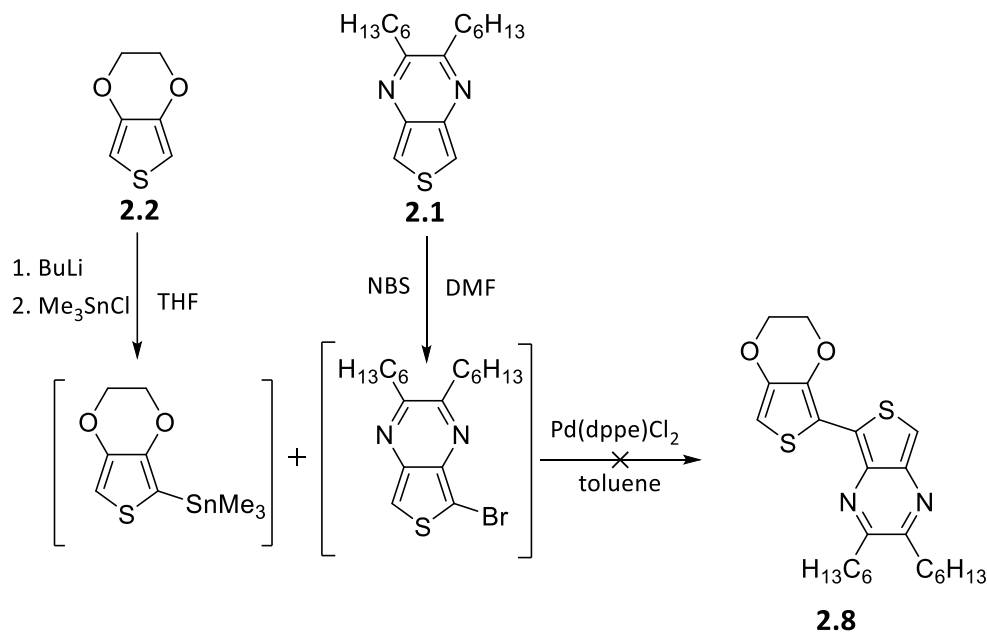
Scheme 2.11. Unsuccessful synthesis attempt of coupling **2.2** and **2.1** in hopes of generating **2.8**.

Rather than having the brominated-TP and the stannyl-EDOT, the functionalization was reversed. Unfortunately, this was not sufficient to synthesize **2.8** (Scheme 2.12) with no measurable amount of the dimer being synthesized. After further investigation in the trimer work that Wen had done with **2.1** and **2.2**, it appeared he also had issues with the coupling.[8]
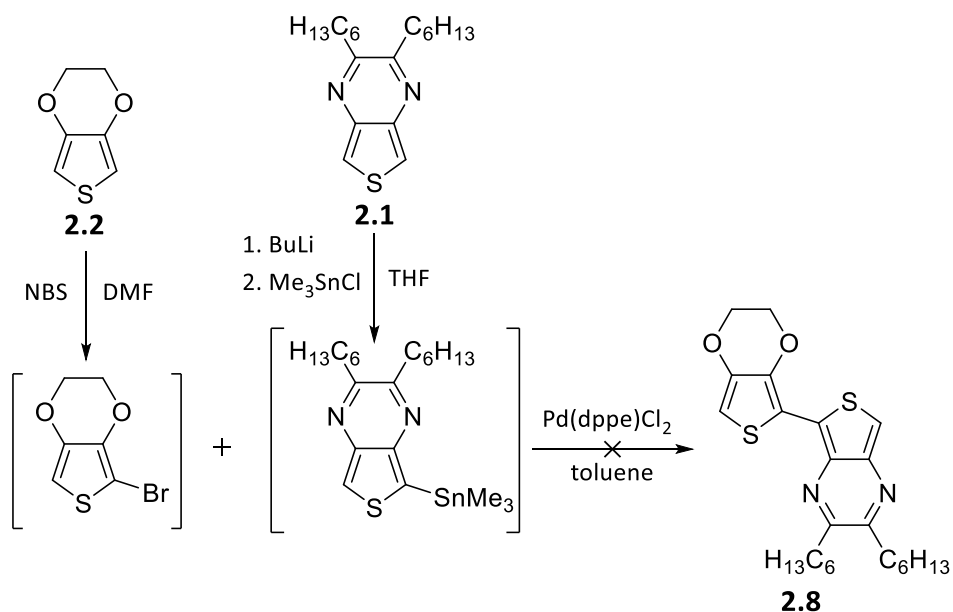
Scheme 2.12. Unsuccessful coupling attempt of **2.2** and **2.1** via Stille coupling to generate **2.8**.

In order to overcome this hurdle, Wen et. al. used copper(I) iodide as a co-catalyst with the palladium catalyst to facilitate the coupling. The CuI reacts with unsaturated stannanes to form an organocopper intermediate, which is able to undergo the transmetalation process much faster than the stannane.[34,35] Employing the co-catalyst conditions (Scheme 2.13) to the dimer system finally resulted in the generation and isolation of **2.8**.
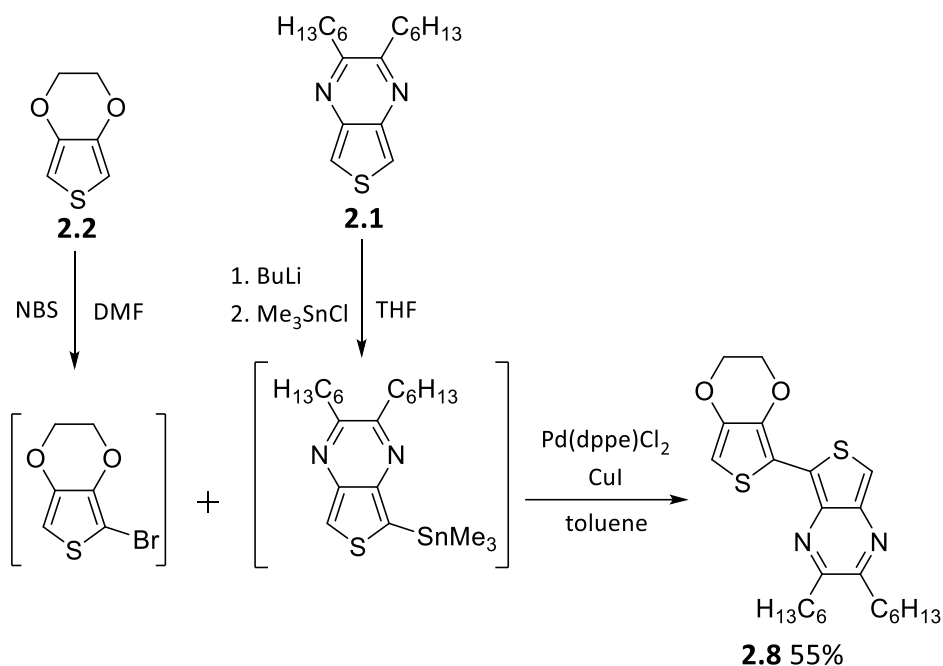
Scheme 2.13. Successful coupling of **2.2** and **2.1** via Stille coupling with co-catalyst CuI to generate **2.8**.

7,7'-Bis(trimethylsilyl)-5,5'-bis(thieno[3,4-b]pyrazine)

The TP dimer was previously synthesized by Wen et. al. as shown in Scheme 2.14.[8] Due to the air sensitivity of TP oligomers, Wen end-capped the dimer with trimethylsilyl (TMS) groups to protect the oligomer from spontaneously polymerizing and/or decomposing through oxidation. This was an issue with the purity lifetime of the other dimers generated without protecting groups, where they needed to be analyzed immediately after synthesis or there were additional peaks present not pertaining to the desired product. Additionally, TMS is an electronically neutral species, meaning it has similar electronic effects as a proton. This means that the protecting group should have little effect on the optical and electronic properties of the oligomer.
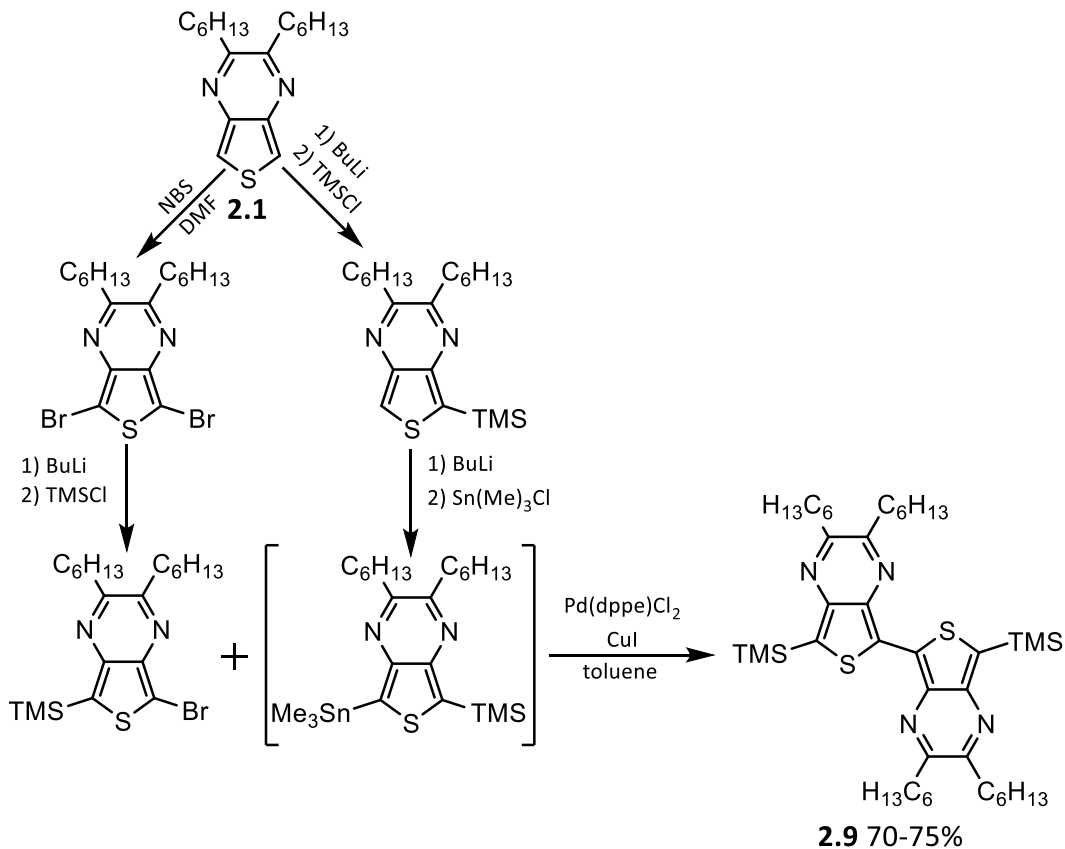
Scheme 2.14. Synthetic scheme of the coupling of **2.1** resulting in the generation of **2.9**.[8]

X-Ray Structural Analysis

Structure of 2.10

     X-ray quality crystals of **2.10** were obtained by vapor diffusion with diethyl ether as the solvent and methanol as the antisolvent. The crystals that were obtained were very thin and needlelike. The thermal ellipsoid plot is shown in Figure 2.3. The molecule **2.10** crystallizes in the triclinic space group P-1, with two molecules per unit cell.
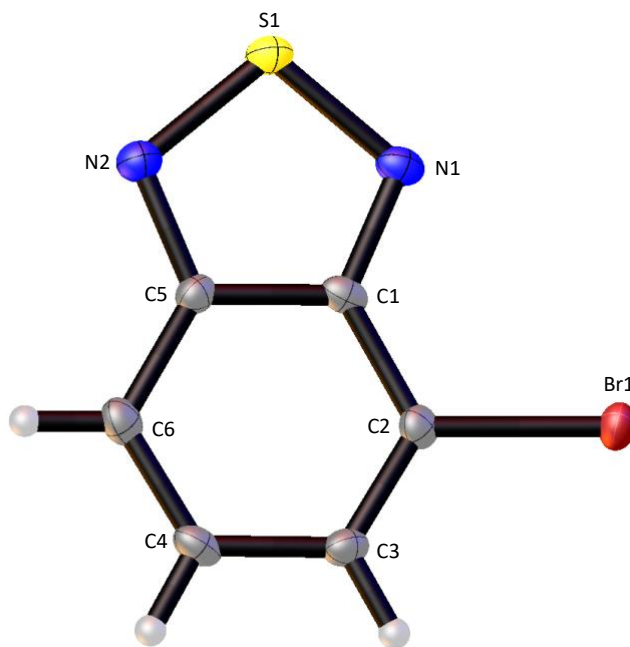
Figure 2.3. Thermal ellipsoid plot of **2.10** at 50% probability level.

Between each *bc*-plane, there are alternating strips of **2.10**. The strips are rotated 180°

from one another in such a way that the bromines are opposite of each other and the benzene and

thiadiazole rings are overlapping between planes. All of the BTD-Br units within the same *bc*-

plane have the same orientation of the bromine and the BTD rings. This can be seen in Figure

2.4.
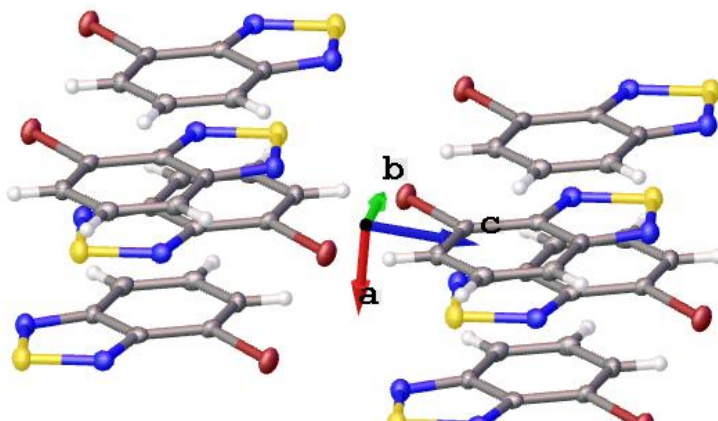
Figure 2.4. Crystal packing of BTD-Br.

Comparing the structural parameters of the unfunctionalized BTD to **2.10** (Table 2.1) demonstrates the impact of the bromine to the BTD unit. There is a consistent elongation in the bonds of the thiadiazole ring of the brominated species. The bonds of the benzene ring are elongating and contracting to compensate for the thiadiazole elongation. This is likely due to the delocalization of electron density caused by the bromine atom.

Table 2.1. Selected experimental bond lengths (Å) of BTD and **2.10**.

Bond	BTD[36]	**2.10**
C(1)-C(2)	1.459	1.427(5)
C(1)-C(5)	1.418	1.423(5)
C(1)-N(1)	1.323	1.346(4)
C(2)-C(3)	1.31	1.358(5)
C(3)-C(4)	1.478	1.419(5)
C(4)-C(6)	1.31	1.367(5)
C(5)-C(6)	1.448	1.420(5)
C(5)-N(2)	1.342	1.358(4)
N(1)-S(1)	1.613	1.620(3)
N(2)-S(1)	1.606	1.618(3)

Structure of 2.5

X-ray quality crystals of **2.5** were grown using the same method used for **2.10**. The thermal ellipsoid plot is shown in Figure 2.5. The molecule **2.5** crystallizes in the monoclinic space group P21/c and has four molecules in each unit cell. The EDOT and BTD rings have an anti-configuration so the fused rings are oriented in opposite directions along the conjugated backbone. This anti-configuration is consistent with what was expected for all of the dimers synthesized in this project. The BTD unit is planar, but there is an 18° rotation along the interannular bond. This results in the EDOT unit being slightly out of the plane, but not enough to break conjugation.
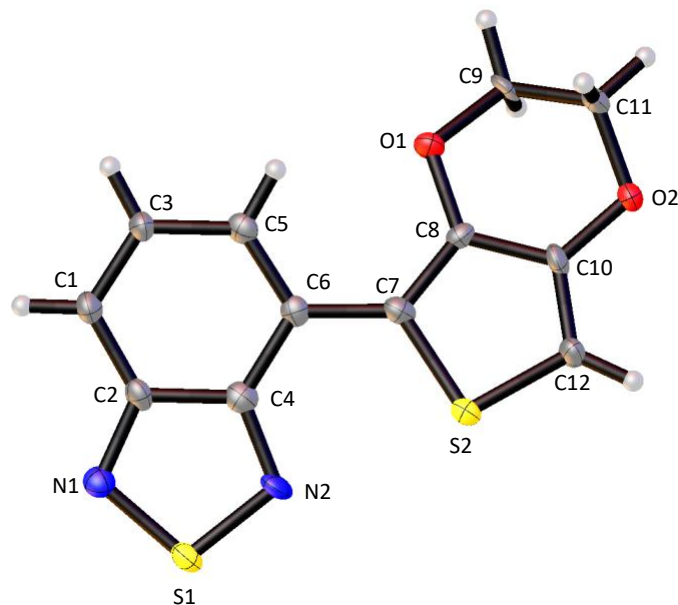
Figure 2.5. Thermal ellipsoid plot of **2.5** at the 50% probability level.

One of the notable aspects of this crystal structure is that it provides the opportunity to analyze the interannular bond C(6)-C(7) that connects the electron-rich donor and the electron-poor acceptor unit. One of the explanations for the effectiveness of HOMO-LUMO gap reduction of the D-A molecules is that the difference in the electron nature of the two species results in a substantial contribution of the quinoidal resonance structure (Figure 2.6). This resonance structure contains a double bond between the two aromatic rings and if there is substantial contribution of this resonance form then the interannular bond between the donor and acceptor unit would be shortened, corresponding to a greater double-bond contribution. This explanation has been used extensively throughout the literature with little but speculation to justify the stance.[37-44] The C(6)-C(7) bond length of **2.5** was found to be 1.469 Å. This length is closer to that of a non-conjugated single bond (approximately 1.52 Å) than a C=C bond (1.35 Å).[45] The bond length is actually larger than the bond length between the thiophene (not as electron rich as EDOT) and the benzene (not as electron deficient as BTD) of 2,5-diphenylthiophene (1.439 Å), where 2,5-diphenylthiophene does not have characteristics of a D-

A molecule.[46] The lack of shortening of the interannular bond, as well as the loss of planarity between the donor and acceptor unit, cast doubt on the theory that D-A interactions result in significant contribution from a quinoidal resonance form and reduced bond length alternation between units.
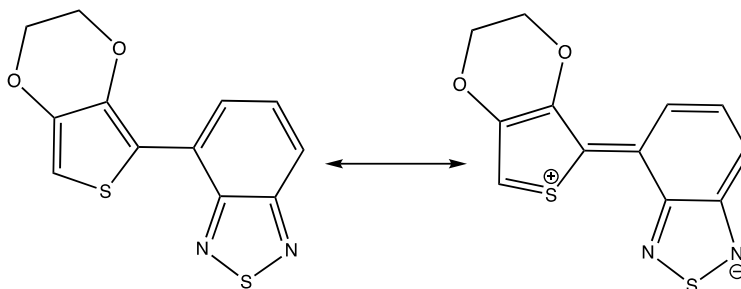
Figure 2.6. Ground state and quinoidal resonance forms of BTD-EDOT dimer.

One example of the intramolecular interactions of the **2.5** dimer is hydrogen bonding that occurs between the two units. The C-H bond at the 5-position of the BTD unit has a distance of 2.916 Å between itself and the adjacent oxygen on the EDOT (Figure 2.7). The angle between the C-H---O is 124.8°, which is of limited linearity. The angle and the C---O distance are both within previously defined parameters for C-H---O hydrogen bonds.[47,48] The C---O distance falls within the range of significant interaction (2.70-3.50 Å)[48] and is even shorter than many documented C-H---O hydrogen bonds (usually 3.0-4.0 Å).[48] The interannular twist that was previously mentioned may be a by-product of maximizing the hydrogen bond interaction with the lone pair of electrons on the oxygen that do not lie within the plane of the aromatic rings.
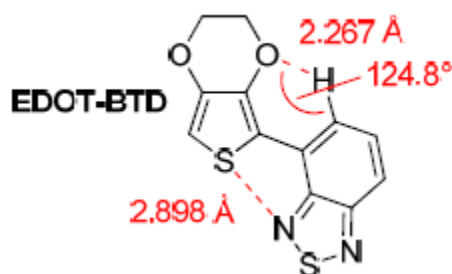
Figure 2.7. Intramolecular interactions observed in EDOT-BTD.[34]

In addition to the hydrogen bonding between the two rings, **2.5** exhibit a S---N contact between the sulfur of the EDOT and the nitrogen on the BTD closest to the EDOT (Figure 2.7). The distance between these two atoms was 2.898 Å, which is less than the sum of the van der Waals radii at 3.35 Å,[49] and has a C-S---N angle of 163.3°. These S---N contacts have also been observed in thiazole species which had even longer contacts (3.064-3.241 Å).[50,51]

Another notable aspect of the **2.5** crystal structure is the twisting of the ethylene bridge of the EDOT ring (Figure 2.8). The difference in the orientation of the hydrogens attached to C(9) and C(11), and the lack of free-rotation due to the bridge being a part of a ring, demonstrates how they are not equivalent and assists with explaining the complicated splitting pattern of the NMR spectra for **2.5**, as well as the splitting that is present in the NMR spectra of all of the non-symmetric EDOT compounds. Each hydrogen experiences ^2J coupling with the hydrogen that it shares a carbon with as well as two different ^3J coupling from the hydrogens on the adjacent carbon due to each of those hydrogens also having a slightly different atmosphere and different interactions with the hydrogen. This splitting pattern is consistent with what has been found in other EDOT compounds.[52-54]
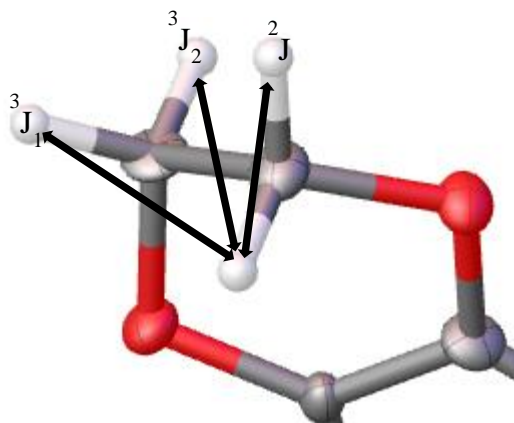
Figure 2.8. Coupling interactions on ethylene bridge of asymmetric EDOT compounds. ^2J shows the geminal coupling and $^3J_1$ and $^3J_2$ indicate the two different vicinal couplings.

Second Order Splitting with EDOT Containing Dimers

While the ^{1}H NMR of **2.2** results in a singlet for the alkyl region due to symmetry, upon

breaking of the symmetry, it no longer appears as a singlet. However, it is not a simple triplet

and has been previously described as a multiplet.[52-55] Second order splitting patterns take place

when the chemical shift difference is less than or the same magnitude as the *J*-coupling. These

splitting patterns are more complicated than first-order spectra and often require modeling to

properly interpret. A freely available NMR simulator that accurately models second-order effects

was used to determine the coupling constants and chemical shift of the dimers containing

EDOT.[56]

Figures 2.9 through 2.11 present all three of the EDOT containing dimers: EDOT$_2$,

EDOT-BTD, and EDOT-TP. The left-most part of each image is a table that shows the splitting

frequencies and chemical shift value for each of the protons as well as the simulated splitting

pattern. Due to the similar nature of the protons it is possible to use the symmetry of the situation

to make the modeling a bit easier to predict. The right portion of the image is the experimental

splitting of the actual ^{1}H NMR of the dimers.
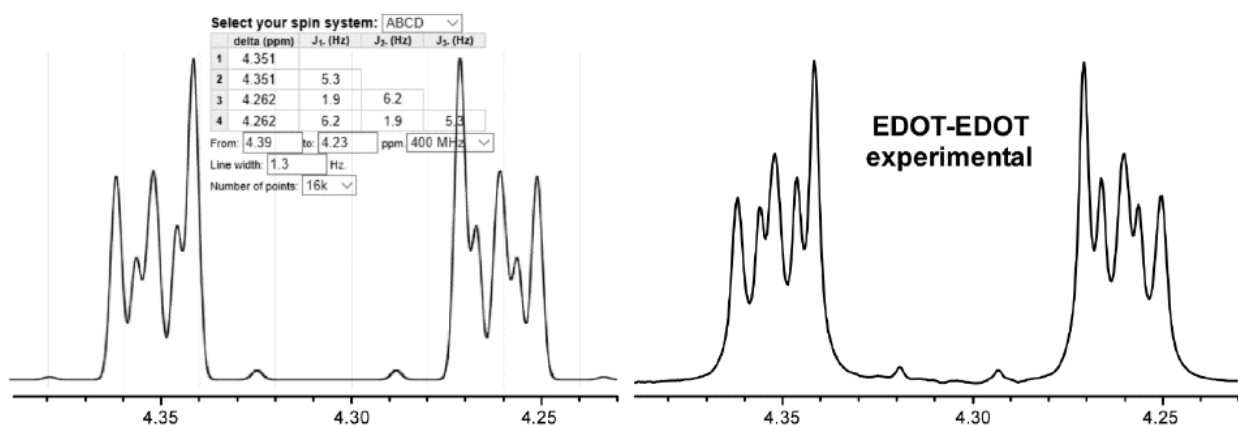
Figure 2.9. Model of the second order splitting for **2.7** compared to the actual 1H spectrum as well as the splitting frequencies.[34]

Select your spin system: ABCD

	delta (ppm)	J_1 (Hz)	J_2 (Hz)	J_3 (Hz)
1	4.419			
2	4.419	3.5		
3	4.326	2.3	6.3	
4	4.326	6.3	2.3	3.5

From: 4.30 to: 4.45 ppm 400 MHz
Line width: 0.9 Hz
Number of points: 16k

EDOT-BTD
experimental
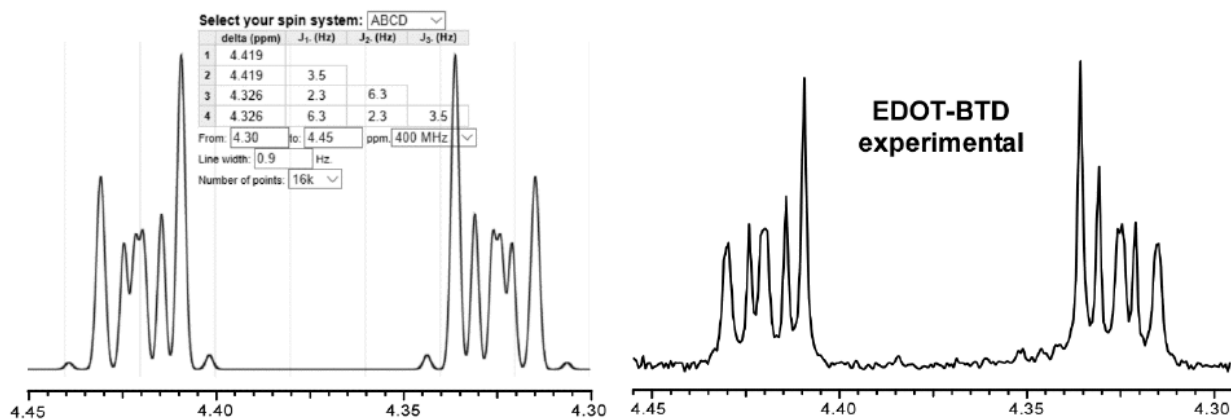
Figure 2.10. Model of the second order splitting for **2.5** compared to the actual 1H spectrum as well as the splitting frequencies.[34]

Select your spin system: ABCD

	delta (ppm)	J_1 (Hz)	J_2 (Hz)	J_3 (Hz)
1	4.439			
2	4.439	5.0		
3	4.301	2.1	6.5	
4	4.301	6.5	2.1	5.0

From: 4.26 to: 4.49 ppm 400 MHz
Line width: 1.3 Hz
Number of points: 16k

EDOT-TP
experimental
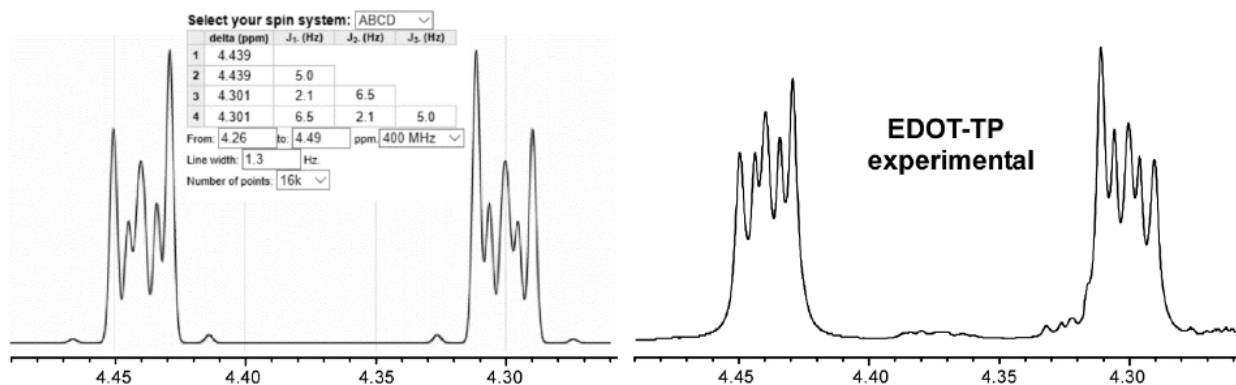
Figure 2.11. Model of the second order splitting for **2.8** compared to the actual 1H spectrum as well as the splitting frequencies.[34]

The crystal structure of **2.5** provided insight on the dihedral between the hydrogens that were on the adjacent carbons. The Karplus equation was used to predict the ^3J coupling constant using the dihedral angle and the values calculated were close to that of the computational model. It should be noted that the dihedral angle of the crystal structure was in the solid state while all of the ^1H NMR were in solution so there should be some expected difference between the two values, but it did provide a good starting value for the modeling. All of the ^3J coupling frequencies were within the range calculated by the Karplus equation. The ^2J coupling was expected to be around 2 Hz and that was the case for all three of the dimers. These values are in similar to those found with a functionalized 1,4-dioxane molecule which also has a CH_2-CH_2

bridge between two oxygen atoms.[57] There was also a family of 3,4-alkylenedioxythiophene molecules synthesized, but there were no J values given in the paper for any of the compounds and all of the protons on the alkyl bridges were described as multiplets.[58] However, this work led to an EDOT molecule that had a functionalized ethylene bridge. While the splitting for the bridge was described as two separate multiplets, a proton on the carbon bonded to the ethylene bridge was described as a doublet of a doublet, but it had a J value that did not match any other J values from the alkyl chain. This proton had a coupling constant of 6.3 Hz and was likely the ^3J from the proton on the ethylene bridge.[59] This value is similar to the values found for the coupling observed with the EDOT containing dimers.

UV-Vis Absorption Spectroscopy

Solution data of dimers in $CHCl_3$ were analyzed via UV-vis spectroscopy. Table 2.2 contains the corresponding absorption data of the dimers. In order to better understand the impact of the ambipolar unit, the following figures contained the three different heterodimers as well as the homodimers of the units that make up each of the heterodimers. All of the dimers exhibit high energy π-π^* transitions . With the exception of the $EDOT_2$ dimer, there is also a lower energy transition that has been designated an intramolecular charge transfer (ICT) from the conjugated backbone to one of the acceptor or ambipolar units. The extinction coefficient (ε) is a measure of how strongly a molecule absorbs light at a given wavelength and is dependent on the cross-sectional area of the molecule and the probability of the electronic transition. The lower ε of these ICT transitions is due to the lower allowedness, and thus lower probability, of the transition because to the lack of overlap of the molecular orbitals between the ground and excited state.[60] The ground state is primarily localized along the backbone of the dimer and the excited state is localized on an acceptor or ambipolar unit. The difference between the ε of the low

energy ICT and high energy π-π* also indicate that there are two different types of transitions with the dimers, excluding **2.7**. Previous work with similar sized molecules has shown that the ε of transitions labeled π-π* have extinction coefficients over 10,000 M^{-1} cm^{-1} and ICT transitions have values between 6,000 and 9,000 M^{-1} cm^{-1} and are usually a broad transition, which is consistent with what was observed with the dimers.[8] The ε values of EDOT-TP are lower than expected and is likely due to an issue with the measurement of the extinction coefficient and not characteristic of the molecule itself. There is work currently being done to collect this data again to ensure proper values.

Table 2.2. UV-vis absorption of the dimers synthesized.

Compound	λ_{max} (nm)	ε (M^{-1} cm^{-1})	Compound	λ_{max} (nm)	ε (M^{-1} cm^{-1})
	309	26000		262	11000
BTD$_2$[a]	316	28600	EDOT-TP	302	12600
	360	9130		451	2400
	251	15400		296	9000
	287	17400		307	10900
BTD-EDOT	306	15300	EDOT$_2$[a]	320	15400
	319	15400		335	13200
	409	6620			
	235	23200		256	21300
	274	12300	TP$_2$[b]	302	16400
BTD-TP	284	12700		504	6890
	316	16200			
	435	5960			

[a] Data from [32] [b] Data from [8]

The BTD-EDOT dimer (**2.5**) serves as the baseline for comparison for donor-acceptor unit with it consisting of the classical donor (EDOT) and acceptor (BTD). Being able to characterize the interaction between these two components allows for the comparison of the ambipolar unit TP as it replaces different units within the dimer family and help to characterize how the ambipolar unit fits within the D-A framework.

Figure 2.12 shows the absorption spectra of the BTD$_2$ (**2.4**), EDOT$_2$ (**2.7**), and **2.5**. The donor-donor dimer **2.7** has the highest-energy onset of absorption (350 nm) while **2.4** has an onset of absorption of 420 nm and **2.5** has an onset of absorption of 480 nm. The absorption of BTD$_2$ is red shifted in comparison to EDOT$_2$ because of the ICT that can occur from the biphenylene backbone to the thiadiazole rings. The lower energy absorption of the mixed dimer BTD-EDOT demonstrates the effectiveness of the donor-acceptor model when an appropriate donor and acceptor are matched. The onset of absorption of **2.5** is at a lower energy because the molecule utilizes the high HOMO of the electron rich EDOT unit and the low lying LUMO of the electron deficient BTD unit.
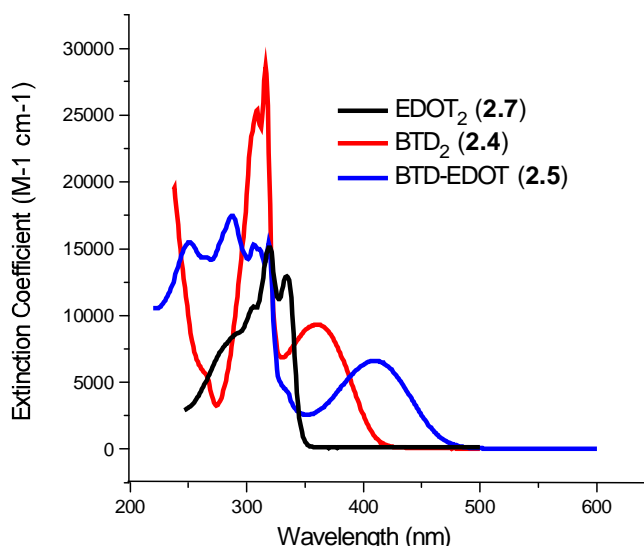
Figure 2.12. The overlay of the absorption of the **2.4**, **2.7**, and **2.5**.

The interaction between the EDOT and BTD monomer units behave as is expected within the D-A framework. If the model was as simple as is currently accepted, this would serve as an appropriate guideline for predicting the impact of coupling based on the categorization as either an acceptor or a donor unit. However, the impact of the TP ambipolar unit will show that there are substantial differences between it and the BTD and EDOT units.

The first of the ambipolar interactions that was investigated was the impact of pairing the ambipolar unit TP with the electron-rich donor unit EDOT. Figure 2.13 shows the absorption spectra of the $EDOT_2$ (**2.7**), TP_2 (**2.9**), and the EDOT-TP (**2.8**) dimers. The most notable aspect of the absorption spectra of the three compounds is the fact that EDOT-TP does not have the highest onset of absorption as would be classically expected of the donor-acceptor dimer. The donor-ambipolar dimer EDOT-TP has an onset of absorption of 530 nm compared to the ambipolar homodimer TP_2 absorbing at 575 nm, both of which are classified as ICT from the bithiophene backbone to the pyrazine ring on the TP. This can be contributed to the EDOT-TP dimer having both units strongly contributing to destabilizing the HOMO and only one unit, the ambipolar TP, contributing to stabilize the LUMO whereas the TP_2 has both units contributing to destabilizing the HOMO and both units contributing to stabilizing the LUMO, resulting in a larger reduction in the HOMO-LUMO gap. Cyclic voltammetry will elucidate more information about the actual energy levels of the HOMO and LUMO of the resulting dimers whereas UV-vis only gives us information about the HOMO-LUMO energy difference.
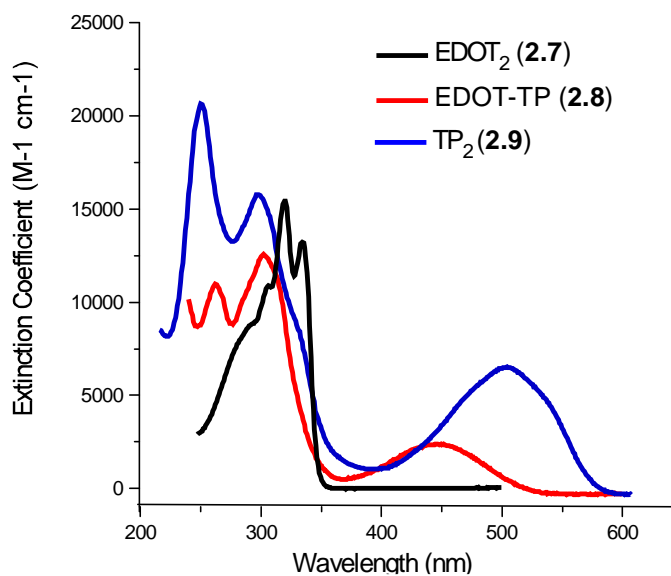
Figure 2.13. The overlay of the absorption of **2.7**, **2.9**, and **2.8**.

Now that the interaction between the ambipolar unit and a donor unit has been investigated it is necessary to analyze the ambipolar and acceptor unit when paired. The paring of the units TP and BTD would be an acceptor-acceptor dimer by the traditional D-A framework and would not be expected to be a viable material due to its expected low lying HOMO characteristic of most acceptors resulting in a large HOMO-LUMO gap. This assumption does not take into account the ambipolar nature of the TP monomer unit. Figure 2.14 shows the absorption spectra of the BTD_2 (**2.4**), BTD-TP (**2.6**), and TP_2 (**2.9**) dimers.
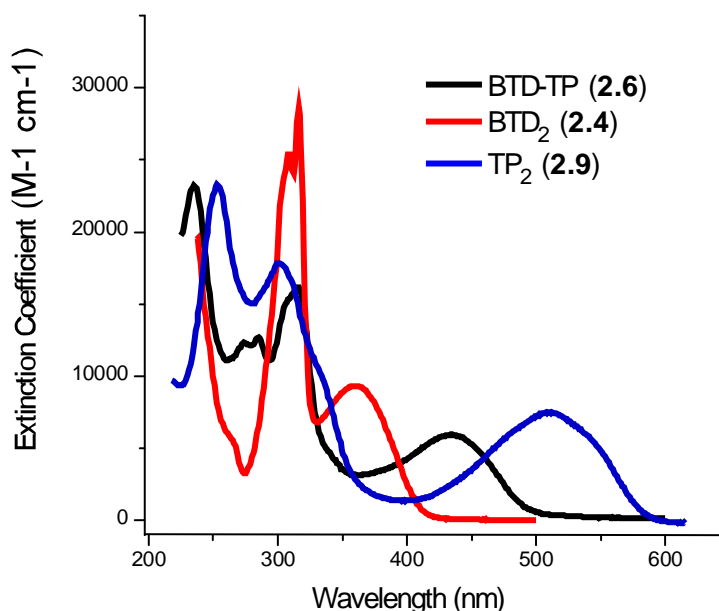
Figure 2.14. The overlay of the absorption of **2.4**, **2.9**, and **2.6**.

The results from the dimers do present some unexpected results from the classical perspective of the D-A framework, but not surprising if the role of the ambipolar unit is included into the system. In the classical D-A framework, all three of these dimers generated would be classified as acceptor-acceptor dimers. However, the ambipolar TP contributes to a destabilized HOMO while both the BTD and TP contribute to stabilize the LUMO. This means that the more ambipolar nature, the smaller the expected HOMO-LUMO gap which is consistent with the results. The larger the ambipolar nature (TP_2>BTD-TP>BTD_2), the higher the onset of

absorption (575 nm, 500 nm, and 420 nm) which relates to a smaller HOMO-LUMO gap. Additionally, the ambipolar-acceptor TP-BTD dimer has a similar onset of absorption (500 nm) as the traditional donor-acceptor EDOT-BTD (480 nm) which indicates that this could be a similarly viable design for conjugated materials.

The compilation of the absorption data of the different dimers gives insight on the role of the ambipolar unit when paired with traditional donor and acceptor units. The onset of absorption is similar when the ambipolar unit is paired with either a donor or an acceptor unit. In this situation, the acceptor-ambipolar dimer, BTD-TP, had an onset of absorption (500 nm) similar to that of the donor-ambipolar dimer, EDOT-TP, onset of absorption (530 nm). This shows that the ambipolar unit does an excellent job of reducing the HOMO-LUMO gap, regardless of it being paired with an electron rich donor unit or an electron deficient acceptor unit. Both the ambipolar-donor and ambipolar-acceptor dimers have a smaller HOMO-LUMO gap than the traditional donor-acceptor dimer (BTD-EDOT) which has an onset of absorption of 480 nm. Despite the great synergy of the ambipolar unit with both donor and acceptor units, the ambipolar homodimer (TP$_2$) has the highest onset of absorption.

Electrochemistry

While the absorption of the dimers does provide a substantial amount of information on the relative energy level differences between the HOMO and the LUMO, it does not give any information on the actual energy levels. Fortunately, cyclic voltammetry (CV) provides a means of estimating the energy levels of the HOMO and the LUMO when analyzed and compared with a standard, which is ferrocene for this study. The actual values of the energy levels are important for organic electronics because of the interactions necessary for charge separation and generation. It is worth noting that if only the oxidation or reduction can be measured by CV, the

onset of absorption can be used to estimate the corresponding undetermined HOMO or LUMO energy levels. The data for **2.4** and **2.7** was collected by Evan Culver and data for **2.9** was collected by Li Wen.[8,32]

The BTD-EDOT dimer (**2.5**) serves as the model example of the donor and acceptor molecule in the D-A framework, with the CV demonstrating how the individual components contribute to the new energy levels of the dimer. Figure 2.15 shows the voltammograms of the BTD$_2$ (**2.4**) and EDOT$_2$ (**2.7**) homodimers, as well as **2.5**. It is worth noting that only the oxidation was measurable for **2.7** within the solvent window.
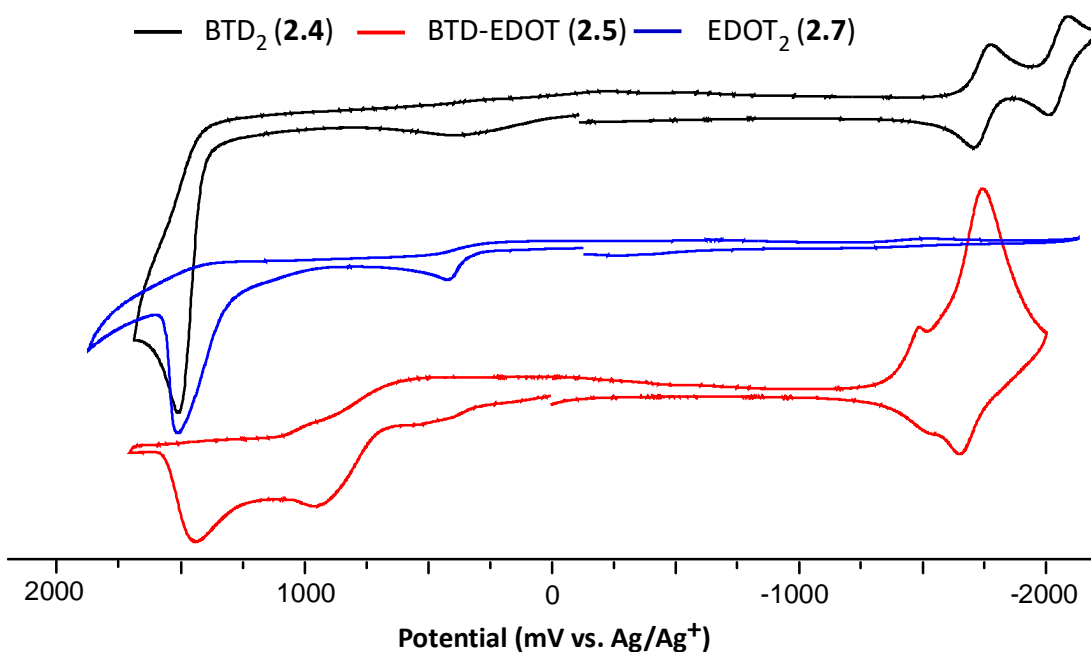
Figure 2.15. Cyclic voltammograms of **2.4**, **2.5**, and **2.7**.

The CV of **2.5** serves as a great example of what would be expected with a donor-acceptor system. The HOMO of the heterodimer has EDOT as the primary contributor, as demonstrated by the similarity between the oxidation of **2.5** and **2.7**. The LUMO of the heterodimer has BTD as the primary contributor, as demonstrated by the similar energy of the reduction of **2.5** and **2.4**. Additionally, this demonstrates that when units behave as expected

52

within the D-A framework, it is a powerful tool for designing molecules. The HOMO-LUMO

gap of **2.5** was 1.95 eV as determined by CV and **2.4** had a HOMO-LUMO gap of 3.05 eV by

CV. The HOMO and LUMO energy levels of the dimers are compiled in Table 2.3.

The EDOT-TP heterodimer (**2.8**) was generated from the ambipolar TP unit (**2.1**) and the

donor EDOT unit (**2.2**). This was the first of the ambipolar heterodimers analyzed by CV. Figure

2.16 shows the cyclic voltammograms of the two homodimers EDOT$_2$ (**2.7**) and TP$_2$ (**2.9**) as well

as the heterodimer. All three of the dimers have similar HOMO levels, as shown by their

oxidations. However, due to the unstable LUMO of EDOT compared to TP, the TP unit will be

the primary contributor to the LUMO, as is shown by the similar reductions of the **2.9** dimer and

2.8 dimer.
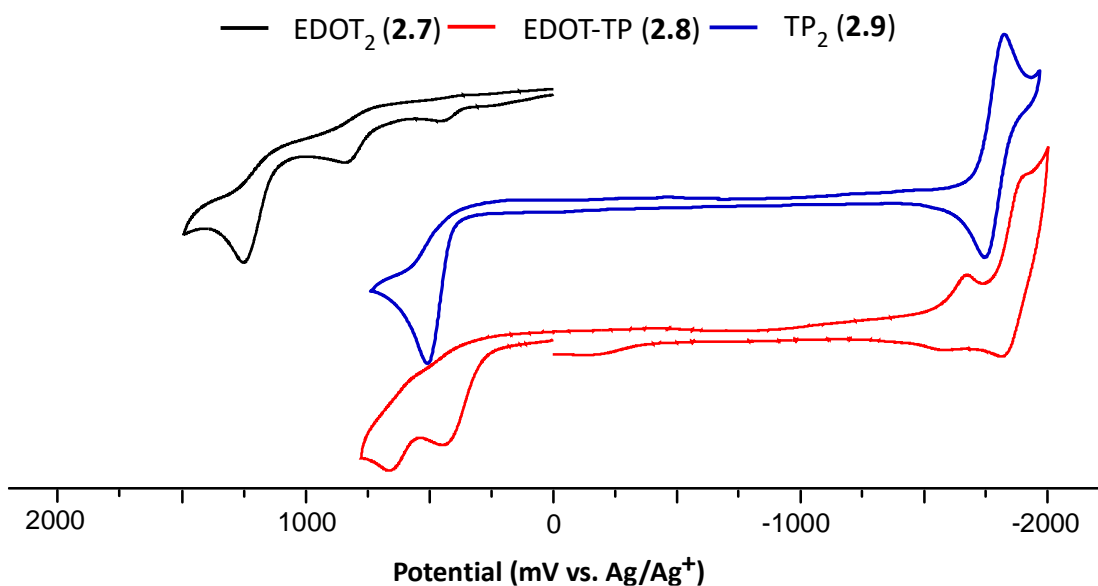
Figure 2.16. Cyclic voltammograms of **2.7**, **2.8**, and **2.9**.

The interaction between the frontier orbitals of the EDOT and the TP units results in a

less stable HOMO for the heterodimer (-5.35 eV) than either of the homodimers (-5.40 eV for

2.7 and -5.45 eV for **2.9**). The heterodimer **2.8** has a smaller HOMO-LUMO gap (2.00 eV) than

2.9 (2.08 eV) and **2.7** (2.70 eV), as would be expected of a classical D-A molecule. However, the

53

D-A framework does not predict the impact that the ambipolar unit has on the HOMO of the resulting molecule. The HOMO of the traditional D-A molecule BTD-EDOT was substantially more stable than the HOMO of the donor-donor dimer **2.7** (-5.80 eV vs. -5.40 eV), whereas the HOMO of the ambipolar-donor dimer was comparable to the homo-dimers that make it up. This is a product of the ambipolar unit substantially contributing to a less stable HOMO when paired with the donor EDOT due to the high lying HOMO of TP while also being the primary contributor to the LUMO of the molecule due to its low lying LUMO. The energy levels for the HOMO and LUMO energy levels for the dimers are compiled in Table 2.3.

The final family of dimers analyzed is the TP and BTD based dimers. Figure 2.17 shows the CVs of the BTD-TP dimer (**2.6**) as well as the BTD_2 (**2.4**) and the TP_2 (**2.9**) homodimers. All three of these dimers would be considered acceptor-acceptor dimers by the classic D-A framework. While the two base units have similar LUMO levels, the difference in the HOMO between TP and BTD has a substantial impact on the resulting dimers.
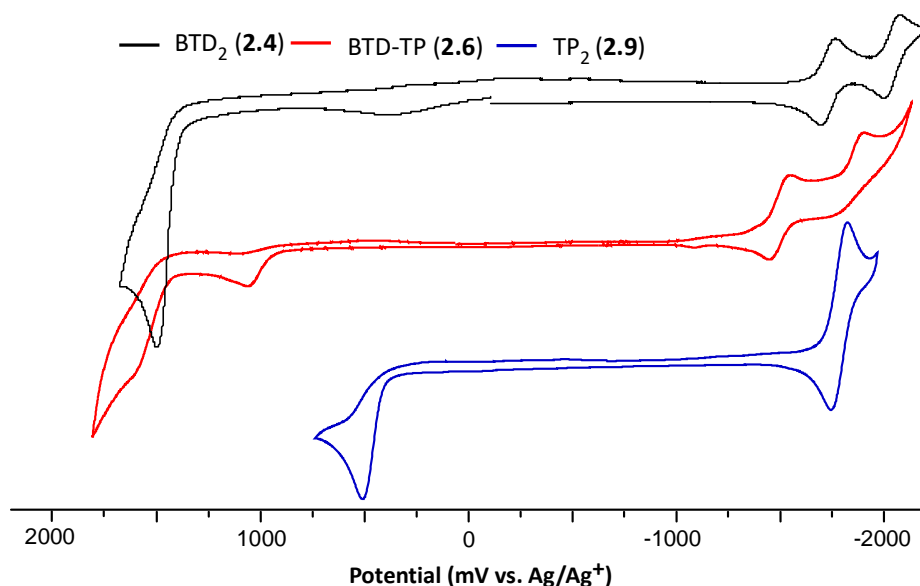
Figure 2.17. Cyclic voltammograms of **2.4**, **2.6**, and **2.9**.

The trend in the HOMO level of the dimers is similar to the trend that was seen with the EDOT and BTD based dimers, the classical donor-acceptor model. The HOMO of the dimers became more destabilized as the more electron rich ambipolar TP content increased. This is an example of the ambipolar unit fulfilling the role of the donor unit and being the primary contributor to the HOMO of the resulting compound due to the high lying HOMO of the TP unit when paired with an acceptor.

One way in which the ambipolar unit behaves differently than the traditional donor unit is in the energy level of the LUMO. All three of these ambipolar- and acceptor-based dimers had similar LUMO energy levels allowing for efficient hybridization of the LUMO orbitals. This results in it not being as clear which unit is the primary contributor LUMO of the resulting heterodimer. It does appear there is an advantage in having two similar, yet distinct low lying LUMO energy levels because the heterodimer had a lower LUMO than either of the homodimers.

The HOMO-LUMO gap for the ambipolar-acceptor **2.6** is close to the HOMO-LUMO gap for the donor-acceptor **2.5**, 2.43 eV and 2.40 eV respectively. This is an indication that polymers based on an ambipolar-acceptor design could have similar electronic properties to the already successful donor-acceptor designed materials. The energy levels for the HOMO and LUMO energy levels for the dimers are compiled in Table 2.3.

Table 2.3. Compilation of CV data for dimers synthesized.

Compound	E_{HOMO} (eV)[a]	E_{LUMO} (eV)[b]	HOMO-LUMO gap (eV)
BTD$_2$ (**2.4**)	-6.49	-3.44	3.05
BTD-EDOT (**2.5**)	-5.80	-3.40	2.40
BTD-TP (**2.6**)	-5.90	-3.47	2.43
EDOT$_2$ (**2.7**)	-5.40	-2.22[c]	3.18[d]
EDOT-TP (**2.8**)	-5.35	-3.35	2.00
TP$_2$ (**2.9**)	-5.45	-3.37	2.08

[a] E_{HOMO}= - ($E_{[onset, ox vs. Fc+/Fc]}$ + 5.1)(eV).[61] [b] E_{LUMO} = - ($E_{[onset, red vs. Fc+/Fc]}$ + 5.1) (eV).[61] [c] Reduction not within solvent window. E_{LUMO} = E_{HOMO} + HOMO-LUMO gap (eV) [d] Optical HOMO-LUMO gap

When compared to the donor and acceptor units, the TP does not behave as only one of those units within the traditional D-A framework. When paired with the donor monomer EDOT, the ambipolar TP contributes to the HOMO along with EDOT and is a substantial contributor to the LUMO of the resulting dimer. However, when paired with the acceptor monomer BTD, the TP is the primary contributor to the HOMO while both units are contributing to the LUMO. This demonstrates the ambipolar nature of the TP unit in its ability to be a strong donor and strong acceptor simultaneously as well as its diversity of being able to be paired with either an electron rich donor or an electron deficient acceptor and synergize to generate a material with a substantially smaller HOMO-LUMO gap. The energy levels of the dimers were graphed to give a clear visual representation of the measured values of the dimers.
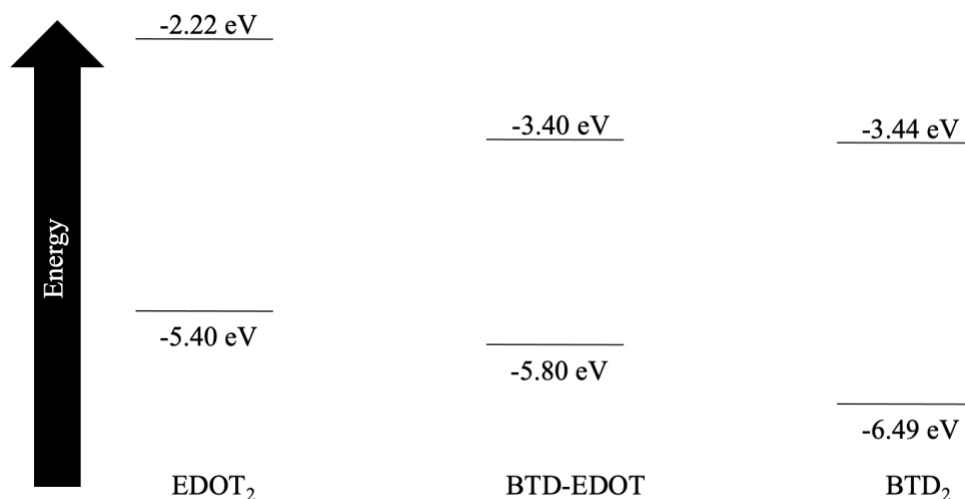
Figure 2.18. Graphical representation of the HOMO and LUMO energy levels (with values) for the EDOT and BTD based dimers.

Figure 2.18 is a representation of the HOMO and LUMO energy levels measure for EDOT$_2$ (**2.7**), BTD-EDOT (**2.5**), and BTD$_2$ (**2.4**). The molecules were arranged to demonstrate how the frontier orbitals interact to result in the reduction in the HOMO-LUMO gap for the donor-acceptor materials. The LUMO of BTD-EDOT (-3.40 eV) is substantially closer to that of the BTD$_2$ (-3.44 eV) than the LUMO of EDOT$_2$ (-2.22 eV) which indicates that the LUMO has more contribution from the BTD than the EDOT unit. As expected, the LUMO of the BTD$_2$ is still lower than that of the BTD-EDOT because of the increased interaction between the LUMO of the two BTD units compared to the mismatch of the LUMOs of the BTD and EDOT units.

The HOMO of BTD-EDOT (-5.80 eV) is closer to the donor dimer EDOT$_2$ (-5.40 eV) than the acceptor dimer BTD$_2$ (-6.49 eV), which indicates that the HOMO of BTD-EDOT has higher contribution from the EDOT unit than the BTD unit. This again demonstrates the effectiveness of designing characteristics of molecules utilizing the donor-acceptor model with the resulting donor-acceptor material having a LUMO more characteristic of the donor material.

One surprising feature of the BTD and EDOT dimer family is how similar in energy levels the LUMOs are between the two acceptor unit dimer (BTD$_2$) and the mixed donor-

57

acceptor dimer (BTD-EDOT). This is likely due to the reduced amount of overlap between the two LUMOs being primarily localized on the thiadiazole rings. With there being a small difference in the LUMO with less acceptor units, it is possible that a 1:1 ratio of donor to acceptor units may not be the optimal ratio in order to minimize the HOMO-LUMO gap. This topic would require the further generation of larger molecules where the ratio of donor to acceptor units is continually controlled. This would eventually lead to polymerization of the molecules to ensure the trend continues on large scale.

Figure 2.19 is representative of the HOMO and LUMO energy levels of EDOT$_2$ (**2.7**), EDOT-TP (**2.8**), and TP$_2$ (**2.9**). The HOMO of all three of the dimers are similar, due to the similarity of the electron richness of the EDOT and TP monomer unit. The LUMO of the donor-ambipolar EDOT-TP (-3.35 eV) has a value that is closer to the ambipolar dimer TP$_2$ (-3.37 eV) than the donor dimer EDOT$_2$ (-2.22 eV), indicating the TP unit of the heterodimer is the primary contributor to the LUMO of the molecule.
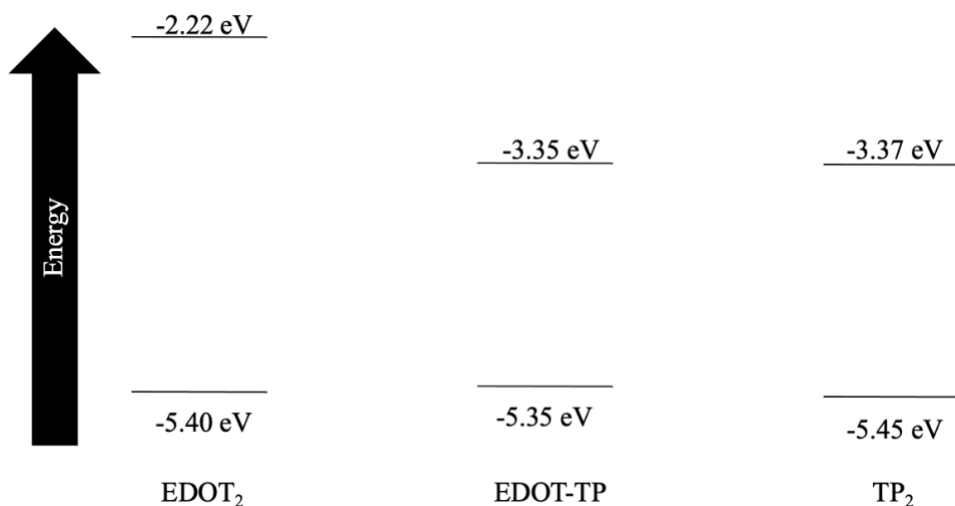
Figure 2.19. Graphical representation of HOMO and LUMO energy levels (with values) for EDOT and TP based dimers.

While the energy levels of the donor-ambipolar EDOT-TP are similar to the classical donor-acceptor EDOT-BTD, the difference in the HOMO energy levels indicate a substantial

difference in the role that TP has compared to BTD. The HOMO of the dimers containing EDOT and TP are all of similar energy levels due to the similarity in the electron richness of EDOT and TP instead of the substantial stabilization of the HOMO caused by the BTD unit when paired with EDOT. TP is the primary contributor to the LUMO of the EDOT-TP dimer and is also contributing with the EDOT to destabilize the HOMO of the dimer, which are behaviors that are not expected of a traditional donor or acceptor unit but has been a defining feature of an ambipolar unit.

One additional trend that was found with the EDOT-TP dimer that occurred with the EDOT-BTD was that there was not a substantial difference in the LUMO of the heterodimer when only one acceptor or ambipolar unit was present compared to two being present in the homodimers, again likely for the same reason of the lack of overlap of the LUMOs on the pyrazine rings. This is even further evidence to deem worthy the investigation of the ratio for the LUMO contributing components of conjugated materials fabricated using the donor-acceptor model.

Figure 2.20 is a representation of the HOMO and LUMO energy levels of BTD$_2$ (**2.4**), TP$_2$ (**2.9**), and BTD-TP (**2.6**). All three of these dimers have very similar LUMO energy levels, having a range of -3.37 eV to -3.47 eV. The HOMO of the acceptor dimer BTD$_2$ has the lowest HOMO (-6.49 eV), while the HOMO increases as there is more ambipolar TP present in the dimer (-5.90 eV for BTD-TP and -5.45 eV for TP$_2$) due to the electron-rich nature of the ambipolar TP unit destabilizing the resulting HOMO, similar to the impact of a donor unit.
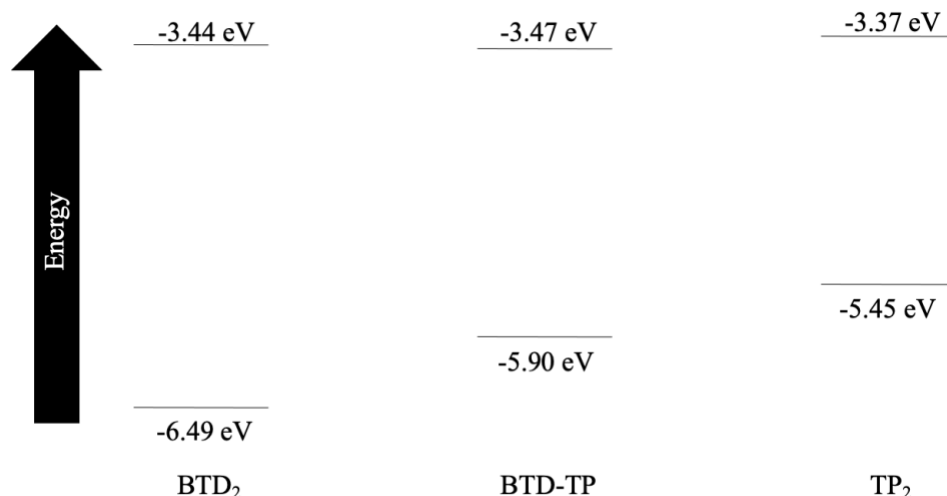
Figure 2.20. Graphical representation of the HOMO and LUMO energies levels (with values) for BTD and TP based dimers.

The HOMO energy levels of the acceptor-ambipolar dimer family consisting of BTD and TP has a similar trend as the donor-acceptor dimer family of BTD and EDOT. As there is an increase in the TP content, the HOMO of the dimer becomes more destabilized. This is an unexpected result from the classical assignment of TP being an acceptor unit and but completely expected with the characteristics of an ambipolar unit. The ambipolar unit, when paired with an acceptor behaves as the primary contributor to the HOMO, as demonstrated by the relationship between the HOMO energy level and the TP content.

The LUMO energy of all three of the dimers are of similar energy. With both TP_2 and BTD_2 having similar LUMO energy levels, it is not as clear whether TP or BTD is the primary contributor to the LUMO of BTD-TP. However, the comparison of the LUMOs of BTD-EDOT and EDOT-TP give insight on the strength of TP and BTD as acceptors. The LUMO for the resulting dimers will have very little contribution from the EDOT due to the mismatch in energy level, so the LUMO can be attributed to the TP or BTD. The LUMO of BTD-EDOT was -3.40 eV while the LUMO of EDOT-TP was -3.35 eV, indicating that BTD is a stronger acceptor than TP and is also likely the primary contributor to the LUMO of BTD-TP. Additionally, the BTD-

TP dimer has a lower LUMO than either of the homo-dimers, which may indicate that the breaking of symmetry of the molecule results in a more stable LUMO. Even with the dimers consisting of monomer units with lower lying LUMOs, the dimers containing EDOT and either BTD or TP all have similar LUMO energy levels. This lack of difference between the dimers containing two units with low lying LUMOs and dimers containing only one unit with a low lying LUMO unit further demonstrates the diminishing return of multiple or excessive units to tune the LUMO of the resulting molecule.

Computational Study

DFT calculations utilizing the B3LYP/6-31G* basis were performed by a M. Carmen Ruiz Delgado (University of Málaga) for the series of dimers for comparison.[32] Figure 2.21 shows the HOMO and LUMO levels for the dimers as determined by DFT calculations. The trend in the HOMO-LUMO energy levels is consistent with the energy levels observed by CV in Table 2.3.
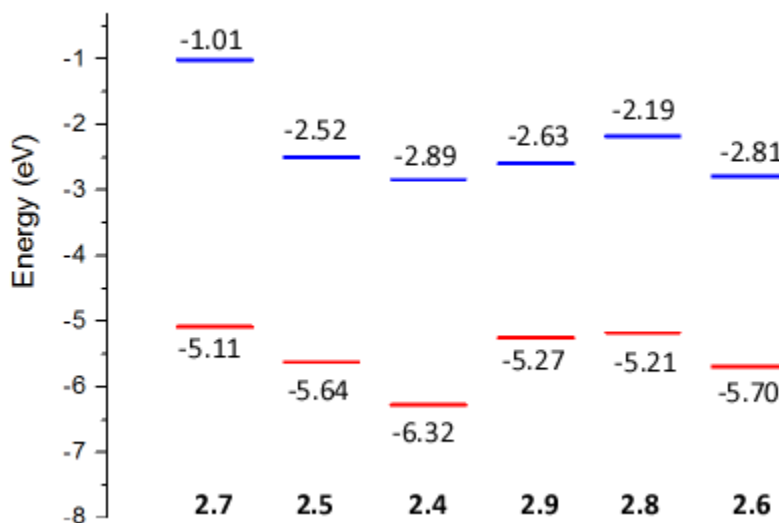
Figure 2.21. Calculated HOMO and LUMO levels for the dimer family.

The comparison of the computational energy levels of a couple of the dimers further demonstrate the oddity that the ambipolar unit is within the D-A framework. The traditional donor-acceptor EDOT-BTD (**2.5**) has a similar HOMO-LUMO gap (3.12 eV) as the dimer consisting of TP paired with EDOT (**2.8**, 3.02 eV) or when TP is paired with BTD (**2.6**, 2.89 eV). This demonstrates TP's ability to reduce the HOMO-LUMO gap whether paired with a donor or an acceptor unit and it does not make sense for it to be classified as one of those two units when it fulfills the role of both of the units.

Conclusion

The work presented describes the synthesis and characterization of a family of dimers based on their roles in the donor-acceptor framework. The traditional donor-acceptor dimer EDOT-BTD was generated as well as the donor-ambipolar EDOT-TP and the ambipolar-acceptor TP-BTD. Homo-dimers of EDOT, BTD, and TP were also compared.[8,32] With the family of dimers synthesized, it was possible to investigate the role of the ambipolar unit within the donor-acceptor framework as well as investigate some claims about molecules within the donor-acceptor framework.

One explanation for the reduced HOMO-LUMO gaps for donor-acceptor molecules is an increase in contribution of the resonance form between the electron rich donor and the electron deficient acceptor that results in a double bond between the two units. This resonance form results in the reduction of bond length alternation, which has been found to decrease to the HOMO-LUMO gap of molecules. However, the crystal structure of EDOT-BTD, a strong donor and a strong acceptor, showed no sign of bond length reduction between the two rings. This indicates that there is not a substantial presence of a resonance form that results in a double bond

between the two units and is not an appropriate explanation for the reduction in the HOMO-LUMO gap for donor-acceptor molecules.

The UV-vis absorption and cyclic voltammetry data provides the basis for the impact that ambipolar units have within the donor-acceptor framework. All of the dimers except for EDOT$_2$ had a low energy intramolecular charge transfer where the electron density becomes localized on either the acceptor or the ambipolar unit. The donor-ambipolar and ambipolar-acceptor dimers both had a similar HOMO-LUMO gap as the donor-acceptor molecule. The CV data indicates that the ambipolar unit is substantially contributing to both the HOMO and the LUMO of the molecules whether it is paired with the donor or acceptor unit. Additionally, these results provide the foundation to explore an ambipolar-acceptor polymer that has the potential to be a low or reduced band gap polymer.

One additional finding that challenges some claims within the donor-acceptor framework is the impact of the ratio of the acceptor unit. There was a small difference between there being only a single unit with a low-lying LUMO, indicating that a 1:1 ratio may not be necessary to minimize the LUMO and a smaller HOMO-LUMO gap could be obtained by having less low-lying LUMO (acceptor or ambipolar) units. Varying the ratio of the donor and acceptor units has been used to shift the onset of absorption to lower energies by reducing the amount of acceptor, but not to minimize the HOMO-LUMO gap.[62] The study showed that decreasing the amount of acceptor did result in a blue shift in the onset of absorption, but the only ratios studied were 2:1, 4:1, and 6:1 of the donor to acceptor material. This was also investigated using two different donors and the same acceptor. Additionally, the ambipolar TP could also have an impact on the ideal ratio of donor or acceptor to ambipolar unit. This topic could be investigated by generating

larger oligomers (4 to 5 units long) with varying amounts of acceptor units to determine how this trend continues to that larger scale.

Experimental Methods

General

Unless stated, all materials were reagent grade and used without further purification. All chromatographic separations were performed with standard chromatography methods with silica gel as the stationary phase (230-400 mesh). Dry THF and toluene were obtained via distillation over sodium and benzophenone. DMF was dried with magnesium sulfate, then passed through silica gel, and then had nitrogen gas bubbled through it for three hours. All glassware was oven-dried, assembled as soon as it could be handled, and cooled under dry nitrogen before use. Transfer of liquids was carried out using standard syringe techniques and all reactions were done in an inert, dry nitrogen atmosphere with a constant stream of nitrogen. Melting points were determined using a digital thermometer couple with a 0.1 °C resolution. The ^{1}H and ^{13}C NMR were completed on a 400 MHz spectrometer. All NMR data was referenced to the chloroform signal and peak multiplicity was reported as follows: s = singlet, d = doublet, t = triplet, q = quartet, p = pentet, dd = doublet of doublets, m = multiplet, and br = broad. HRMS was performed in house.

Materials

2,5-Dibromo-3,4-dinitrothiophene,[63] benzo[c][1,2,5]thiadiazole,[64] 2,3-dihexylthieno[3,4-b]pyrazine,[65] and 7,7' bis(trimethylsilyl)-5,5'-bis(2,3-dihexylthieno[3,4-b]pyrazine),[8] 2,2'-bis(3,4-ethylenedioxthiophene),[32] and 4,4'-bis(benzo[c][1,2,5]thiadiazole[32] were prepared as previously described. 3,4-Ethylenedioxythiophene was dissolved in THF and then dried with magnesium sulfate. This was followed by the solvent being removed by reduced pressure and the

EDOT stored in an inert atmosphere after it was dried. Acetonitrile was dried over CaH_2 prior to use.

4-Bromobenzo[c][1,2,5]thiadiazole (2.10)

Benzo[c][1,2,5]thiadiazole (1.98 g, 14.5 mmol) and 47% HBr (145 mL) were added to a round bottom flask with a condenser attached. Br_2 (0.75 mL, 14.5 mmol) was added to the round bottom flask and it was then heated to reflux for one hour. After one hour, water was added to the reaction mixture to quickly cool it. The mixture of benzo[c][1,2,5]thiadiazole, 4-bromobenzo[c][1,2,5]thiadiazole, and 4,7-dibromobenzo[c][1,2,5]thiadiazole was then extracted with $CHCl_3$ and the solvent was removed by reduced pressure. The mixture was then purified by steam distillation, with the distillate consisting of benzo[c][1,2,5]thiadiazole and 4-bromobenzo[c][1,2,5]thiadiazole. This was then purified by recrystallization in MeOH, allowing for the isolation of the 4-bromobenzo[c][1,2,5]thiadiazole as a fluffy, white solid. 40.% yield. mp 65.9-66.9 °C. ^{1}H NMR: δ 7.98 (dd, 1H, $J = 8.8$, 0.9 Hz), 7.85 (dd, 1H, $J = 7.2$, 0.9 Hz), 7.48 (dd, 1H, $J = 8.8$, 7.2 Hz) ; ^{13}C NMR: δ 154.9, 153.7, 132.3, 130.3, 121.2, 114.8.

4-(3,4-Ethylenedioxythiophen-2-yl)benzo[c][1,2,5]thiadiazole (2.5)

3,4-Ethylenedioxythiophene (0.21 mL, 2.0 mmol) was dissolved in dry THF (80 mL) and cooled to -78 °C with acetone-dry ice bath. BuLi (0.88 mL of 2.5 M in hexanes, 2.2 mmol) was added and the mixture was stirred for 30 minutes. Me_3SnCl (2.2 mL of 1.0 M in THF, 2.2 mmol) was added and stirred for 30 minutes. After the 30 minutes, the mixture was removed from the acetone bath and allowed to warm to room temperature and stirring continued for 2 hours. The reaction was concentrated by solvent removal under reduced pressure. This was then directly used without characterization or purification. 4-Bromobenzo[c][1,2,5]thiadiazole (0.43 g, 2.0 mmol), tris(dibenzylideneacetone)dipalladium(0) ($Pd_2(dba)_3$) (0.037 g, 2%), and tri(o-

tolyl)phosphine (P(*o*-tol)₃) (0.049 g, 8%) were added and a nitrogen atmosphere was obtained.

Toluene (60 mL) was then added and the solution was heated to 98 °C for 20 hours. The solution

was then quenched with distilled water and extracted with chloroform. A red powder was

collected after the product was purified with silica gel column chromatography with ethyl acetate

and hexane as the eluent (v/v=5/95: yield: 90.%). mp 78.1-78.8 °C ^{1}H NMR: δ 8.33 (dd, 1H, $J =$

7.1, 1.0 Hz), 7.85 (dd, 1H, $J =$ 8.8, 1.0 Hz), 7.63 (dd, 1H, $J =$ 7.1, 8.8 Hz), 6.59 (s, 1H), 4.40 (m,

2H), 4.31 (m, 2H) ^{13}C: δ 155.63, 154.99, 152.51, 142.00, 140.74, 130.27, 126.42, 119.33,

113.63, 102.64, 65.39, 64.70; HRMS m/z 298.9933 [M+Na]$^+$ (calcd for $C_{12}H_8N_2O_2S_2Na$

298.9925).

5-(3,4-Ethylenedioxythiophen-2-yl)-2,3-dihexylthieno[3,4-b]pyrazine (2.8)

2,3-Dihexylthieno[3,4-*b*]pyrazine (0.61 g, 2.0 mmol) was dissolved in dry THF (60 mL)

and cooled to -78 °C with acetone-dry ice bath. BuLi (0.88 mL of 2.5 M in hexanes, 2.2 mmol)

was added and the mixture was stirred for 30 minutes. Me₃SnCl (2.2 mL of 1.0 M in THF, 2.2

mmol) was added and stirred for 30 minutes. After the 30 minutes, the mixture was removed

from the acetone bath and allowed to warm to room temperature and stirring continued for 2

hours. The solution was concentrated by reduced pressure.

3,4-Ethylenedioxythiophene (0.21 mL, 2.0 mmol) was added to 20 mL of DMF in an

inert atmosphere. The solution was cooled to 0 °C by an ice bath. NBS (0.39 g, 2.2 mmol) was

dissolved in 20 mL of DMF and transferred to an addition funnel. The NBS solution was added

over 10 minutes to the EDOT solution and then stirred for 20 minutes after the addition was

complete. The solution was then removed from the ice bath and was allowed to stir for 2 hours.

The solution was washed with distilled water and extracted with ethyl acetate. The organic phase

was thoroughly washed with water to remove residual DMF. The solvent was removed by reduced pressure.

The stannyl-TP, EDOT-Br, Pd(dppe)Cl$_2$ (0.12 g, 10%), and CuI (0.038 g, 10%) were added to a round bottom flask and a nitrogen atmosphere was obtained. Toluene (60 mL) was added to the flask and the solution was heated at 98 °C for 20 hours. The solution was then quenched with distilled water and extracted with chloroform and dried with magnesium sulfate. The final product was an orange powder which was purified with silica gel column chromatography with ethyl acetate and hexane as the eluent (v/v= 5/95: yield: 55%). mp 81.7-82.4 °C ^{1}H NMR: δ 7.60 (s, 1H), 6.43 (s, 1H), 4.45 (m, 2H), 4.30 (m, 2H), 2.95 (m, 4H), 2.00 (p, 2H, J = 7.4 Hz), 1.80 (p, 2H, J = 7.7 Hz), 1.56-1.33 (m, 12H), 0.92 (m, 6H) ^{13}C NMR: δ 159.98, 154.79, 147.01, 141.54, 138.58, 133.50, 116.19, 111.71, 100.97, 65.69, 65.06, 35.95, 35.34, 32.29, 32.04, 30.08, 30.00, 28.58, 27.29, 23.05, 22.95, 14.52, 14.42; HRMS m/z 445.1968 [M]$^+$ (calcd C$_{24}$H$_{32}$N$_2$S$_2$O$_2$ 445.1983).

4-(2,3-Dihexylthieno[3,4-b]pyrazin-5-yl)-benzo[c][1,2,5]thiadiazole (2.6)

2,3-Dihexylthieno[3,4-*b*]pyrazine (0.61 g, 2.0 mmol) was dissolved in dry THF (60 mL) and cooled to -78 °C with acetone-dry ice bath. BuLi (0.88 mL of 2.5 M in hexanes, 2.2 mmol) was added and the mixture was stirred for 30 minutes. Me$_3$SnCl (2.2 mL of 1.0 M in THF, 2.2 mmol) was added and stirred for 30 minutes. After the 30 minutes, the mixture was removed from the acetone bath and allowed to warm to room temperature and stirring continued for 2 hours. The solution was concentrated by reduced pressure.

4-Bromobenzo[*c*][1,2,5]thiadiazole (0.43 g, 2.0 mmol), Pd$_2$(dba)$_3$ (0.037 g, 2%), and P(*o*-tol)$_3$ (0.049 g, 8%) were added and a nitrogen atmosphere was obtained. Toluene (60 mL) was added and the solution was heated to 98 °C for 20 hours. The solution was then quenched with

distilled water and extracted with chloroform. The final product was an orange powder was purified with silica gel column chromatography with ethyl acetate and hexane as the eluent (v/v= 5/95: yield: 85%). Mp. 102.9-103.5 °C. ^{1}H NMR: δ 9.37 (dd, 1H, J = 7.2, 0.9 Hz), 7.99 (s, 1H), 7.94 (dd, 1H, J = 8.7, 0.9 Hz), 7.76 (dd, 1H, J = 8.7, 7.2 Hz), 3.02 (t, 2H, J = 7.5 Hz), 3.00 (t, 2H, J = 7.8 Hz), 1.96 (m, 2H), 1.83 (m, 2H), 1.58-1.33 (broad m, 12H), 0.94 (m, 6H) ^{13}C NMR: δ 156.7, 156.2, 155.6, 152.7, 142.8, 140.1, 130.5, 128.5, 127.3, 127.1, 119.9, 118.1, 35.9, 35.6, 32.2, 32.0, 29.7, 29.5, 28.5, 27.8, 23.0, 22.9, 14.5, 14.4 HRMS *m/z* 439.1981 [M]$^+$ (calcd $C_{24}H_{30}N_4S_2$ 439.1990).

Electrochemistry

All electrochemical techniques were performed on a Bioanyltical Systems BAS 100B/W electrochemical analyzer. Cyclic voltammetry (CV) experiments were performed using a three-electrode cell consisting of a Pt-disc working electrode, Pt coil wire auxiliary electrode, and an Ag/Ag$^+$ reference electrode. A 0.1 M electrolyte solution was prepared with tetrabutylammonium hexafluorophosphate (TBAPF$_6$) using MeCN distilled over CaH$_2$ under dry nitrogen. The solutions were deoxygenated with argon for at least 20 min prior to each scan and blanketed with argon during the experiments. CV experiments were performed in the described cell at a sweep rate of 100 mV/s. E_{HOMO} and E_{LUMO} values were determined in a reference to ferrocene (5.1 V vs. vacuum).

UV-Vis Absorption Spectroscopy

All absorption spectroscopy was performed on a Carry 500 dual-beam UV-vis-NIR spectrophotometer. Solution-state spectra were analyzed in CHCl$_3$ using matched 1 cm quartz cuvettes. The HOMO-LUMO gaps were determined by generating a Tauc plot from the data and determining the gap based on the intercept of the most linear portion of the plot.

References

1. Yu, G.; Gao, J.; Hummelen, J. C.; Wudl, F.; Heeger, A. J. *Science* **1995,** *270,* 1789.

2. Friend, R. H.; Gymer, R. W.; Holmes, A. B.; Burroughes, J. H.; Marks, R. N.; Taliani, C.; Bradley, D. D. C.; Santos, D. A. D.; Brédas, J. L.; Logdlund, M.; Salaneck, W. R. *Nature* **1999,** *397*, 121.

3. Zhou, Y.; Fuentes-Hernandez, C.; Shim, J.; Meyer, J.; Giordano, M.; Dindar, A.; Haske, W.; Najafabadi, E.; Khan, T. M.; Sojoudi, H.; Barlow, S.; Graham, S.; Brédas, J.-L.; Marder, S. R.; Kahn, A.; Kippelen, B. *Science* **2012,** *336*, 327.

4. Havinga, E. E.; ten Hoeve, W.; Wynberg, H. *Polym. Bull. (Berlin)* **1992,** *29,* 119.

5. Lewis, F. D.; Burch, E. L. *J. Phys. Chem.* **1996,** *100,* 4055.

6. Mulholland, M. E.; Konkol, K. L.; Anderson, T. E.; Schwiderski, R. L.; Rasmussen, S. C. *Aust. J. Chem.* **2015**, *68*, 1759.

7. Pandey, L.; Risko, C.; Norton, J. E.; Brédas, J.-L. *Macromolecules* **2012,** *45*, 6405.

8. Wen, L.; Heth, C. L.; Rasmussen, S. C. *Phys. Chem. Chem. Phys.,* **2014,** *16*, 7231.

9. Velusamy, M.; Thomas, K. R. J.; Lin, J. T.; Hsu, Y.-C.; Ho, K.-C. *Org. Lett.* **2005,** *7,* 1899.

10. Jungsuttiwong, S.; Yakhanthip, T.; Surakhot, Y.; Khunchalee, J.; Sudyoadsuk, T.; Promarak, V.; Kungwan, N.; Namuangruk, S. *J. Comput. Chem.* **2012,** *33,* 1517.

11. Wu, C. G.; Chung, M. F.; Tsai, H.-H. G.; Tan, C. J.; Chen, S. C.; Chang, C. H.; Shih, T. W. *ChemPlusChem,* **2012,** *77,* 832.

12. Havinga, E. E.; ten Hoeve, W.; Wynberg, H. *Synth. Met.,* **1993,** *55,* 299.

13. Roncali, J. *Chem. Rev.* **1997,** *97*, 173.

14. Pomerantz, M.; Chaloner-Gill, B.; Harding, L. O.; Tseng, J. J.; Pomerantz, W. J. J. *Chem. Soc. Chem. Commun.* **1992,** 1672.

15. Kastner, J.; Kuzmany, H.; Vegh, D.; Landl, M.; Cuff, L.; Kertesz, M. *Synth. Met.* **1995,** *69,* 593.

16. Hagan, A. J.; Moratti, S. C.; Sage, I. C. *Synth. Met.* **2001,** *119,* 147.

17. Petersen, M. H.; Hagemann, O.; Nielsen, K. T.; Jørgensen, M.; Krebs, F. C. *Sol. Energy Mater. Sol. Cells* **2007,** *91,* 996.

18. Sonmez, G.; Sonmez, H. B.; Shen, C. K. F.; Jost, R. W.; Rubin, T.; Wudl, F. *Macromolecules* **2005,** *38*, 669.

19. Zhang, F.; Perzon, E.; Wang, X.; Mammo, W.; Andersson, M. R.; Inganäs, O. *Adv. Funct. Mater.* **2005,** *15,* 745.

20. Akoudad, S.; Roncali, J. *Chem. Commun.* **1998,** 2081.

21. Sonmez, G.; Sonmez, H. B.; Shen, C. K. F.; Wudl, F. *Adv. Mater.* **2004,** *16*, 1905.

22. Perepichka, I. F.; Levillain, E.; Roncali, J. *J. Mater. Chem.* **2004,** *14,* 1679.

23. Wen, L.; Duck, B. C.; Dastoor, P. C.; Rasmussen, S. C. *Macromolecules* **2008,** *41*, 4576.

24. Mammo, W.; Admassie, S.; Gadisa, A.; Zhang, F.; Inganas, O.; Anderrson, M. R. *Sol. Energy Mater. Sol. Cells* **2007,** *91,* 1010.

25. Wen, L.; Nietfeld, J. P.; Amb, C. M.; Rasmussen, S. C. *J. Org. Chem.* **2008,** *73,* 8529.

26. Gigli, G.; Anni, M.; Theander, M.; Cingolani, R.; Barbarella, G.; Favaretto, L.; Inganäs, Ol. *Synth. Met.* **2001,** *119,* 581.

27. Mulholland, M. E.; Konkol, K. L.; Anderson, T. E.; Schwiderski, R. L.; Rasmussen, S. C. *Aust. J. Chem.* **2015,** *68,* 1759.

28. Konkol, K. L.; Schwiderski, R. L.; Rasmussen, S. C. *Materials* **2016,** *9,* 404.

29. Kenning, D. D.; Funfar, M. R.; Rasmussen, S. C. *Polymer Preprints* **2001,** *42,* 506.

30. Kenning, D. D.; Mitchell, K. A.; Calhoun, T. R.; Funfar, M. R.; Sattler, D. J.; Rasmussen, S. C. *J. Org. Chem.* **2002,** *67,* 9073.

31. Mulholland, M. *PhD Dissertation,* North Dakota State University, Fargo, ND, 2013.

32. Anderson, T. E.; Culver, E. W.; Badía-Domínguez, Irene; Delgado, M. C. R.; Buysse, C. E; Rasmussen, S. C. *Phys. Chem. Chem. Phys.* Manuscript in Preparation.

33. Pilgram, K.; Zupan, M.; Skiles, R. *J. Heterocycl. Chem.* **1970,** *7,* 629.

34. Farina, V.; Kapadia, S.; Krishnan, B.; Wang, C.; Liebeskind, L. S. *J. Org. Chem.* **1994,** *59,* 5905.

35. Tanaka, S.; Yamashita, Y. *Synth. Met.* **1995,** *69,* 599.

36. Luzzati, V. *Acta Crystallogr.* **1951**, *4*, 193.

37. Bundgaard, E.; Krebs, F. *Solar Energy Materials and Solar Cells* **2007**, *91*, 954.

38. Chen, M.; Perzon, E.; Andersson, M. R.; Marcinkevicius, S.; Jönsson, S. K. M.; Fahlman, M.; Berggren, M. *Appl. Phys. Lett.*, **2004,** *84*, 3570.

39. Kitamura, C.; Tanaka, S.; Yamashita, Y. *J. Chem. Soc. Chem. Commun.* **1994,** 1585.

40.   Ajayaghosh, A. *Chem. Soc. Rev.* *2003, 32,* 181.

41.   Chochos, C. L.; Choulis, S. A. *Progress in Polymer Science* **2011**, *36*, 1326.

42.   Havinga, E. E.; ten Hoeve, W.; Wynberg, H. *Polym. Bull.* **1992,** *29*, 119.

43.   Brocks, G.; Tol, A. *J. Phys. Chem.* **1996,** *100*, 1838.

44.   van Mullekmo, H. *Materials Science and Engineering: R: Reports* **2001**, *32*, 1.

45.   *CRC Handbook of Chemistry and Physics;* Lide, D. R., Frederikse, H. P. R., Eds.; CRC Press: Boca Raton, FL, 1995; p. 9-4.

46.   Pouzet, P.; Erdelmeier, I.; Ginderow, D.; Momon, J.-P.; Dansette, P. M.; Mansuy, D. *J. Heterocyclic Chem.* **1997**, *34*, 1567.

47.   Sarma, J. A. R. P.; Desiraju, G. R. *Acc. Chem. Res.* **1986**, *19*, 222.

48.   Desiraju, G. R. *Acc. Chem. Res.* **1991**, *24*, 290.

49.   *Handbook of Chemistry and Physics*, 68th ed.; Weast, R. C., Ed.; CRC Press, Inc., Boca Raton, **1987**, p. D-188.

50.   Getmanenko, Y. A.; Singh, S.; Sandhu, B; Wang, C.-Y.; Timofeeva, T.; Kippelen, B.; Marder, S. R. *J. Mater. Chem C* **2014**, *2*, 124.

51.   Uzelac, E. J.; McCausland, C. B.; Rasmussen, S. C.; *J. Org. Chem.* **2018**, *83*, 664.

52.   Turbiez, M.; Frère, P.; Allain, M.; Videlot, C.; Ackermann, J.; Roncali, J. *Chem. Eur. J.* **2005,** *11,* 3742.

53.   Apperloo, J. J.; Groenendaal, L.; Verheyen, H.; Jayakannan, M.; Janssen, R. A. J.; Dkhissi, A.; Beljonne, D.; Lazzaroni, R.; Brèdas, J. L. *Chem. Eur. J.* **2002,** *8,* 2384.

54.   Turbiez, M.; Frère, P.; Roncali, J. *J. Org. Chem.* **2003,** *68*, 5357.

55.   Belletête, M.; Beaupré, S.; Bouchard, J.; Blondin, P.; Leclerc, M.; Durocher, G. *J. Phys. Chem. B* **2000,** *104,* 9118.

56.   Castillo, A. M.; Patiny, L.; Wist, J. *J. Mag. Res.* **2011**, *209*, 123.

57.   Modarresi-Alam, A. R.; Dabbagh, H. A. *Turk J Chem* **2009,** *33,* 607.

58.   Kumar, A.; Welsh, D. M.; Morvant, M. C.; Piroux, F.; Abboud, K. A.; Reynolds, J. R. *Chem. Mater.* **1998,** *10,* 896.

59.   Schwendeman, I.; Gaupp, C. L.; Hancock, J. M.; Groenendaal, L. B.; Reynolds, J. R. *Adv. Funct. Mater.* **2013,** *13,* 541.

60.   Konkol, K. L.; Schwiderski, R. L.; Rasmussen, S. C. *Materials* **2016**, *9*, 404.

61.   Cardona, C. M.; Li, W.; Kaifer, A. E.; David, S. D.; Bazan, G. C. *Adv. Mater.* **2011,** *23,* 2367.

62.   Beaujuge, P. M.; Ellinger, S.; Reynolds, J. R. *Nat. Mater.* **2008**, *7*, 795.

63.   Wen, L.; Rasmussen, S. C. *J. Chem. Crystallogr.* **2007,** *37,* 387.

64.   Tao, Y. M.; Li, H. Y.; Xu, Q. L.; Zhu, Y. C.; Kang, L. C.; Zheng, Y. X.; Zuo, J. L.; You, X. Z. *Synth. Met.* **2011,** *161,* 718.

65.   Kenning, D. D.; Mitchell, K. A.; Calhoun, T. R.; Funfar, M. R.; Sattler, D. J.; Rasmussen, S. C. *J. Org. Chem,* **2002,** *67,* 9073.

CHAPTER 3. A NEW DESIGN PARADIGM FOR LOW BAND GAP CONJUGATED

POLYMERS[†]

Introduction

The donor-acceptor (D-A) model has proven to be an incredibly effective model for generating low band gap (E_g) materials.[1-3] It requires an electron-rich unit (the donor) and an electron-deficient unit (the acceptor) that are coupled together in an alternating sequence to generate a polymer with a HOMO-LUMO gap smaller than either of the units would be able to generate as a homopolymer, which results in a smaller E_g in the solid state. While the D-A model has been used to generate polymers with desirable electronic characteristics, it is an oversimplified model for the explanation of the optoelectronic properties and needs improvement in order to serve as a better model for the synthesis of organic electronic materials. There have been little changes to the model since its initial conception in 1993.[4] Monomer units are simply assigned the classification of being either a donor or acceptor species and the resulting optoelectronic characteristics are attributed to the D-A model and little additional analysis is presented. However, some recent work has findings that are not consistent with the current D-A model.

As was previously discussed, thieno[3,4-*b*]pyrazine (TP) based molecules simultaneously behave as both an acceptor and a donor, meaning it behaves as both the traditional donor and acceptor units in the D-A model.[5-9] While it is commonly viewed as an acceptor unit, it has the

---

uncommon characteristic of generating a homopolymer with a smaller E_g than when paired with a donor unit as would be predicted by the D-A model. It is because of this reason it was deemed necessary to specify a new monomer class to properly describe the TP unit. As such, it has been proposed to call this new monomer class as *ambipolar units*: a unit that has characteristics of both a donor and an acceptor simultaneously.

In order to synthesize conjugated co-polymers it is necessary to use directable carbon-carbon coupling methods, such as Migita—Stille, Kumada, Heck, Miyaura—Suzuki, or Negishi coupling.[10-13] While these methods are effective at generating polymers, they require additional synthetic steps to prepare the monomers for the coupling and also results in the production of metal-based byproducts, some of which are toxic (i.e. organotin compounds). An alternative method of synthesizing these copolymers that requires fewer synthetic steps and generates less byproducts would be a substantial step toward the commercialization of these organic electronic materials.[14] Direct arylation polymerization (DArP) appears to be a potential new method of polymer synthesis that has these advantages.[15-18]

DArP results in the cross coupling between two aromatic molecules. The new C-C bond is formed as a result of the condensation between an aryl C-H bond and an aryl halide, commonly C-Br or C-I. One of the benefits of this polymerization method is the generation of only halo acids as byproducts. The currently proposed mechanism of DArP (Scheme 3.1) consists of the oxidative addition (1) of the aryl halide substrate to a palladium(0) catalyst, similar to other more common cross-coupling methods. The unfunctionalized aromatic molecule undergoes a palladium catalyzed C-H bond activation, typically via a concerted metalation-deprotonation pathway (2).[19,20] This intramolecular proton transfer is assisted by the presence of a coordinated base.[21] Most of the arenes seem to follow a concerted metalation-deprotonation

process.[22,23] The new C-C bond is then formed upon the reductive elimination of the two aryl

ligands (3).
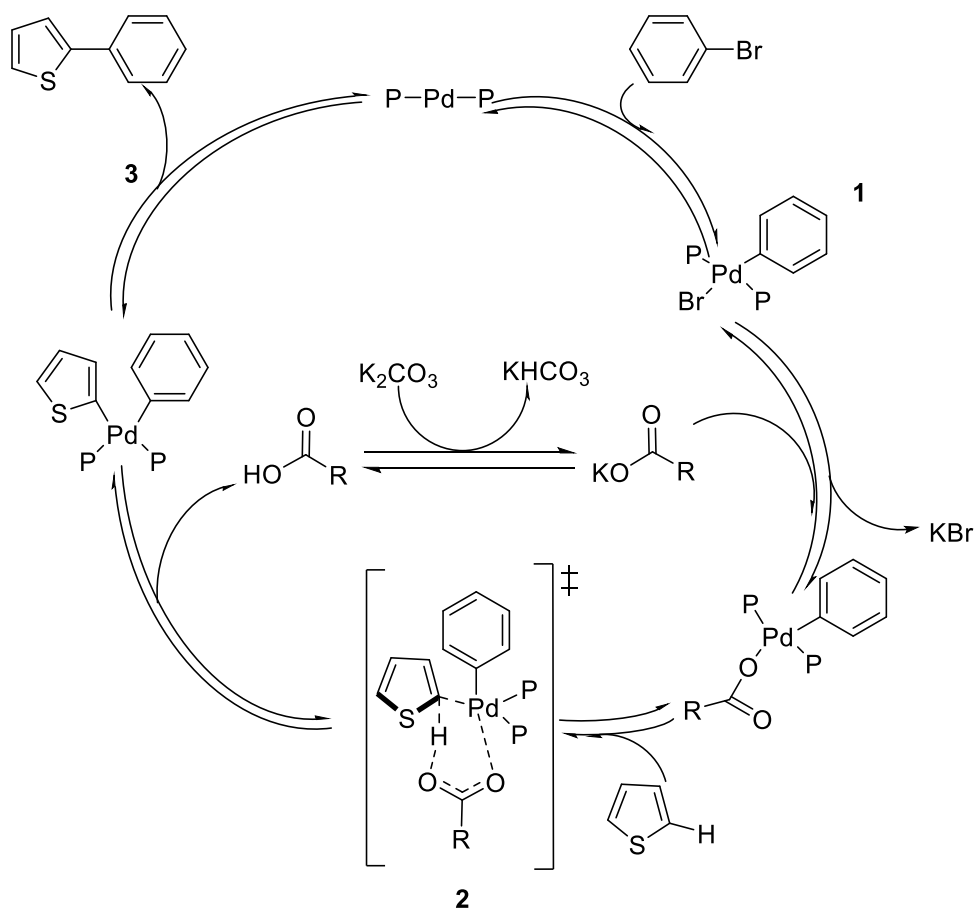
Scheme 3.1. Proposed mechanism for direct heteroarylation between thiophene and bromobenzene with a carboxylate additive. Significant steps in the coupling are oxidative addition (1), coordinated base-assisted concerted metalation-deprotonation (2), and reductive elimination (3).[24]

There are a number of different aspects of the DArP synthesis process that can be varied

to optimize the characteristics of the resulting polymer. Initial solvent investigations were

between amide-containing polar solvents, such as DMF, compared to less polar solvents, such as

THF.[24] Another method of varying the reaction conditions for DArP is the use of different

organic acids and bases. The carboxylic acid assists with the proton transfer and nearly any

carboxylic acid will do. However, it was found that, after screening 24 carboxylic acids that with

different alkyl chains (linear, tertiary, secondary, tertiary cyclic, secondary cyclic and bicyclic),

the shorter chained tertiary carboxylic acids resulted in polymers with a higher yield, higher

molecular weight, and a smaller polydispersity index (PDI) when synthesizing poly(3-

hexylthiophene) (P3HT).[25] In addition to work optimizing the organic acid, there has been a

substantial amount of work with respect to the base used for the DArP. Wand and Wang found

that the highest molecular weights, yields, and degrees of polymerization were obtained with

carbonate and phosphate bases, with cesium carbonate slightly edging out the other options.[26]

The base plays an important role in the deprotonation step and the addition of Cs_2CO_3 to the

reaction mixture during the generation of P3HT polymers resulted in a higher yield (99% vs

50%) and higher regioregularity (99% vs 93.5%) of head-to-tail orientation.[27,28] Initial studies

used a molar ratio of 0.3:2.3 of acid to base on small molecules and this was expanded to

polymers and met with significant polymer generation.[29-32] In 2013, Ozawa found that the ratio

of 1:3 acid to base generated the largest degree of polymerization for the generation of a P3HT

polymer.[33] While each polymerization requires fine tuning, this 1:3 ratio became a standard

starting point for subsequent DArP polymerizations.[15-18,24,34]

One of the biggest drawbacks of DArP is the limitation of the monomers that can be used

when preparing polymers. Controlling the site of the halogen will guide the new bond to be

formed with that carbon. While the most reactive C-H site will result in the relative majority of

the bonds, it does not mean it will be the only C-H site that forms a C-C bond. Kanbara and co-

workers found that there was substantial β-branching when using a 2,2'-bithiophene monomer.[35]

This was avoided by blocking those carbons that allowed for β-branching with methyl groups,

but this can result in poor packing and significant torsion angle between the aromatic units,

greatly increasing the E_g of the resulting polymer.[36] Monomer choice and choice of halogenation

site have a large impact on the success for the polymerization via DArP. It is important that there must be a significantly more reactive C-H site or cross-coupling will occur, resulting in a branched polymer instead of a linear polymer.

While the ambipolar nature of the TP based molecules has been investigated in model dimers, it is important to investigate how it interacts once extended to a conjugated polymer. Since TP has always been treated like an acceptor unit there is already substantial data on its interactions when polymerized with a donor unit to generate a low E_g material.[37-43] However, the fabrication of polymers with the ambipolar TP paired with acceptor units (Figure 3.1) would provide addition insight of the role of ambipolar units within the donor-acceptor framework. The generation of poly(2,3-dihexylthieno[3,4-*b*]pyrazine-*alt*-benzo[*c*][1,2,5]thiadiazole) (**3.1**) would provide a scenario where an acceptor stronger than TP is paired with the ambipolar unit. To determine if the pairing of the ambipolar TP works with acceptors weaker than it the polymer poly(2,3-dihexylthieno[3,4-*b*]pyrazine-*alt*-2,3-dihexylquinoxaline) (**3.2**) was generated. The third ambipolar-acceptor polymer was comprised of a hexyloxy functionalized TP being paired with an acceptor to yield poly(2,3-bis(hexyloxy)thieno[3,4-*b*]pyrazine-*alt*-2,3-dihexylquinoxaline) (**3.3**). The hexyloxy functionalization of the TP results in a destabilizing of the HOMO and LUMO energy levels of the monomer, which would lead to a reduction in the E_g of the final polymer when paired with a strong acceptor. These polymers are the first low E_g ambipolar-acceptor polymers to expand the current donor-acceptor framework. Portions of this chapter have been included in two published papers.[44,45]

3.1 **3.2** **3.3**
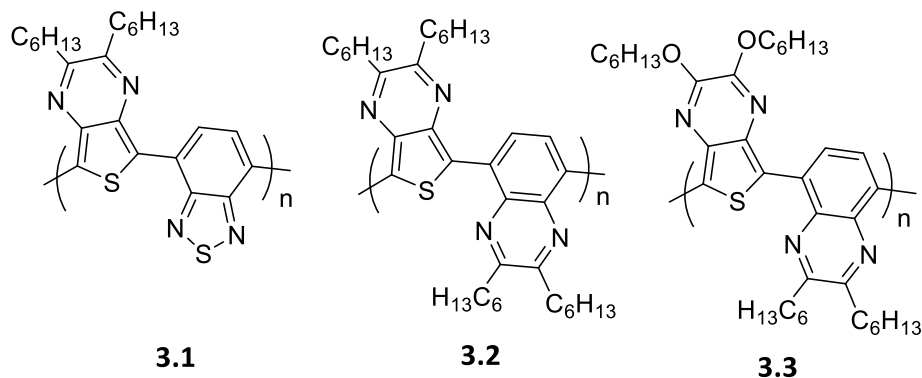
Figure 3.1. The three ambipolar-acceptor polymers that were the target compounds for this project.

Results and Discussion

Synthesis

Synthesis of monomers

The synthesis for most of the monomer components of the polymers was already developed. The synthesis of 2,3-dihexylthieno[3,4-*b*]pyrazine (**3.4**)[46] 2,3-bishexyloxythieno[3,4-*b*]pyrazine,[47] and 4,7-dibromobenzo[*c*][1,2,5]thiadiazole (**3.5**)[48] is well established and there were not any noteworthy changes, although the purification of **3.5** was optimized.

The one monomer that was not already synthesized was the quinoxaline unit. While quinoxaline has been thorough studied for its application in conjugated polymers, most of the quinoxaline units are 2,3-diaryl functionalized.[49-51] The presence of these aryl substituents could introduce additional steric interactions that would negatively affect the characteristics of the resulting polymer.[44] One possible reason for the low number of dialkyl quinoxalines is because of the difficulties in producing the alkyl-functionalized α-dione. Fortunately, these are the same α-diones that are necessary to synthesize **3.4**, which has been previously optimized by the Rasmussen group.[52]

78

The first attempt at generating the brominated quinoxaline was by generating 2,3-

dihexylquinoxaline (**3.7**), and then brominating with Br_2 and HBr in hopes of generating 5,8-

dibromo-2,3-dihexylquinoxaline (**3.8**), expecting similar results as the bromination of

benzo[*c*][1,2,5]thiadiazole (**3.9**). However, the bromination was not as selective as **3.9** and a

mixture of brominated species was collected that proved difficult to separate by column

chromatography (Scheme 3.2).
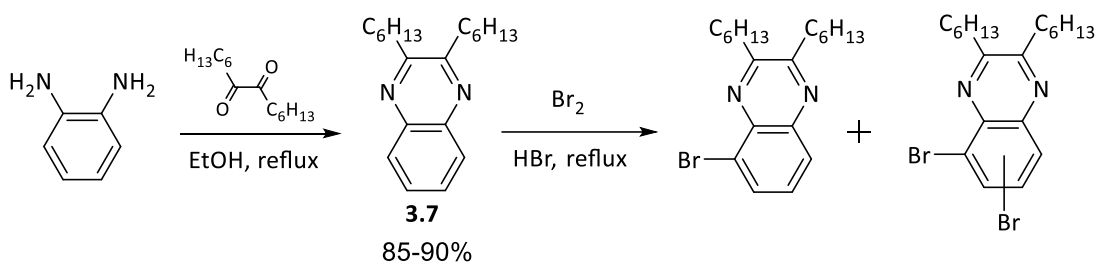
Scheme 3.2. Attempted bromination of **3.7** to generate **3.8**.

A more elegant and less direct approach was necessary in order to generate the

brominated quinoxaline. Fortunately, a clever means of generating compounds similar to **3.8** had

already been developed (Scheme 3.3).[53] Rather than the condensation of the 1,2-diaminobenzene

followed by bromination, it was first necessary to generate **3.9**, which can then be brominated

generating **3.5** which then yields 2,3-diamino-1,4-dibromobenzene upon ring opening when

reduced with sodium borohydride. The desired **3.8** could then be obtained after the condensation

with an α-dione.
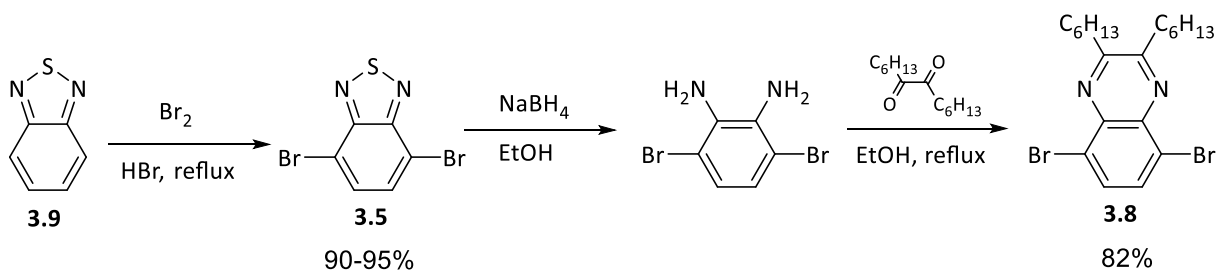
Scheme 3.3. Successful synthetic route starting with the bromination of **3.9** followed by its
reduction and the condensation to generate the desired **3.8**.

Synthesis of Polymers

The polymers were generated with one of the monomers being brominated and the other having only two active protons to limit any polymer defects. The monomers **3.4** and **3.5** were polymerized to generate poly(2,3-dihexylthieno[3,4-*b*]pyrazine-*alt*-benzo[*c*][1,2,5]thiadiazole) (p(TP-BTD) **3.1**), as shown in Scheme 3.4. The second polymer generated (Scheme 3.5) was the pairing of **3.4** and **3.8**, which generated poly(2,3-dihexylthieno[3,4-*b*]pyrazine-*alt*-2,3-dihexylquinoxaline) (p(TP-Qx) **3.2**). The third and final polymer (Scheme 3.6) was the pairing of **3.6** and **3.8** which yielded poly(2,3-bis(hexyloxy)thieno[3,4-*b*]pyrazine-*alt*-2,3-dihexylquinoxaline) (p(TPOR-Qx) **3.3**).
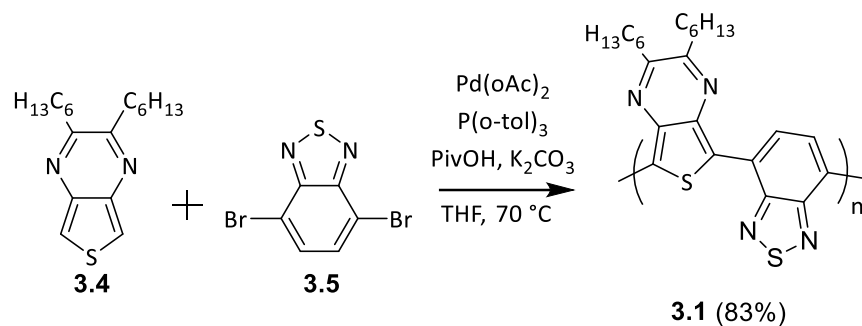
Scheme 3.4. Coupling of **3.4** and **3.5** via DARP to generate **3.1**.
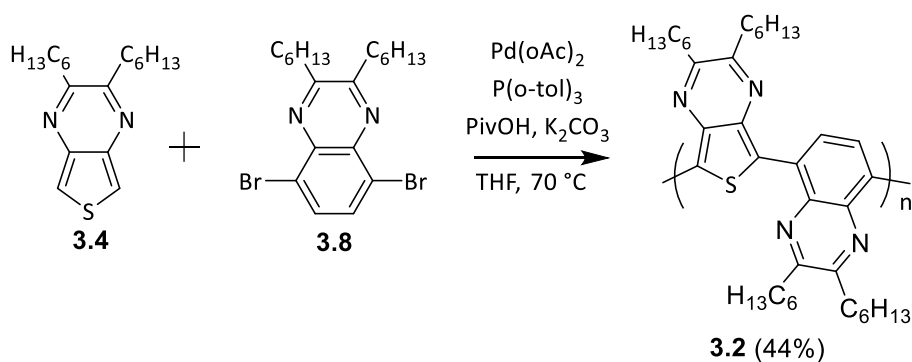
Scheme 3.5. Coupling of **3.4** and **3.8** via DARP to generate **3.2**.
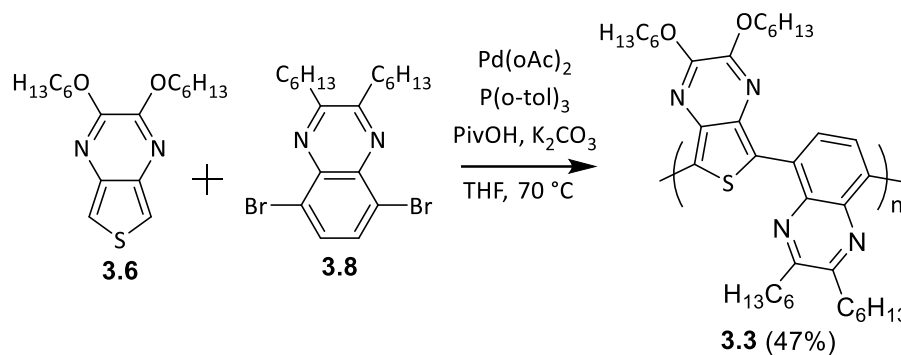
Scheme 3.6. Coupling of **3.6** and **3.8** via DARP to generate **3.3**.

The molecular weight of the polymer has a substantial impact on the characteristics of the polymer. The molecular weight is directly related to the conjugation length because more units along the polymeric backbone results in an increase in the orbital blending due to increased conjugation as long as the effective conjugation length has not been reached and there are not other factors that would break conjugation.[54] The polymerization of the conjugated materials results in a wide range of molecular weights and the highest molecular weight fraction is collected by Soxhlet extraction with sequential washes of methanol, acetone, hexane, and chloroform, with the chloroform fraction containing the highest molecular weight fraction of the soluble material.

The high molecular weight fractions of polymers were analyzed by gel permeation chromatography (GPC) to determine the molecular weight of the polymer as well as the PDI to quantify the extent of the polymerization. This data is present in Table 3.1.

Table 3.1. Yields and molecular weight data for the polymers.

Entry	Yield (%)	M_n[a]	PDI[a]	Degree of Polymerization (n)
3.1	83	1900	1.57	4-5
3.2	44	2700	1.28	4-5
3.3	47	2300	1.45	3-4

[a] Determined via GPC

The polymer **3.3** had a reduced degree of polymerization likely due to the reactivity of the alkoxy functionalized monomer unit **3.6**. It is expected that the electron donating alkoxy groups would result in a significant reduction in the rate of oxidative addition, resulting in a lower molecular weight material.[55,56] The obtained molecular weight of 2300 for **3.3** is just shy of the range of other reported polymers containing **3.6** that ranged from 2700-4800 so the lower molecular weight is not unprecedented and the degree of polymerization is comparable.[6,55,57]

Impact of Pivalic Acid

DArP is a continually developing means of polymerization that focuses on providing a polymerization option without the use of additional functionalizations that produce toxic byproducts. The initial works done focused on using solely a palladium catalyst and a phosphine ligand.[58] The initial attempt at generating **3.1** used the DArP conditions of a palladium catalyst, a phosphine ligand, and a base to assist with the deprotonation step of the reaction mechanism. The resulting polymer was generated with a lower yield than desired, with only 45% of the high molecular weight fraction after the Soxhlet purification.

After further investigation in the development of the DArP, it was found that the addition of a carboxylic acid to the reaction mixture would greatly improve the polymerization process.[59] The presence of pivalic acid in the Schlenk tube during the polymerization of **3.1** resulted in an increase in the yield of the high molecular weight fraction to 83%. It is worth noting that the solution absorbance of the two polymers showed little difference, as shown in Figure 3.2. This indicates that the addition of pivalic acid did not significantly increase the molecular weight of the polymer, but it did result in a substantial increase in the yield of the high molecular weight portion of the polymer.
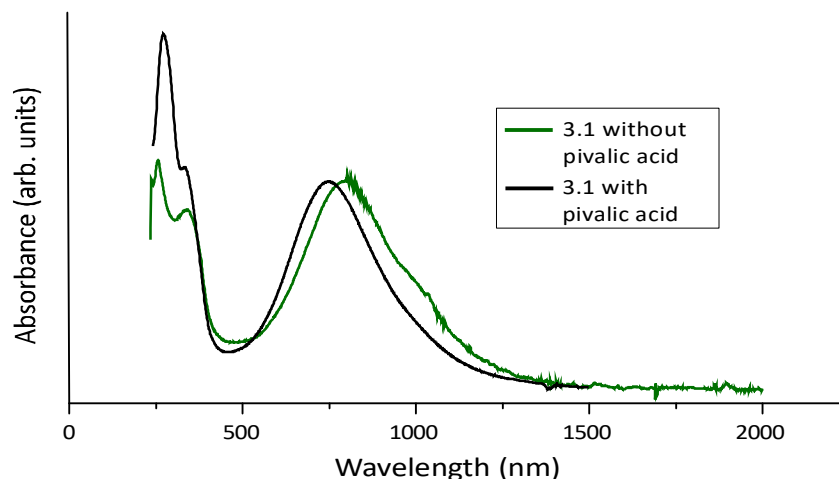
Figure 3.2. Absorption of **3.1** in CHCl$_3$ with and without pivalic acid during the polymerization.

UV-Vis Absorption Spectroscopy

Absorption data for the film and solution of the three polymers are shown in Figures 3.3 through 3.6. The related absorption data for all three polymers can be seen in Table 3.2. All of the polymers exhibit two absorption bands. The high energy band is assigned a π-π* transition and the low energy band is assigned to an intramolecular charge transfer (ICT) transition from the polymer backbone to one of the acceptor or ambipolar units. Two of the three polymers generated were low band gap materials with E$_g$ values of 0.94 eV for **3.1** and 1.33 eV for **3.2**. The polymer **3.3** was just shy of the 1.50 eV cutoff with an E$_g$ of 1.56 eV. It is worth noting that these are two of only a few low E$_g$ polymers generated by DArP.[60-64]

Table 3.2. Optical properties of polymers.

Entry	Solution λ$_{max}$(nm)[a]	Solid λ$_{max}$(nm)[b]	Band gap (eV)[c]
3.1	266, 329, 742	334,779	0.94
3.2	193, 261, 625	276, 341, 687	1.33
3.3	294, 333, 593	296, 335, 605	1.56

[a] In CH$_3$Cl. [b] Film formed via spin coating on glass plate from CHCl$_3$. [c] Optical E$_g$.
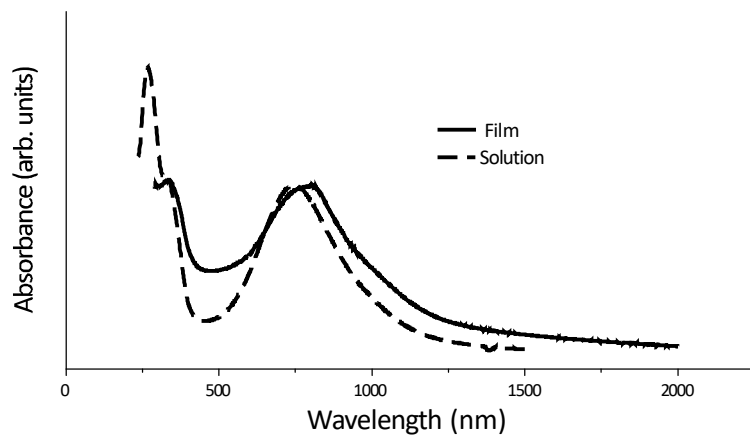
Figure 3.3. Solution, in CHCl$_3$, and solid state absorption data of **3.1**.
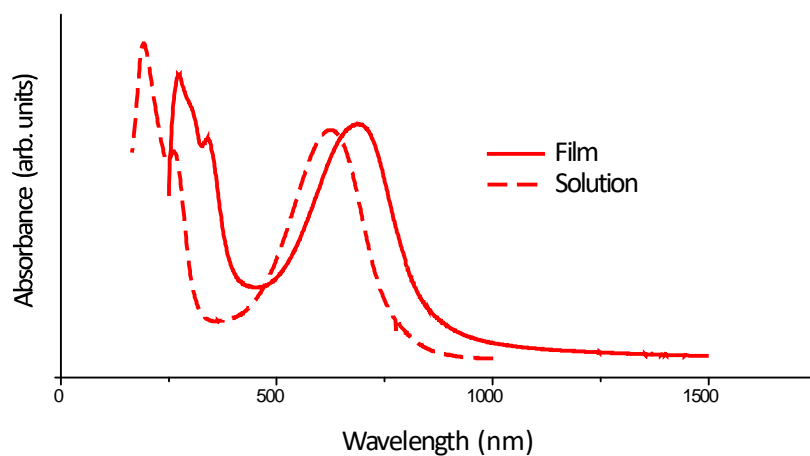
Figure 3.4. Solution, in CHCl$_3$, and solid state absorption data of **3.2**.
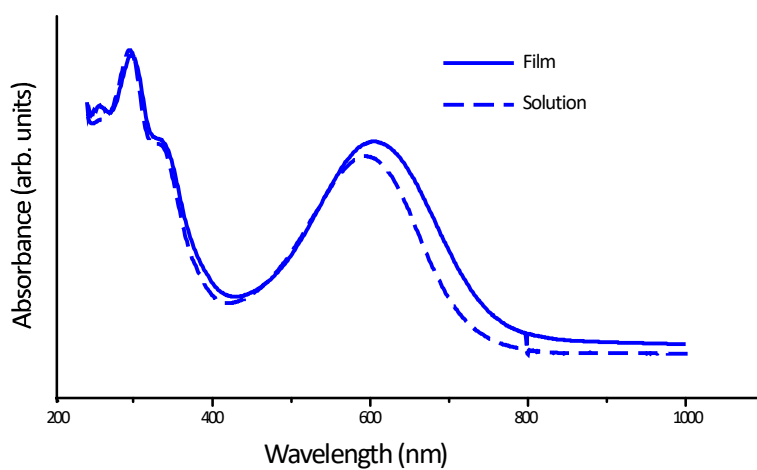
Figure 3.5. Solution, in CHCl$_3$, and solid state absorption data of **3.3**.

There was a notable difference in the processability of the polymers as well. The polymers **3.1** and **3.2** easily formed films when spin-cast with $CHCl_3$. However, the polymer film would undergo decomposition upon thermal annealing when exposed to air. It was possible to avoid this by thermally annealing under nitrogen. It was difficult to generate a film of **3.3** via spin-casting, so a combination of drop-casting and spin-casting was used. This required the formation of a film by initially drop casting, followed by the addition of a small amount of a solubilizing solvent and spin-casting at reduced speeds. Figure 3.6 shows the compilation of absorption of the films of the three polymers.

The ICT of the ambipolar-acceptor polymers may have some characteristics different than the classical donor-acceptor polymers. The ICT is understood to be a charge transfer from the polymer backbone to the acceptor unit in the classical D-A molecules. However, the ambipolar-acceptor polymers could contain two separate ICT if the LUMOs of the ambipolar and acceptor are similar, with each corresponding to the charge transfer to either the ambipolar unit or the acceptor unit. It is also possible that the LUMOs of the ambipolar and acceptor unit could hybridize to form a LUMO with contribution from both the ambipolar and acceptor unit. In the polymers generated there is only one broad ICT absorption that was observed. This indicates that there is either a single ICT from the polymer backbone to the LUMO localized on either the acceptor or ambipolar unit or a hybridized LUMO of the ambipolar and acceptor unit. The other possible explanation is that there are two ICTs that have overlapping absorption profiles and only a single broad absorption is observed. TD-DFT calculations by M. Carmen Ruiz Delgado (University of Málaga) support the single ICT transition from HOMO to LUMO localized on the acceptor or ambipolar unit.[45]
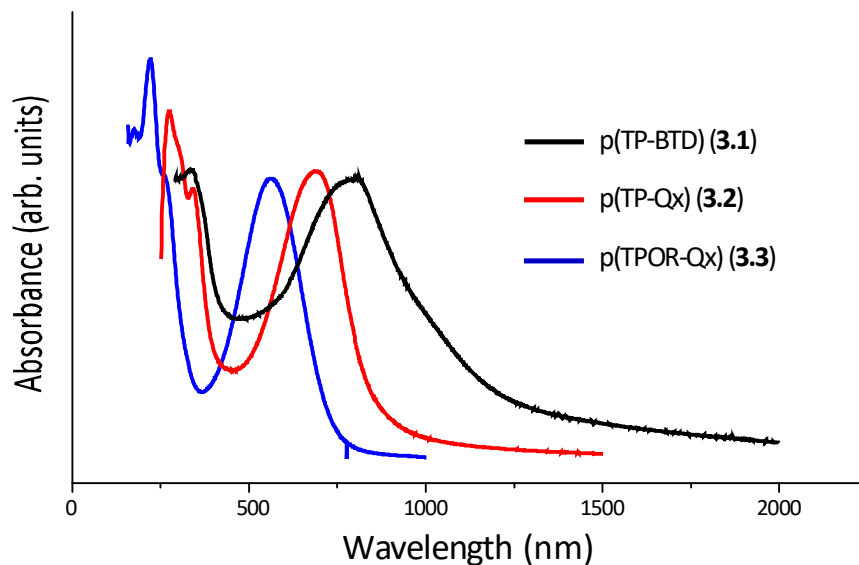
Figure 3.6. Solid state absorption of **3.1**, **3.2**, and **3.3**.

Electrochemistry of Ambipolar-Acceptor Copolymers

The cyclic voltammetry (CV) experiments were performed on the ambipolar-acceptor copolymers with data found in Table 3.3 and representative CVs in Figure 3.7. The reason the HOMO of **3.3** is much lower than the other two polymers' is most likely due to the smaller molecular weight because the HOMO energy levels of all the monomers that make up the other polymers were similar. The HOMO of **3.3** would actually be expected to be higher than the other two polymers due to the destabilized energy levels caused by the alkoxy functionalization compared to the alkyl functionalization on the TP unit. The LUMO of each of the polymers was determined by using the optical E_g with the measured HOMO.

Table 3.3. Electrochemical properties of the acceptor-ambipolar polymers.

Polymer	HOMO (eV)[a]	LUMO (eV)[b]	E_g (eV)[c]
3.1	-5.0	-4.1	0.94
3.2	-5.2	-3.9	1.33
3.3	-5.3	-3.7	1.55

Film formed by drop casting from a $CHCl_3$ solution of the polymer onto a Pt disc for **3.1** and a carbon disc for **3.2** and **3.3** as the working electrode. Potentials vs Ag/Ag^+ in 0.1 M $TBAPF_6$ in MeCN. [a] $E_{HOMO} = -(E_{[onset, ox vs. Fc+/Fc]} + 5.1)(eV)$.[65] [b] $E_{LUMO} = E_{HOMO} - E_g$. [c] Optical E_g.
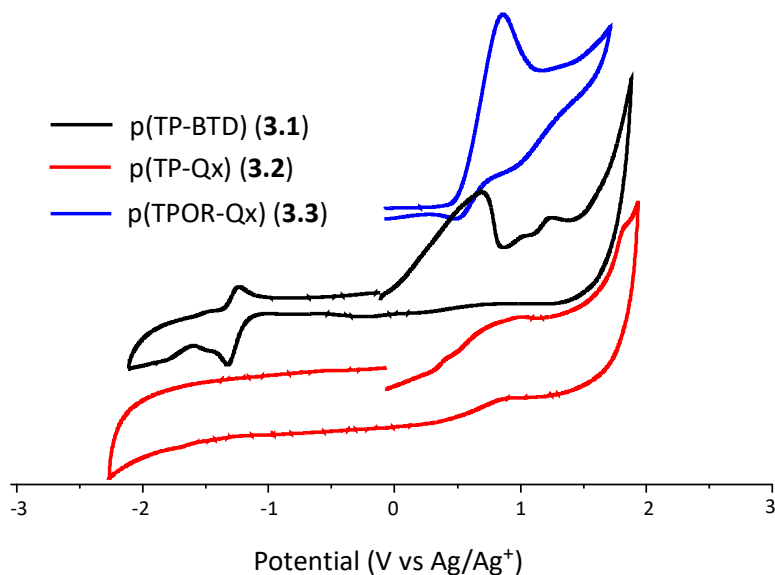
Figure 3.7. Cyclic voltammograms of ambipolar-acceptor polymers **3.1**, **3.2**, and **3.3**.

The pairing of TP with BTD and Qx for polymers show that the ambipolar-acceptor polymer design is effective with acceptors weaker or stronger than TP. The LUMO of BTD (-3.2 eV)[66] makes it a stronger acceptor than TP (-3.0 eV),[46] while the LUMO of Qx (-2.7 eV)[67] makes it a weaker acceptor than TP. The difference in the LUMO of polymers **3.1** (-4.4 eV) and **3.2** (-4.2 eV) are consistent with the trend of the LUMOs of the BTD and Qx unit. This indicates that the LUMO of the resulting polymers can be adjusted by using acceptors of different strength, with the stronger acceptors being expected to generate a more stabilized polymer LUMO.

The design of **3.3** was to utilize the ambipolar TP that was functionalized with hexyloxy substituents to destabilize the HOMO and LUMO energy levels of the TP unit, resulting in a higher HOMO of the polymer it is incorporated in.[47] When paired with another acceptor, the destabilized HOMO of the TP and the LUMO of the TP and the acceptor unit (Qx) would hopefully result in a low E_g material. The low molecular weight limited the success of the polymer, however it does provide insight on the polymer design. The HOMO of **3.3** (-5.3 eV) was similar to that of **3.2** (-5.2 eV) indicating that despite the limited molecular weight and

87

conjugation length of **3.3**, the objective of obtaining a more destabilized HOMO through the alkoxy functionalized TP has potential to work using this polymer design. Unfortunately, polymer **3.3** had an E_g just above the low E_g threshold, causing it to not be categorized as a low E_g polymer. In order to properly evaluate the effectiveness of the polymer design the limited molecular weight issue needs to be overcome.

Conclusion

The work presented demonstrates the successful synthesis of three ambipolar-acceptor polymers via DArP: poly(2,3-dihexylthieno[3,4-*b*]pyrazine-*alt*-2,1,3-benzothiadiazol) (**3.1**), poly(2,3-dihexylthieno[3,4-*b*]pyrazine-*alt*-2,3-dihexylquinoxaline (**3.2**), and poly(2,3-bis(hexyloxy)thieno[3,4-*b*]pyrazine-*alt*-2,3-dihexylquinoxaline (**3.3**). The polymers **3.1** and **3.2** were both low E_g polymers and are two of only a few low E_g polymers synthesized via DArP.[60-64] While **3.3** had a larger E_g, likely due to its low degree of polymerization, the design could still generate a low E_g material if the polymerization were optimized. This shows that the ambipolar-acceptor polymer design is an effective means for generating low E_g polymers. Additionally, this new design helps overcome the issue of the high lying HOMOs of most TP based low E_g materials.[68]

The pairing of 2,3-dihexyl TP with both Qx and BTD to generate low E_g polymers also indicates that the ambipolar-acceptor design works with acceptors that are stronger (BTD) and weaker (Qx) than TP. Additionally, the resulting of the LUMO of the polymer trends with the strength and of the acceptor unit. This allows for a level of tunability of the LUMO by varying the strength of the acceptor unit paired with the ambipolar TP unit.

Additional work with this project would consist of optimizing the synthesis conditions for the polymerization. Leclerc has claimed that the reaction conditions for each set of monomers

can be specific and requires optimization.[17] One method that was used to optimized the polymer synthesis was the use of superheated solvent under pressure in a sealed microwave vial which resulted in higher molecular weight polymers.[44,45] If additional ambipolar units were identified, more ambipolar-acceptor polymers could be synthesized by replacing the TP unit with the new ambipolar unit. This would further support the ambipolar-acceptor polymer design and its inclusion within the donor-acceptor framework.

These new ambipolar-acceptor polymers could be used as acceptor materials in bulk-heterojunction solar cells. The solution fluorescence of higher-molecular weight **3.1** and P3HT revealed partial quenching of the P3HT emission and some change of the emission profile.[45] This shows that there is some charge transfer between the two polymers and there is potential for these ambipolar-acceptor polymers to serve as acceptor materials for bulk-heterojunction solar cells.[69-71] The tunable LUMO of these polymers also could broaden the donor materials that could be used for solar cells as well.

Experimental

General

Unless stated, all materials were reagent grade and used without further purification. All chromatographic separations were performed with standard chromatography methods with silica gel as the stationary phase (230-400 mesh). Dry THF was obtained via distillation over sodium and benzophenone. Acetonitrile was dried over CaH_2 and distilled prior to use. All glassware was oven-dried, assembled as soon as it could be handled, and cooled under dry nitrogen before use. Transfer of liquids was carried out using standard syringe techniques and all reactions were done in an inert, dry nitrogen atmosphere with a constant stream of nitrogen. Melting points were determined using a digital thermometer couple with a 0.1 °C resolution. The ^1H and ^{13}C NMR

were completed on a 400 MHz spectrometer. All NMR data was referenced to the chloroform signal and peak multiplicity was reported as follows: s = singlet, d = doublet, t = triplet, q = quartet, p = pentet, dd = doublet of doublets, m = multiplet, and br = broad. HRMS was performed in house.

Materials

2,5-Dibromo-3,4-dinitrothiophene,[72] benzo[*c*][1,2,5]thiadiazole (**3.9**),[73] 4,7-dibromobenzo[*c*][1,2,5]thiadiazole (**3.5**),[48] 2,3-dihexylthieno[3,4-*b*]pyrazine(**3.4**),[46] 2,3-bis(hexyloxy)thieno[3,4-*b*]pyrazine(**3.6**),[47] and 2,3-diamino-1,4-dibromobenzene(**3.5**)[74] were prepared as previously reported.

5,8-Dibromo-2,3-dihexylquinoxaline (3.8)

3.5 (0.30 g, 1.13 mmol) was dissolved in absolute ethanol (60 mL) in a round bottom flask. This was then purged with nitrogen three times. 7,8-Tetradecane-dione (0.28 g, 1.25 mmol) was added to the round bottom flask and was then flushed with nitrogen two more times. The reaction was then heated at reflux for three hours. After three hours the solvent was removed by reduced pressure and the sample was purified by silica gel column chromatography with ethyl acetate and petroleum ether as the eluent (v/v=5/95: yield 82%), leaving a white solid. Mp. 69.8-70.4 °C. ^{1}H NMR: δ 7.81 (s, 2H), 3.07 (t, 4H, J = 7.6 Hz), 1.91 (m, 4H), 1.49 (m, 4H), 1.37 (m, 8H), 0.91 (t, 6H, J = 7.0 Hz) ^{13}C NMR: δ 158.6, 132.3, 123.7, 35.1, 32.1, 29.5, 28.1, 23.0, 14.5.

Poly(2,3-dihexylthieno[3,4-b]pyrazine-alt-benzo[c][1,2,5]thiadiazole) (3.1)

Dry THF was degassed by bubbling nitrogen through it for two hours. To a dry Schlenk tube was added **3.4** (0.108 g, 0.355 mmol), **3.5** (0.104 g, 0.355 mmol), palladium (II) acetate (0.010 g, 0.041 mmol, 12%), tris(*o*-methoxyphenyl)phosphine (0.022 g, 0.062 mmol, 18%), potassium carbonate (0.147 g, 1.065 mmol), and pivalic acid (0.036 g, 0.355 mmol) and a

nitrogen atmosphere was obtained. The degassed THF (10.0 mL) was then added to the Schlenk

tube and the reaction was heated to 70 °C by a mineral oil bath for five days. The reaction was

shielded from all sources of light for the duration of the polymerization. The polymerization was

stopped by cooling to room temperature and precipitating the polymer in methanol. The polymer

was filtered and then purified by Soxhlet extractions of methanol, acetone, hexane, and

chloroform. The polymer was obtained from the chloroform fraction upon removal of the solvent

by reduced pressure. The polymer obtained was a blue/black solid (130 mg, 83 % isolated).

GPC: $M_w = 3000$, $M_n = 1900$, PDI = 1.6.

Poly(2,3-dihexylthieno[3,4-b]pyrazine-alt-2,3-dihexylquinoxaline) (3.2)

Dry THF was degassed by bubbling nitrogen through it for two hours. To a dry Schlenk

tube was added **3.4** (0.108 g, 0.355 mmol), **3.8** (0.162 g, 0.355 mmol), palladium (II) acetate

(0.010 g, 0.041 mmol, 12%), tris(*o*-methoxyphenyl)phosphine (0.022 g, 0.062 mmol, 18%),

potassium carbonate (0.147 g, 1.065 mmol), and pivalic acid (0.036 g, 0.355 mmol) and a

nitrogen atmosphere was obtained. The degassed THF (10.0 mL) was then added to the Schlenk

tube and the reaction was heated to 70 °C by a mineral oil bath for five days. The reaction was

shielded from all sources of light for the duration of the polymerization. The polymerization was

stopped by cooling to room temperature and precipitating the polymer in methanol. The polymer

was filtered and then purified by Soxhlet extractions of methanol, acetone, hexane, and

chloroform. The polymer was obtained from the chloroform fraction upon removal of the solvent

by reduced pressure. The polymer obtained was a blue/black solid (93 mg, 44 % isolated). GPC:

$M_w = 3400$, $M_n = 2700$, PDI 1.3.

Poly(2,3-bis(hexyloxy)thieno[3,4-b]pyrazine-alt-2,3-dihexylquinoxaline) (3.3)

Dry THF was degassed by bubbling nitrogen through it for two hours. To a dry Schlenk tube was added **3.6** (0.108 g, 0.355 mmol), **3.8** (0.162 g, 0.355 mmol), palladium (II) acetate (0.010 g, 0.041 mmol, 12%), tris(*o*-methoxyphenyl)phosphine (0.022 g, 0.062 mmol, 18%), potassium carbonate (0.147 g, 1.065 mmol), and pivalic acid (0.036 g, 0.355 mmol) and a nitrogen atmosphere was obtained. The degassed THF (10.0 mL) was then added to the Schlenk tube and the reaction was heated to 70 °C by a mineral oil bath for five days. The reaction was also shielded from all sources of light for the duration of the polymerization. The polymerization was stopped by cooling to room temperature and precipitating the polymer in methanol. The polymer was filtered and then purified by Soxhlet extractions of methanol, acetone, hexane, and chloroform. Nothing was collected from the chloroform fraction, so the hexane fraction was obtained upon removal of the solvent by reduced pressure. The polymer obtained was a blue/black solid (106 mg, 47 % isolated). GPC: M_w = 3400, M_n = 2300, PDI = 1.5.

Electrochemistry

All electrochemical techniques were performed on a Bioanyltical Systems BAS 100B/W electrochemical analyzer. Cyclic voltammetry (CV) experiments were performed using a three-electrode cell consisting of a Pt-disc working electrode, Pt coil wire auxiliary electrode, and an Ag/Ag^+ reference electrode. A 0.1 M electrolyte solution was prepared with tetrabutylammonium hexafluorophosphate ($TBAPF_6$) using MeCN distilled over CaH_2 under dry nitrogen. The solutions were deoxygenated with argon for at least 20 min prior to each scan and blanketed with argon during the experiments. Solutions of the polymers dissolved in $CHCl_3$ were drop cast on the working electrode and dried to generate a solid film. CV experiments were performed in the described cell at a sweep rate of 100 mV/s. E_{HOMO} values were determined in a

reference to ferrocene (5.1 eV vs. vacuum) and the E$_{LUMO}$ values were determined based on the E$_{HOMO}$ value and the optical band gap.

UV-Vis Absorption Spectroscopy

All absorption spectroscopy was performed on a Carry 500 dual-beam UV-vis-NIR spectrophotometer. Solution-state spectra were analyzed in chloroform and solid-state spectra were analyzed with the polymer spin coated on a glass plate from a CHCl$_3$ solution. The optical band gaps were determined by generating a Tauc plot from the data and determining the gap based on the intercept of the most linear portion of the plot.

References

1. Amb, C. M.; Chen, S.; Graham, K. R.; Subbiah, J.; Small, C. E.; So, F.; Reynolds, J. R. *J. Am. Chem. Soc.* **2011,** *133,* 10062.

2. Helgesen, M.; Krebs, F. C. *Macromolecules* **2010,** *43,* 1253.

3. Zhang, X.; Steckler, T. T.; Dasari, R. R.; Ohira, S.; Potscavage, W. J.; Tiwari, S. P.; Coppée, S.; Barlow, S.; Brédas, J.-L.; Kippelen, B.; Reynolds, J. R.; Marder, S. R. *J. Mater. Chem.* **2010,** *20,* 123.

4. Havinga, E. E.; ten Hoeve, W.; Wynberg, H. *Synth. Met.,* **1993,** *55,* 299.

5. Wen, L.; Heth, C. L.; Rasmussen, S. C. *Phys. Chem. Chem. Phys.* **2014,** *16*, 7231.

6. Mulholland, M. E.; Konkol, K. L.; Anderson, T. E.; Schwiderski, R. L.; Rasmussen, S. C. *Aust. J. Chem.* **2015,** *68,* 1759.

7. Konkol, K. L.; Schwiderski, R. L.; Rasmussen, S. C. *Materials* **2016,** *9,* 404.

8. Kenning, D. D.; Funfar, M. R.; Rasmussen, S. C. *Polymer Preprints* **2001,** *42,* 506.

9. Kenning, D. D.; Mitchell, K. A.; Calhoun, T. R.; Funfar, M. R.; Sattler, D. J.; Rasmussen, S. C. *J. Org. Chem.* **2002,** *67,* 9073.

10. Carsten, B.; He, F.; Son, H. J.; Xu, T.; Yu, L. *Chem. Rev.* **2011**, *111*, 1493.

11. Loewe, R. S.; Ewbank, P. C.; Liu, J.; Zhai, L.; McCullough, R. D. *Macromolecules* **2001**, *34*, 4324.

12. Sakamoto, J.; Rehahn, M.; Wegner, G.; Schluter, A. D. *Macromol. Rapid Commun.* **2009**, *30*, 653.

13.   Morin, P.-O.; Bura, T.; Leclerc, M. *Mater. Horiz.* **2016**, *3*, 11.

14.   Po, R.; Bernardi, A.; Calabrese, A.; Carbonera, C.; Corso, G.; Pellegrino, A. *Energy Environ. Sci.* **2014**, *7*, 925.

15.   Pouliot, J.-R.; Grenier, F.; Blaskovits, J. T.; Beaupré, S.; Leclerc, M. *Chem. Rev.* **2016,** *116,* 14225.

16.   Bura, T.; Blaskovits, J. T.; Leclerc, M. *J. Am. Chem. Soc.* **2016,** *138,* 10056.

17.   Mercier, L. G.; Leclerc, M. *Acc. Chem. Res.* **2013**, *46*, 1597.

18.   Bohra, H.; Wang, M. *J. Mater. Chem. A* **2017,** *5,* 11550.

19.   Gorelsky, S. I.; Lapointe, D.; Fagnou, K. *J. Org. Chem.* **2012,** *77,* 658.

20.   Ackermann, L. *Chem. Rev.* **2011,** *111,* 1315.

21.   Schipper, D. J.; Fagnou, K. *Chem. Mater.* **2011**, *23*, 1594.

22.   Biswas, B.; Sugimoto, M.; Sakaki, S. *Organometallics* **2009**, *19*, 3895.

23.   Gorelsky, S. I.; Lapointe, D.; Fagnou, K. *J. Am. Chem. Soc.* **2008**, *130*, 10848.

24.   Bura, T.; Blaskovits, J. T.; Leclerc, M. *Journal of the American Chemical Society* **2016**, *138*, 10056.

25.   Rudenko, A. E.; Thompson, B. C.; *Macromolecules* **2015**, *31*, 569.

26.   Wang, X.; Wang, M. *Polym. Chem.* **2014**, *5*, 5784.

27.   Wang, Q.; Takita, R.; Kikuzaki, Y.; Ozawa, F. *J. Am. Chem. Soc.* **2010**, *132*, 11420.

28.   Pouliot, J. R.; Wakioka, M.; Ozawa, F.; Li, Y.; Leclerc, M. *Macromol. Chem. Phys.* **2016**, *217*, 1493.

29.   Lafrance, M.; Fagnou, K. *J. Am. Chem. Soc.* **2006**, *128*, 16496.

30.   Segawa, Y.; Maekawa, T.; Itami, K. *Angew. Chem., Int. Ed.* **2015**, *54*, 66.

31.   Kuwabara, J.; Yamazaki, K.; Yamagata, T.; Tsuchida, W.; Kanbara, T. *Polym. Chem.* **2015**, *6*, 891.

32.   Mercier, L. G.; Aich, B. R.; Najari, A.; Beaupre, S.; Berouard, P.; Pron, A.; Robitaille, A.; Tao, Y.; Leclerc, M. *Polym. Chem.* **2013**, *4*, 5252.

33.   Wakioka, M.; Kitano, Y.; Ozawa, F. *Macromolecules* **2013**, *46*, 370.

34.   Iizuka, E.; Wakoika, M.; Ozawa, F. *Macromolecules* **2015,** *48,* 2989.

35. Fujinami, Y.; Kuwabara, J.; Lu, W.; Hayashi, H.; Kanbara, T. *ACS Macro Lett.* **2012**, *1*, 67.

36. Kuwabara, J.; Nohara, Y.; Choi, S. J.; Fujinami, Y.; Lu, W.; Yoshiumura, K.; Oguma, J.; Suenobu, K.; Kanbara, T.*Polym. Chem.* **2013**, *4*, 947.

37. Nietfeld, J. P.; Heth, C. L.; Rasmussen, S. C. *Chem. Commun.* **2008,** 981.

38. Sonmez, G.; Sonmez, H. B.; Shen, C. K. F.; Jost, R. W.; Rubin, T.; Wudl, F. *Macromolecules* **2005,** *38,* 669.

39. Sonmez, G.; Sonmez, H. B.; Shen, C. K. F.; Wudl, F. *Adv. Mater.* **2004,** *16,* 1905.

40. Sonmez, G.; Shen, C. K. F.; Rubin, Y.; Wudl, F. *Angew. Chem. Int. Ed.* **2004,** *43,* 1498.

41. Berlin, A.; Zotti, G.; Zecchin, S.; Schiavon, G.; Vercelli, B.; Zanelli, A. *Chem. Mater.* **2004,** *16,* 3667.

42. Wienk, M. M.; Turbiez, M. G. R.; Struijk, M. P.; Fonrodona, M.; Janssen, R. A. *J. Appl. Phys. Lett.* **2006,** *88,* 153511.

43. Perepichka, I. F.; Levillain, E.; Roncali, J. *J. Mater. Chem.* **2004,** *14,* 1679.

44. Anderson, T. E.; Culver, E. W.; Almyahi, F. A.; Dastoor, P. C.; Rasmussen, S. C. *Synlett* **2018,** *29,* 2542.

45. Culver, E. W.; Anderson, T. E.; Navarrete, J. T. L.; Delgado, M. C. R.; Rasmussen, S. C. *ACS Macro Lett.* **2018,** *7,* 1215.

46. Kenning, D. D.; Mitchell, K. A.; Calhoun, T. F.; Funfar, M. R.; Sattler, D. J.; Rasmussen, S. C. *J. Org. Chem.* **2002,** *67,* 9073.

47. Wen, L.; Nietfeld, J. P.; Amb, C. M.; Rasmussen, S. C. *J. Org. Chem.* **2008,** *73,* 8529.

48. Wang, R.; Zhang, C.; Wang, W.; Liu, T. *J. Polym. Sci. A* **2010,** *48,* 4867.

49. Yuan, J.; Ouyang, J.; Cimrova, V.; Leclerc, M.; Najarid, A.; Zou, Y. *J. Mater. Chem. C* **2017,** *5,* 1858.

50. Gedefaw, D.; Prosa, M.; Bolognesi, M.; Seri, M.; Andersson, M. R. *Adv. Energy Mater.* **201,** *7,* 1700575.

51. Liu, M.; Gao, Y.; Zhang, Y.; Liu, Z.; Zhao, L. *Polym. Chem.* **2017,** *8,* 4613.

52. Kenning, D. D.; Mitchell, K. A.; Calhoun, T. R.; Funfar, M. R.; Sattler, D. J.; Rasmussen, S. C. *J. Org. Chem.* **2002,** *67,* 9073.

53. Edelmann, M. J.; Raimundo, J. –M.; Utesch, N. F.; Diederich, F.; Boudon, C.; Gisselbrecht, J. –P.; Gross, M. *Helv. Chim. Acta.* **2002,** *85,* 2195.

54. Kroon, R.; Lenes, M.; Hummelen, J. C.; Blom, P. W. M.; De Boer, B. *Polym. Rev.* **2008,** *48*, 531.

55. Evenson, S. J.; Mulholland, M. E.; Anderson, T. E.; Rasmussen, S. C. *Asian J. Org. Chem.* **2020,** *9,* 1333.

56. Puri, M.; Gatard, S.; Smith, D. A.; Ozerov, O. V. *Organometallics* **2011,** *30,* 2472.

57. Mulholland, M. E.; Wen, L.; Rasmussen, S. C. *Topol. Supramol. Polym. Sci.* **2015,** *2,* 18.

58. Lafrance, M.; Rowley, C. N.; Woo, T. K.; Fagnou, K. *J. Am. Chem. Soc.* **2006,** *316,* 8754.

56. Rudenko, A. E.; Thompson, B. C. *Macromolecules* **2015,** *48,* 569.

57. Guo, Q.; Dong, J.; Wan, D.; Wu, D.; You, J. *Macromol. Rapid Commun.* **2013,** *34*, 522.

58. Nakanishi, T.; Shirai, Y.; Han, L. *J. Mater. Chem. A* **2015,** *3,* 4229.

59. Homyak, P.; Liu, Y.; Liu, F.; Russel, T. P.; Coughlin, E. B. *Macromolecules* **2015,** *48,* 6978.

60. Wang, K.; Huang, J.; Ko, J.; Leong, W. L.; Wang, M. *J. Polym. Sci., Part A: Polym. Chem.* **2017,** *55*, 3205.

61. Nakabayashi, K.; Fukuzawa, H.; Fujita, K.; Mori, H. *J. Polym. Sci., Part A: Polym. Chem.* **2018,** *56,* 430.

62. Cardona, C. M.; Li, W.; Kaifer, A. E.; Stockdale, D.; Bazan, G. C. *Adv. Mater.* **2011,** *23,* 2367.

63. Vasilieva, N. V.; Irtegova, I. G.; Gritsan, N. P.; Lonchakov, A. V.; Makarov, A. Y.; Shundrin, L. A.; Zibarev, A. V. *J. Phys. Org. Chem.* **2010,** *23,* 536.

64. Chénard, E.; Sutrisno, A.; Zhu, L.; Assary, R. S.; Kowalski, J. A.; Barton, J. L.; Bertke, J. A.; Gray, D. L.; Brushett, F. R.; Curtiss, L. A.; Moore, J. S. *J. Phys Chem. C* **2016,** *120,* 8461.

65. Rasmussen, S. C.; Schwiderski, R. L.; Mulholland, M. E. *Chem. Commun.* **2011,** *47,* 11394.

66. Zhang, J.; Kan, B.; Pearson, A. J.; Parnell, A. J.; Cooper, J. F. K.; Liu, X.-K.; Conaghan, P. J.; Hopper, T. R.; Wu, Y.; Wan, X.; Gao, F.; Greenham, N. C.; Bakulin, A. A.; Chen, Y.; Friend, R. H. *J. Mater. Chem. A* **2018**, *6*, 18225.

67. Zhang, J.; Tan, H. S.; Guo, X.; Facchetti, A.; Yan, H. *Nat Energy* **2018**, *3*, 720.

68. Yan, C.; Barlow, S.; Wang, Z.; Yan, H.; Jen, A. K.-Y.; Marder, S. R.; Zhan, X. *Nat Rev Mater* **2018**, *3*, 18003.

69.   Wen, L.; Rasmussen, S. C. *J. Chem. Crystallogr.* **2007,** *37,* 387.

70.   Tao, Y.-M.; Li, H.-Y.; Xu, Q.-L.; Zhu, Y.-C.; Kang, L.-C.; Zheng, Y.-X.; Zuo, J.-L.; You, X.-Z. *Synthetic Metals* **2011,** *161,* 718.

71.   Yamamoto, T.; Sugiyama, K.; Kanbara, T.; Hayashi, H.; Etori, H. *Macromol. Chem. Phys.* **1998,** *199*, 1807.

CHAPTER 4. ATTEMPTED GENERATION OF 2,3-DIALKYLTHIENO[2,3-*b*]PYRAZINE

Introduction

There has been a recent increase in interest in conjugated oligomeric materials, primarily because of the additional control of the properties of the oligomer material compared to the polymer material.[1-4] From a computational perspective, polymers do not have well defined structures and computational techniques are significantly less developed for infinite polymers than for well-defined molecules.[5] In addition, the polydispersity of molecular weights of polymers makes predicting the electronic properties difficult and can also result in difficulties determining trends.

Conjugated oligomers have the advantage of their well-defined structure, easier purification, fewer defects, and the possibility of more easily introducing functionalities to the final oligomer.[6] The high level of ordering attainable by the small molecules also attributes to a higher mobility, which is a desirable feature for applications such as solar cells, light emitting diodes, field effect transistors, and electrochromics.[7-19] In fact, the top charge mobilities achieved by oligomers is an entire order of magnitude higher than that of polymers.[20] In addition, with the molecules themselves being well defined, the physical properties are reproducible between batches. The well-defined structure provides the added benefit of improving the understanding of established structure-function relationships, such as the roles of donors, acceptors, and ambipolar units in the donor-acceptor framework.

However, oligomers do come with drawbacks. One of which is in the potential complicated synthetic process of generating the small molecules. Polymer synthesis requires the preparation of the monomers to be functionalized for coupling and then the polymerization

carried out. The growth of the small molecule requires an additional step of synthesis and purification for each additional unit. In addition, the processing of small molecules is usually done by vacuum deposition, which is an expensive alternative to the solution-based techniques of spin casting, screen printing, doctor blading, ink-jet printing, and roll-to-roll processing that the soluble polymers can undergo.[21-25]

The design behind small molecules commonly employs the donor-acceptor (D-A) framework. One of the main incentives of using small molecules is the increased control over the molecule itself and the fine tuning that can be done to the HOMO and LUMO energy levels by adding the appropriate unit to the molecule. The thieno[3,4-*b*]pyrazine-based compounds (TP, **4.1**) have been thoroughly investigated by the Rasmussen group and their work has added to the family of TP units with different functionalization.[26] Computational work predict that the different functionalizations result in a range of HOMO (-5.80 to -7.35 eV) and LUMO energy levels (-1.17 to -3.43) for the TP unit, as shown in Figure 4.1.[27] This wide range of energy levels make TP units ideal for small molecule systems because the different functionalization can be used to finely tune the energy levels in the desired manner.

The end cap of small molecules serves an important role for a number of reasons. The first of which is to maintain the oligomer characteristic and inhibit the molecule from undergoing some form of polymerization. This requires an end group that is stable or does not have sites that would allow for polymerization, such as a reactive hydrogen. It has also been shown that the end groups can be adjusted to affect the solubility of the oligomer.[28] A desirable small molecule end cap would therefore consist of a molecule or molecule family that can avoid polymerization, positively influence the solubility, and also have tunable electronic properties to adjust the electronics of the resulting oligomer.
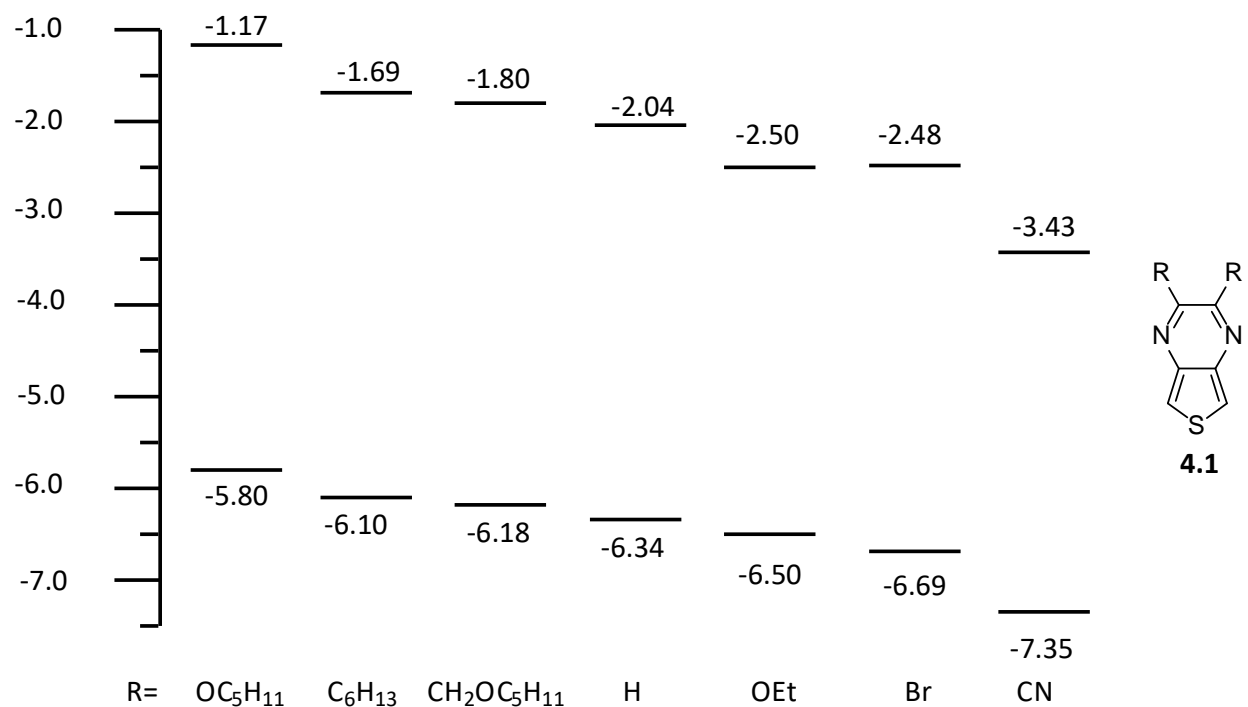
Figure 4.1. Calculated HOMO and LUMO energy levels (in eVs) for select 1st and 2nd generation TPs.[27]

The goal of this project is to generate a TP isomer that would serve as a good end cap

unit. With the large background of work already done with TPs, the new molecule would want to

have a similar synthetic design so the previous work is still applicable.[26,29-31] This would allow

for the unit to serve as a tunable end cap for conjugated small molecules. The traditional TP is

very reactive and does not satisfy the need of an end cap that would inhibit polymerization.

However, the isomer 2,3-difunctionalized thieno[2,3-*b*]pyrazine (**4.2**, Figure 4.2) would serve as

a good end capping unit that can hopefully utilize the work that has been done with TP. Upon

addition to the small molecule chain, the functionalized **4.2** would only have one aromatic

hydrogen that would allow for polymerization, but it would be highly hindered on the thiophene

ring, making polymerization unlikely and the molecule desirable for an end cap unit for

conjugated oligomers.

4.1   **4.2**
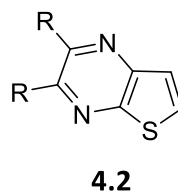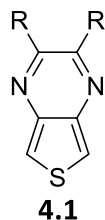
Figure 4.2. The well-established **4.1** and the desired compound of the project **4.2**.

The TP isomer thieno[2,3-*b*]pyrazine has been previously synthesized by a couple of different routes. These previous methods all focused on building the thiophene ring onto the pyrazine ring. For example, the generation of ethyl 7-aminothieno[2,3-*b*]pyrazine-6-carboxylate (**4.3**) was prepared by reacting ethyl α-mercaptoacetate with 2-chloro-3-cyanopyrazine (**4.4**) in the presence of sodium carbonate (Scheme 4.1).[32] While this did not generate the unfunctionalized thieno[2,3-*b*]pyrazine, it did prove that it was possible to generate the functionalized parent.
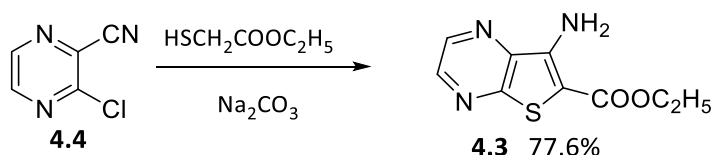
Scheme 4.1. Successful synthesis starting with **4.4** and generating **4.3**.[32]

Three additional steps were necessary in order to generate the unfuctionalized thieno[2,3-b]pyrazine from **4.3**.[33] The previous functionalized derivative **4.3** was first treated with sodium nitrite in sulfuric acid and then reduced with hypophosphorus acid to generate ethyl thieno[2,3-*b*]pyrazine-6-carboxylate (**4.5**). This then underwent saponification with potassium hydroxide in absolute ethanol to yield thieno[2,3-*b*]pyrazine-6-carboxylic acid (**4.6**). The final step was the decarboxylation with copper powder to produce thieno[2,3-*b*]pyrazine (**4.7**). The entire synthetic scheme can be seen in Scheme 4.2. This resulted in an overall yield of 32%.
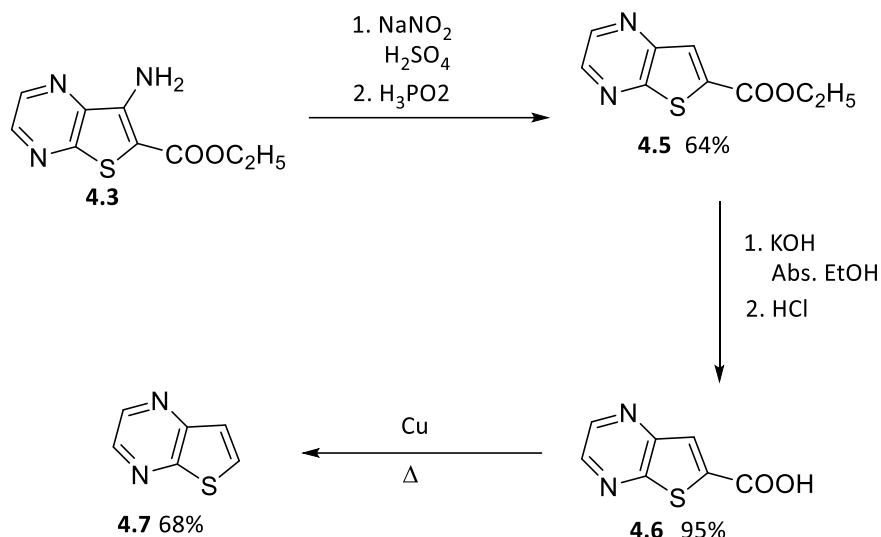
Scheme 4.2. Synthetic pathway to remove functional groups of **4.3** to generate **4.7**.[33]

Bourguignon and coworkers developed two additional methods of synthesizing

thieno[2,3-*b*]pyrazine, both of which start with the pyrazine ring and adding the fused thiophene

to it.[34] The synthesis process started with 2-chloro-3-methylpyrazine (**4.8**) and the substitution of

the chlorine atom with ethyl thioglycolate to yield ethyl 2-[(3-methylpyrazin-2-

yl)sulfanyl]acetate (**4.9**). The methyl group on the pyrazine ring was then oxidized by selenium

dioxide to generate ethyl 2-[(3-formylpyrazin-2-yl)sulfanyl]acetate (**4.10**). The ring closure was

then accomplished with the use of sodium carbonate in absolute ethanol that was heated at reflux

for two hours, resulting in ethyl thieno[2,3-*b*]pyrazine-6-carboxylate (**4.11**). The final step was

the decarboxylation which was accomplished by heating **4.11** and copper powder with an open

flame, extracting with ether, and washing with 10% sodium bicarbonate solution (Scheme 4.3).

The overall yield for this reaction was 27%.
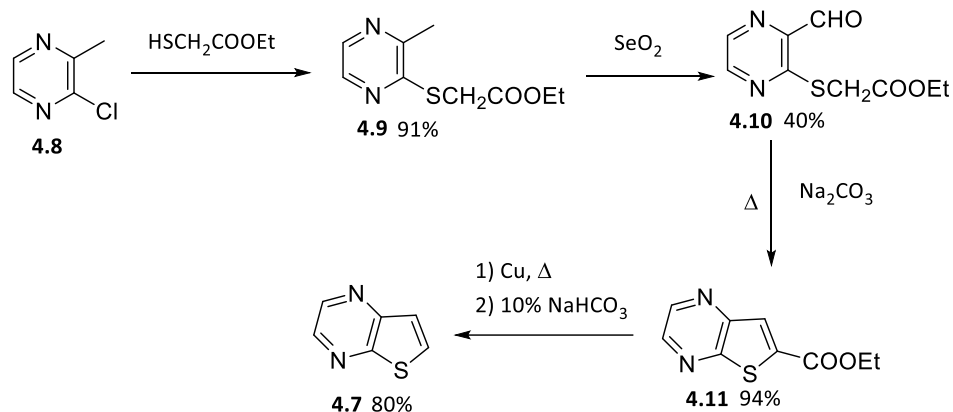
Scheme 4.3. Synthetic pathway from **4.8** to **4.7**.[34]

The second method Bourguignon developed started with 2-chloro-3-methylpyrazine (**4.8**) which then underwent a substitution by methanethiolate in absolute ethanol, generating 2-methyl-3-(methylsulfanyl)pyrazine (**4.12**). This was then oxidized by selenium dioxide to yield 2-formyl-3-(methylsulfanyl)pyrazine (**4.13**). The next step was the Wittig reaction of **4.13** with (ethoxycarbonylmethyl)triphenylphosphine which resulted in ethyl 3-[3-(methylsulfanyl)-2-pyrazinyl]propanoate (**4.14**). This was then brominated by liquid Br_2 in carbon tetrachloride, yielding ethyl 2,3-dibromo-3-[3-(methylsulfanyl)-2-pyrazinyl]propanoate (**4.15**). This would then undergo a ring closing in pyradinium chloride at high temperatures which resulted in the final product **4.7** (Scheme 4.4). The overall yield to this reaction was 7%.
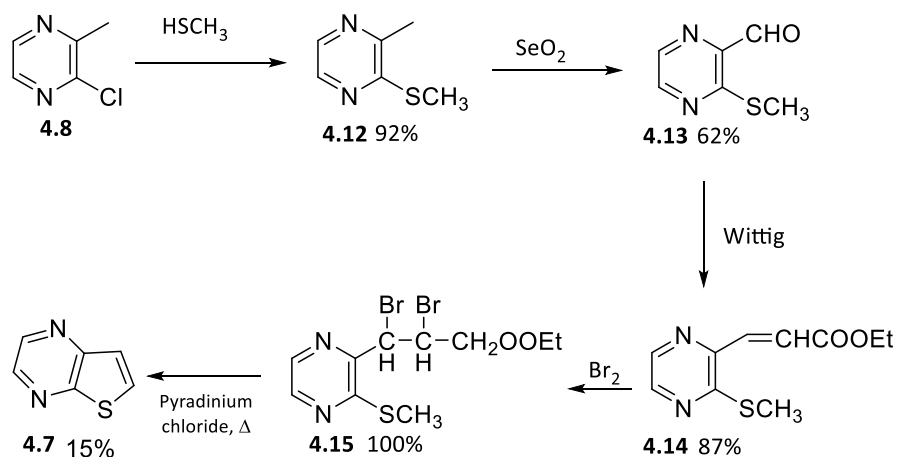
Scheme 4.4. Alternative synthetic pathway from **4.8** to generate **4.7**.[34]

103

While these routes all proved successful at generating the desired product, none of these easily allow for the incorporation of divergent methods for the production of 2,3-difunctionalized analogues, which is essential for the incorporation of solubilizing chains. However, if the synthetic scheme commonly used for generating **4.1** was adjusted to generate **4.2**, it would be possible to utilize the previous work on changing substituents on the pyrazine ring to tune the HOMO and LUMO levels of the new isomer as well as add solubilizing chains.

The proposed synthetic path to generate **4.2** would be similar to the generation of **4.1**, with the main difference being the isomeric dibromothiophene used. The proposed synthetic pathway begins with unfunctionalized thiophene which undergoes a series of brominations and debrominations to yield the desired 2,3-dibromothiophene. This compound would undergo a nitration followed by a reduction to generate the diammonium salt. It would then be possible to neutralize the salt and perform a condensation with an α-dione to generate the desired functionalized **4.2**. The proposed synthetic scheme for the target compound can be seen in Scheme 4.5.
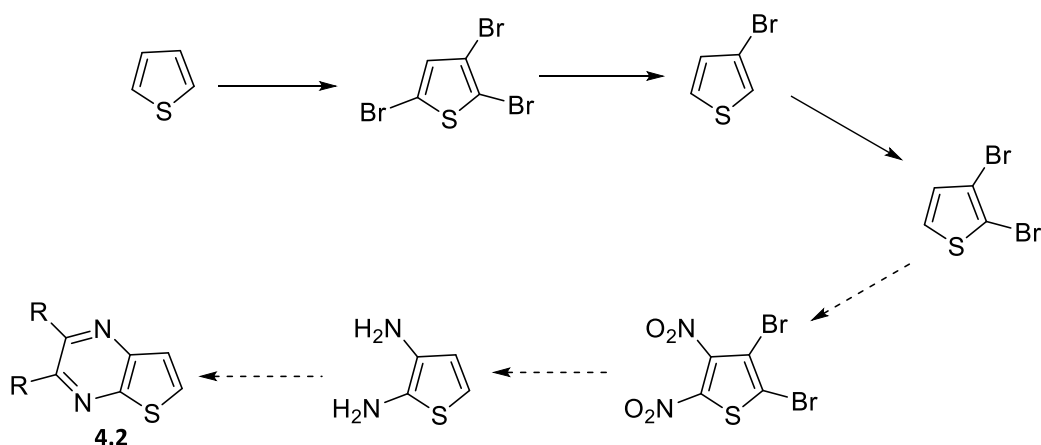
Scheme 4.5. Proposed synthetic scheme for the generation of 2,3-dialkylthieno[2,3-*b*]pyrazine starting from unfunctionalized thiophene and mirroring the method used to generate 2,3-dialkylthieno[3,4-*b*]pyrazine.

Results and Discussion

Synthesis of 2,3-dibromothiophene

Just as thieno[3,4-*b*]pyrazine (**4.1**) molecules require the generation of a dibromo species before the nitration, the thieno[2,3-*b*]pyrazine (**4.2**) isomer will also require a dibromo species. The α-position on the thiophene is the most reactive site and direction nitration would not result in the desired compound. Direct nitration of thiophene will result in nitro groups at the incorrect sites and could result in the decomposition of the thiophene ring.[35-37] The active *α*-positions was convenient when synthesizing the 2,5-dibromothiophene in one step from unfunctionalized thiophene and could then undergo nitration in the synthetic route of **4.1**. However, the necessary dibromo species for **4.2** requires 2,3-dibromothiophene (**4.16**), which necessitates additional steps.

A means of directly synthesizing **4.16** from thiophene (**4.17**) has not yet been developed, however it can be accomplished in a three-step process (Scheme 4.6). Unfunctionalized **4.17** is first brominated with three equivalences of Br_2 to generate the 2,3,5-tribromothiophene (**4.18**), as well as a lesser amount of 2,5-dibromothiphene and 2,3,4,5-tetrabromothiophene. The desired **4.18** is then isolated by distillation.

Unfortunately, at this point the 5- position is brominated and it is difficult to selectively debrominate the 5- position while leaving the bromine at the 2- position intact. Instead, zinc metal is added in the presence of acetic acid to debrominate **4.18** at both positions to yield 3-bromothiophene (**4.19**). The monobromo- **4.19** can then be gently brominated with Br_2 in HBr to generate the desired **4.16** in high yields.

4.17

4.16

Br$_2$/HBr
Diethyl ether

Br$_2$
AcOH

Br
Br   S   Br

4.18

Zn
AcOH
H$_2$O

Br

4.19
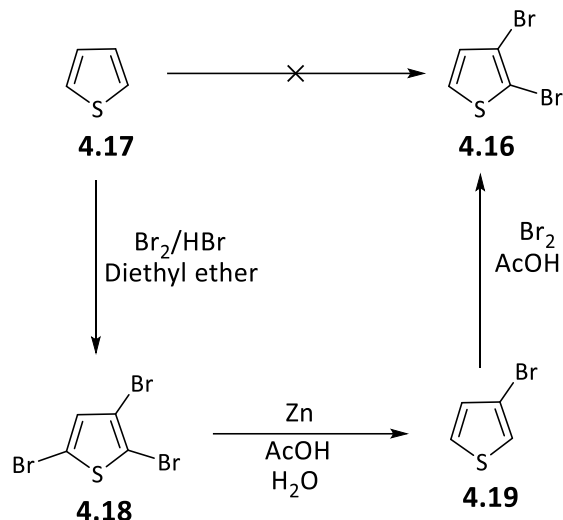
Scheme 4.6. The three-step synthetic pathway used to brominate **4.17**, resulting in the desired **4.16**.

Synthesis of 2,3-dibromo-4,5-dinitrothiophene

With **4.16** being isolated it was now necessary to generate the 2,3-dibromo-4,5-dinitrothiophene (**4.20**) in order to proceed toward the desired **4.2**. Fortunately, there was a substantial amount of work done with the synthesis and characterization of 2,5-dibromo-3,4-dinitrothiophene that provides a solid foundation for the generation of the new species.[37-43] The conditions used to nitrate the 2,5-dibromothiophene were also used to nitrate **4.16**, resulting in a red crystalline material (Scheme 4.7).

Br
S   Br

4.16

HNO$_3$
H$_2$SO$_4$
H$_2$SO$_4$ (fuming)

O$_2$N   Br
O$_2$N   S   Br

4.20
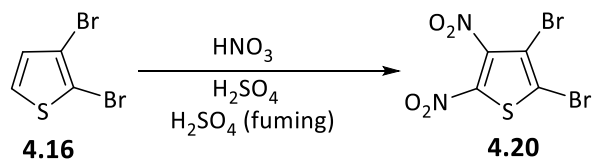
Scheme 4.7. Nitration of **4.16**, resulting in **4.20**.

It is worth noting that during the synthesis process, there was a calculation mistake during one of the reactions that resulted in only a single equivalence of nitric acid being added rather than two equivalences (Scheme 4.8), resulting in 2,3-dibromo-5-nitrothiophene (**4.21**).

106

This is important due to the difficulties with characterizing the nitrated species and this provides a step between the starting dibromo species and the desired dibromo, dinitro species.
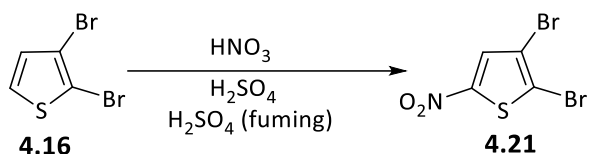
Scheme 4.8. Nitration of **4.16**, resulting in **4.21** when only one equivalence of HNO$_3$ was added.

Difficulties with the Reduction of 4.20

In hopes of maintaining synthetic consistencies with **4.1**, the same synthetic approach was taken for the debromination and reduction of **4.20** in order to generate 2,3-diammoniumthiophene salt (**4.22**), with the appropriate counterions also present as Cl$^-$ and SnCl$_6^{2-}$ (Scheme 4.9). This required adding **4.20** to a solution of HCl cooled by an ice bath followed by tin metal being added slowly, maintaining the solution at 0 °C and the mixture stirring for 20 hours. Unfortunately, after the reduction there was little material collected by vacuum filtration. A red solution was obtained after extracting with petroleum ether. The solvent was removed by reduced pressure and a red material was collected, which upon characterization had different spectral and physical features than **4.20**, demonstrating that a reaction had occurred but the compound could not be further characterized. This compound would be consistently collected for all of the further reduction attempts. The duration of the reduction was increased from 20 hours to 40 hours, but there was no change in the resulting product.

More intense reduction methods were employed in hopes of generating the desired **4.22**. The first method was to increase the stirring temperature for the HCl and tin to room temperature instead of maintaining 0 °C. This unfortunately did not have any noticeable changes to the products isolated, with nothing additional being collected by vacuum filtration after cooling and no noticeable change in the extraction.

The next change was to perform the reduction with SnCl$_2$ in a 1:1 mixture by volume of ethanol and HCl. This was heated at reflux for 20 hours and was then collected by vacuum filtration after the solvent was removed by reduced pressure and the solution was cooled. There was still no isolated material by vacuum filtration. The duration of reflux was increased to 72 hours, with no noticeable change in the reaction outcome.
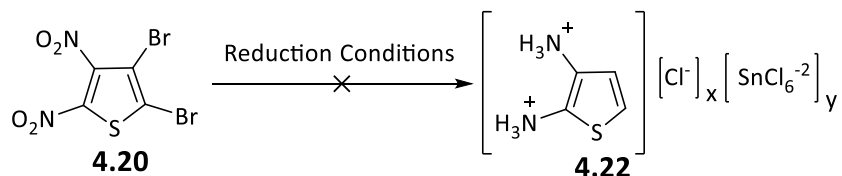
Scheme 4.9. The attempted reaction of the reduction of **4.20** by the different methods shown in Table 4.1 to generate **4.22**.

Table 4.1. The different reduction conditions used for the generation of **4.22**, as shown in Scheme 4.9.

Reduction Attempt	Reagents	Temperature	Duration (h)
1	Sn, HCl	0 °C	20
2	Sn, HCl	0 °C	40
3	Sn, HCl	RT	40
4	SnCl$_2$, EtOH, HCl	Reflux	20
5	SnCl$_2$, EtOH, HCl	Reflux	72

The different methods of reduction were then all repeated, with the reaction mixture no longer trying to be isolated by vacuum filtration, but instead being extracted with petroleum ether, neutralized by a solution of 1.0 M KOH (Scheme 4.10), and then extracted with ethyl acetate and removing the solvent by reduced pressure in hopes of directly isolating 2,3-diaminothiophene (**4.23**) rather than the salt **4.22**. The solution became very cloudy upon addition of the base, similar to what occurs upon the neutralization of the 3,4-diammonium thiophene salt during the synthesis of **4.1**. Unfortunately, upon extraction with ethyl acetate the

crude ^{1}H NMR showed no signs of the anticipated **4.23**. The crude materials were then purified

by column chromatography in hopes of being able to isolate a portion of the desired product, but

this was met with no success.
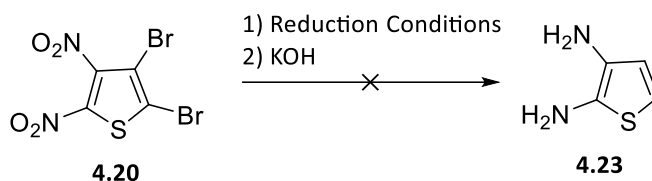
Scheme 4.10. Attempted reduction and neutralization of **4.20** to generate **4.23**.

^{13}C NMR

The characterization of **4.20** came with some difficulties. Due to its lack of protons, [1]H

NMR would not be a fruitful means of characterization other than to determine a lack of

completion in the reaction. There were also difficulties using the high-resolution mass

spectroscopy that resulted in no relatable values being obtained. Attempts were also made at

recrystallizing the compound but came with no success. This made it difficult to ascertain

whether the compound was being synthesized, or if the nitration was causing the compound to

undergo decomposition, which is a concern when nitrating thiophene species.[35,41,42]

Fortunately, the ^{13}C NMR provided a means for characterizing the compound. Figure 4.3

shows the relevant region for the ^{13}C NMR of **4.20**. It is worth noting that only two carbons were

detected, whereas there should be four present. The carbons bound to the nitro functionalities

have been known to have long relaxation times.[37] The delay time increased to 5 s and the number

of scans was greatly increased well beyond standard NMR parameters, but the nitro carbons

were unable to be observed. However, what this does indicate is that either the two carbons were

not able to be observed via ^{13}C NMR and the desired species was generated, or all of the carbons

are accounted for and it is a symmetric species, which is very unlikely considering the starting

material.
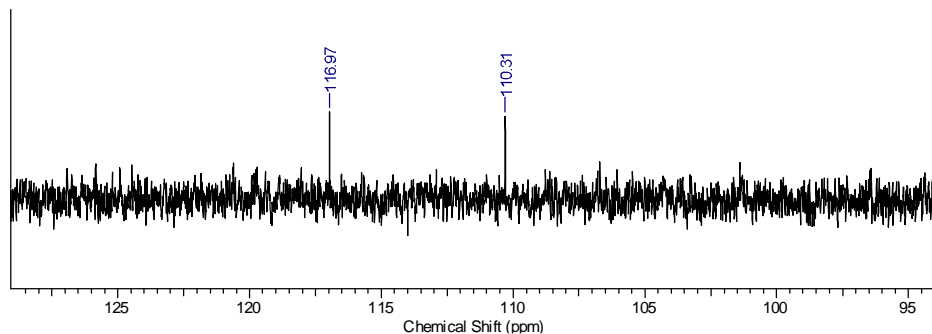
Figure 4.3. ^{13}C NMR of **4.20**. Nitro-carbons were not observed due to long relaxation times.

It was mentioned in the synthesis section that there was an issue during the early stages of the synthesis of the **4.20** that only a single equivalence of nitric acid was added instead of two equivalences, resulting in the generating of what was assumed to be 2,3-dibromo-5-nitrothiophene (**4.21**). This proves to be useful because it can act as a characterizable halfway point between **4.16** and the desired **4.20**. Figure 4.4 presents the ^{13}C NMR of **4.21**.
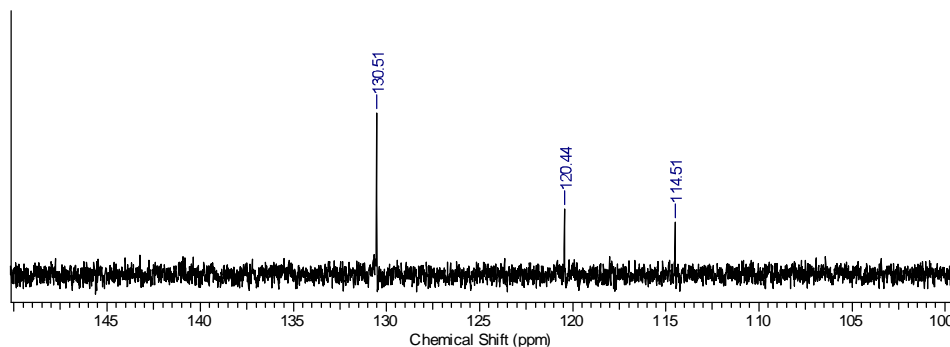
Figure 4.4. ^{13}C NMR of **4.21**. Nitro-carbon was not observed due to long relaxation time.

There are a number of notable aspects of Figure 4.4 that support that **4.20** was generated. The first of which is the presence of the peaks at 120.44 and 114.51 ppm of Figure 4.4 that compare closely to the 116.97 and 110.31 ppm peaks in Figure 4.3. It is feasible that the presence of the nitro group at the 4 position would result in the shift noted between the two compounds. In addition, the intensity of the peak at 130.51 ppm of Figure 4.4 indicates that the carbon has a faster relaxation time than the other species. The ^{1}H NMR also had a single peak at

7.79 ppm, providing additional support that the dinitration was not completed and the compound

is also not undergoing decomposition upon addition of the first nitro group.

UV-Vis Absorption Spectroscopy

Solution absorption data in CH_3CN of **4.20** and **4.21** were analyzed via UV-vis

spectroscopy. The representative absorption spectra are shown in Figure 4.5. While there was not

a substantial amount of structural information apparent from the absorption, it does provide some

useful answers about the progress of the synthesis process.
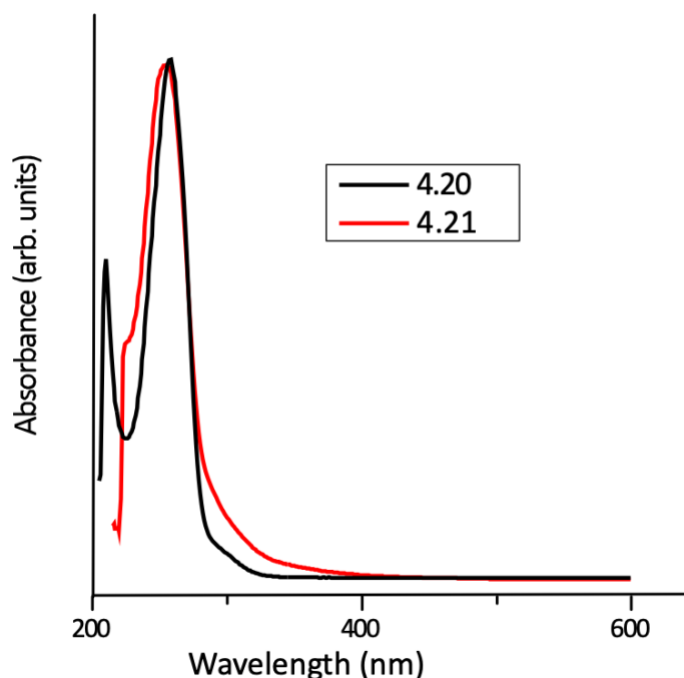
Figure 4.5. Absorbance comparison of **4.20** and **4.21** in CH_3CN.

The differences and similarities in the absorptions indicate that they are similar

compounds. The onset of absorption of **4.20** compared to **4.21** does indicate that the compound

did not undergo some sort of oligiomerization because that would have resulted in a noticeable

shift in the onset of absorption. It is also an indication that **4.20** did not undergo decomposition

or ring opening during the nitration process.

111

<div align="center">**Conclusion**</div>

The synthesis of the 2,3-dialkylthieno[2,3-*b*]pyrazine (**4.2**) did not prove to be successful by adjusting the well-established method of synthesizing 2,3-dialkythieno[2,3-*b*]pyrazine (**4.1**). The work presented demonstrates that the synthetic process was effective until reduction of the 2,3-dibromo-4,5-dinitrothiophene (**4.20**). It was at this point the previously established reduction methods did not prove efficient and even utilizing more rigorous means of reduction did not generate 2,3-diammoniumthiophene salt (**4.22**) as desired. In order to generate the desired **4.2**, a means of reduction not investigated must be employed, such as Raney nickel, hydrazine, or using a palladium catalyst, although care will need to be taken to ensure the thiophene ring does not also get reduced.[43] If alternative reduction methods do not work a synthetic route involving the building of the thiophene onto the pyrazine ring may have to be implemented, with adjustments made to allow for functionalization.

The majority of the work presented is focused on establishing that **4.20** was successfully synthesized. The reason for all of this emphasis on the successful generation of the **4.20** is to bring to the light the fact that the reduction step was the limiting factor in the success of this project and not the unsuccessful synthesis of **4.20**. Despite **4.20** having difficulties with its characterization, there is evidence indicating that it was successfully generated, but was unable to undergo the reduction in the desired manner to allow for the eventual generation of **4.2** by this synthetic route.

<div align="center">**Experimental**</div>

General

Unless stated, all materials were reagent grade and used without further purification. All chromatographic separations were performed with standard chromatography methods with silica

gel as the stationary phase (230-400 mesh). Dry THF was obtained via distillation over sodium and benzophenone. All glassware was oven-dried, assembled hot and cooled under dry nitrogen before use. Transfer of liquids was carried out using standard syringe techniques and all reactions were done in an inert, dry nitrogen atmosphere with a constant stream of nitrogen. Melting points were determined using a digital thermometer couple with a 0.1 °C resolution. The ^{1}H and ^{13}C NMR were completed on a 400 MHz spectrometer. All NMR data was referenced to the chloroform signal and peak multiplicity was reported as follows: s = singlet. HRMS was performed in house.

Materials

2,3,5-Tribromothiophene (**4.18**),[44] 3-bromothiophene (**4.19**),[45] and 2,3-dibromothiophene (**4.16**)[46] were prepared as previously reported. Acetonitrile was dried over CaH_2 and distilled prior to use.

2,3-Dibromo-4,5-dinitrothiophene (4.20)

To a 150 mL, round bottom flask was added sulfuric acid (10 mL, 0.18 mol) and 20% fuming sulfuric acid (30 mL, 0.54 mol). The solution was then cooled to 0 °C by an ice bath. Once cooled to this temperature, 2,3-dibromothiophene (10.97 g, 0.045 mol) was slowly added via addition funnel, maintaining a temperature below 10 °C. After finishing the addition of the thiophene, nitric acid (12 mL, 0.29 mol) was slowly added maintaining a temperature below 20 °C. The reaction was then allowed to stir for three hours after the nitric acid was completely added, maintaining a temperature below 10 °C for the duration. The mixture was then poured onto 500 mL of ice. The organic phase was then extracted with ethyl acetate and thoroughly washed with water. The solvent was removed by reduced pressure and then recrystallized with

methanol. The solid was then collected by vacuum filtration, resulting in 10. g (67%) of red, crystalline material. Mp. 137.5 °C (dec); ^{13}C NMR: δ 117.3, 110.6.

2,3-Dibromo-5-nitrothiophene (4.21)

To a 150 mL, round bottom flask was added sulfuric acid (10 mL, 0.18 mol) and 20% fuming sulfuric acid (30 mL, 0.54 mol). The solution was then cooled to 0 °C by an ice bath. Once cooled to this temperature, 2,3-dibromothiophene (10.97 g, 0.045 mol) was slowly added via addition funnel, maintaining a temperature below 10 °C. After finishing the addition of the thiophene, nitric acid (2.8 mL, 0.068 mol) was slowly added maintaining a temperature below 20 °C. The reaction was then allowed to stir for three hours after the nitric acid was completely added, maintaining a temperature below 10 °C for the duration. The mixture was then poured onto 500 mL of ice. The organic phase was then extracted with ethyl acetate and thoroughly washed with water. The solvent was removed by reduced pressure and then recrystallized with methanol. The solid was then collected by vacuum filtration, resulting in 5.8 g (45%) of red, crystalline material. Mp. 122.0 °C (dec); ^{1}H NMR: δ 7.76 (s, 1H); ^{13}C NMR: δ 130.8, 120.8, 114.8.

Reduction attempts using Sn and HCl

To a 250 mL, 3-neck round bottom flask was added HCl (25 mL, 0.29 mol) and 2,3-dibromo-4,5-dinitrothiophene (0.27 g, 0.81 mmol). The solution was cooled to 0 °C by an ice bath and stirred with a mechanical stirrer for its entirety. Tin (0.77 g, 6.5 mmol) was slowly added, maintaining a temperature below 10 °C. This was then allowed to stir for different durations and temperatures, as shown in Table 4.1. Vacuum filtration resulted in no product being collected. The filtrate was extracted with petroleum ether which yielded a red solid upon

the solvent being removed by reduced pressure. Its spectra was not the same as the starting material but it could not be definitively characterized.

Reduction attempts using SnCl₂

To a 150 mL, 3-neck round bottom flask was added 2,3-dibromo-4,5-dinitrothiophene (1.33 g, 4.00 mmol), $SnCl_2$(6.82 g, 36.0 mmol), ethanol (30 mL), and HCl (30 mL). An inert nitrogen atmosphere was obtained by flushing the solution three times. This solution was then heated at reflux for the durations stated in Table 4.1. After reflux, the solution was cooled to 0 °C by an ice bath and then collected by vacuum filtration but not product was collected. The filtrate was extracted with petroleum ether which yielded a red solid upon the solvent being removed by reduced pressure. Its spectra was not the same as the starting material but it could not be definitively characterized.

References

1. Roders, M.; Kolaczkowki, M. A.; Hollingsworth, W. R.; Seban, R.; Liu, Y.; Ayzner, A. L. *J. Phys. Chem. C* **2019**, *123*, 27305.

2. Heo, Y.-J.; Lim, B.; Jung, Y.-S.; Hwang, K.; Kim, J.-E.; Lee, D.; Lim, D.-H.; Park, J. M.; Kim, D.-Y. *ACS Appl. Energy Mater* **2019**, *2*, 8885.

3. Lin, Y.; Li, Y.; Zhan, X. *Chem. Soc. Rev.* **2012**, *41*, 4245.

4. Sathiyan, G.; Sivakumar, E. K. T.; Ganesamoorthy, R.; Thangamuthu, R.; Sakthivel, P. *Tetrahedron Lett*. **2016**, *57*, 243.

5. Zade, S. S.; Zamoshchik, N.; Bendikov, M. *Acc. Chem. Res*. **2011**, *44*, 14.

6. Ellinger, S.; Ziener, U.; Thewalt, U.; Landfester, K.; Moeller, M. *Chem. Mater*. **2007**, *19*, 1070.

7. Gunes, S.; Neugebauer, H.; Sariciftci, N. S. *Chem. Rev.* **2007**, *107*, 1324.

8. Cheng, Y. J.; Yang, S. H.; Hsu, C. S. *Chem. Rev.* **2009**, *109*, 5868.

9. Dennler, G.; Scharber, M. C.; Brabec, C. *J. Adv. Mater.* **2009**, *21*, 1323.

10. Helgesen, M.; Sondergaard, R.; Krebs, F. C. *J. Mater. Chem.* **2010**, *20*, 36.

11.   Kamtekar, K. T.; Monkman, A. P.; Bryce, M. R. *Adv. Mater.* **2010**, *22*, 572.

12.   Grimsdale, A. C.; Chan, K. L.; Martin, R. E.; Jokisz, P. G.; Holmes, A. B. *Chem. Rev.* **2009**, *109*, 897.

13.   Perepichka, I. F.; Perepichka, D. F.; Meng, H.; Wudl, F. *Adv. Mater.* **2005**, *17*, 2281.

14.   Perepichka, D. F.; Perepichka, I. F.; Meng, H.; Wudl, F. In *Organic Light-Emitting Materials and Devices*; Li, Z. R., Meng, H., Eds.; CREC Press, Boca Raton, FL, 2006, Chapter 2.

15.   Facchetti, A. *Mater. Today* **2007**, *10*, 28.

16.   Allard, S.; Forster, M.; Souharce, B.; Thiem, H.; Scherf, U. *Angew. Chem., Int. Ed.* **2008**, *47*, 4070.

17.   Beaujuge, P. M.; Reynolds, J. R. *Chem. Rev.* **2010**, *110*, 268.

18.   Mortimer, R. J.; Dyer, A. L.; Reynolds, J. R. *Displays* **2006**, *27*, 2.

19.   Sonmez, G. *Chem. Commun.* **2005**, 5251.

20.   Arias, A. C.; MacKenzie, J. D.; McCulloch, I.; Rivnay, J.; Sallco, A. *Chem. Rev.* **2010**, *110*, 3.

21.   Hoppe, H.; Sariciftci, N. S. J. *Mater. Chem.* **2006**, *16*, 45.

22.   Pardo, D. A.; Jabbour, G. E.; Peyghambarian, N. *Adv. Mater.* **2000**, *12*, 1249.

23.   Padinger, F.; Brabec, C. J.; Fromherz, T.; Hummelen, J. C.; Sariciftci, N. S. *Opto-Electronics Rev.* **2000**, *8*, 280.

24.   Singh, M.; Haverinen, H. M.; Dhagat, P.; Jabbour, G. E. *Adv. Mater.* **2010**, *22*, 673.

25.   Krebs, F. C. *Org. Electron.* **2009**, *10*, 3.

26.   Rasmussen, S. C.; Schwiderski, R. L.; Mulholland, M. E. *Chem. Commun.* **2011**, *47*, 11394.

27.   Wen, L.; Nietfeld, J. P.; Amb, C. M.; Rasmussen, S. C. *J. Org. Chem.* **2008**, *73*, 8529.

28.   Cote, M.; Rogueda, P. G. A.; Griffiths, P. C. *JPP* **2008**, *60*, 593.

29.   Rasmussen, S. C.; Mulholland, M. E.; Schwiderski, R. L.; Larsen, C. A. J. *Heterocyclic Chem.* **2012**, *49*, 479.

30.   Rasmussen, S. C.; Pomerantz, M. In *The Handbook of Conducting Polymers*, 3rd ed.; Skotheim, T. A., Reynolds, J. R., Eds.; CRC Press: Boca Raton, FL, 2007; Volume 1, Chapter 12.

31.   Rasmussen, S. C.; Ogawa, K.; Rothstein, S. D. In *The Handbook of Organic Electronics and Photonics*; Nalwa, H. S., Ed.; American Scientific Publishers: Stevenson Ranch, CA, 2008; Volume 1, Chapter 1.

32.   Schneller, S. W.; Clough, F. W. *J. Heterocyclic Chem.* **1975**, *12*, 513.

33.   Schneller, S. W.; Clough, F. W.; Hardee, L. E. *J. Heterocyclic Chem.* **1976**, *13*, 273.

34.   Bourguignon, J.; Lemarchand, G.; Quéguiner, G. *J. Heterocyclic Chem.* **1980**, *17*, 257.

35.   Taylor, R. In *Thiophene and Its Derivatives*; Granowitz, S., Ed.; The Chemistry of Heterocyclic Compounds, Volume. 44, part 2; John Wiley & Sons: New York, 1985; p. 1.

36.   Butler, A. R.; Hendry, J. B. *J. Chem. Soc. B* **1971**, 102.

37.   Wen, L.; Rasmussen, S. C. *J. Chem. Crystallogr.* **2007**, *37*, 387.

38.   Kreis, H. *Chem. Ber.* **1884**, *17*, 2073.

39.   Mozingo, R.; Harris, S. A.; Wolf, D. E.; Hoffhine, C. E.; Easton, N. R.; Folkers, K. *J. Am. Chem. Soc.* **1945**, *67*, 2902.

40.   Kenning, D. D.; Mitchell, K. A.; Calhoun, T. R.; Funfar, M. R.; Sattler, D. J.; Rasmussen, S. C. *J. Org. Chem.* **2002**, *67*, 9073.

41.   Butler, A. R.; Hendry, J. B. *J. Chem. Soc. B* **1971**, 102.

42.   Katritzky, A. R.; Pozharskii, A. F. In *Handbook of Heterocyclic Chemistry*, 2nd ed.; Pergamon: New York, 2000; p 317.

43.   Orlandi, M.; Brenna, D.; Harms, R.; Jost, S.; Benaglia, M. *Org. Process Res. Dev.* **2018**, *22*, 430.

44.   Brandsma, L.; Verkruijsse, H. D. *Synth. Commun.* **1988**, *18*, 1763.

45.   Heinrich, A. C. J.; Thiedemann, B.; Gates, P. J.; Staubitz, A. *Org. Lett.* **2013**, *15*, 4666.

46.   Gronowitz, S.; Zhang, Y.; Hörnfeldt, A.-B. *Acta Chem. Scand.* **1992**, *46*, 654.

CHAPTER 5. INVESTIGATION OF THE IMPACT OF SOLUTION TEMPERATURE ON THE POWER CONVERSION EFFICIENCY OF POLY(3-HEXYLTHIOPHENE):[6,6]-PHENYL-C61-BUTYRIC ACID METHYL ESTER ORGANIC SOLAR CELLS[‡]

Introduction

One promising application of conjugated polymers (CPs) is their use to fabricate organic photovoltaics (OPVs).[1-4] OPVs provide a means to generate electricity from light with a method that is less expensive to fabricate compared to inorganic solar cells. There are multiple methods of OPV fabrication, each with their own benefits and limitations.[5] OPVs have greatly increased in efficiency since their early days.[6] Initial OPVs had power conversion efficiencies (PCE) of less than 1% but are now exceeding 16%.[6,7]

In order for charge generation to occur in OPVs, the donor material must first absorb a photon, leading to the formation of a bound electron-hole pair, called an exciton (Figure 5.1). Classically, the donor material used is a conjugated polymer. This is not to be confused with the donor that was previously discussed when dealing with the synthesis of polymeric materials using a donor-acceptor framework. The exciton needs to diffuse to a donor-acceptor interface within its lifetime. Once there it is necessary to have a charge transfer occur between the donor and the acceptor material, resulting in the hole being present on the donor and the electron on the acceptor. In order to effectively have the charge transfer occur, it is important that the LUMO of the acceptor be lower in energy than the LUMO of the donor. The acceptor is commonly a

---

[‡] The material in this chapter was co-authored by Trent E. Anderson and Muhammet Erkhan Köse. Trent Anderson was responsible for designing the project, fabricating and characterizing the solar cells, analyzing the data, and writing the manuscript. Erkhan Köse was responsible for advising the analysis and editing the manuscript.

fullerene-based material, with [6,6]-phenyl-C61-butyric acid methyl ester (PC$_{60}$BM, Figure 5.2) being the most common. There has substantial progress toward the use of conjugated polymers also being used as acceptors.[4] Upon charge separation, the charges can then be transported to their respective electrodes and charge is generated.[8]
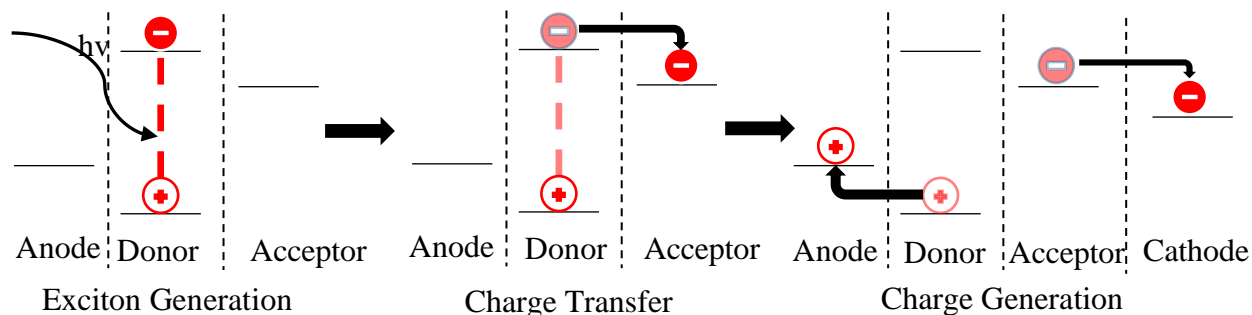
Figure 5.1. Simplified model of an exciton within an OPV resulting in charge generation.
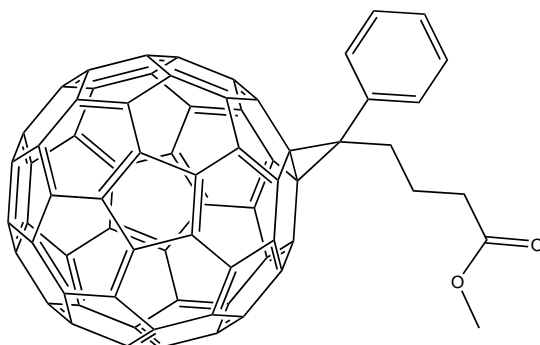
Figure 5.2. Structure of PC$_{60}$BM.

While the physical processes that occur during the generation of charge from OPVs is well understood, the fabrication of devices to accomplish these tasks is more complicated. One of the most influential changes that has occurred throughout the history of OPV device fabrication is the arrangement of the donor and acceptor material within the device.[6] It is essential with the organization of the donor and acceptor material to allow for charge separation as well as having there be a pathway for the charge to flow to its respective electrode. The first OPV design used a bilayer device (Figure 5.3 A), in which a layer of the donor material was first

deposited onto the OPV device, either by spray coating, vacuum deposition, or spin coating. The acceptor layer would then be added on top of the donor layer to allow for the charge carriers to complete its circuit upon charge generation. However, there were a number of issues with this design. The lifetime of an exciton is so short that the charge must be generated within 10-20 nm from the donor-acceptor interface in order for the exciton to diffuse to the donor-acceptor interface and separate before recombination. This requires there to be very thin films ($\approx$30-40 nm), which then minimizes the amount of light the film can absorb to generate the charge carriers.[9-17] The combination of these two issues were substantial enough that improved methods were necessary for the fabrication of OPVs to be viable.

In order to increase the interfacial area between the donor and acceptor material the two components are blended together and then cast onto the substrate, most commonly through spin coating or spray coating. This alternative method of fabricating solar cells as a mixture rather than as layers is described as bulk heterojunction (BHJ) (Figure 5.3 C). This new means of preparing the solar cell heavily increases the interfacial area and allows for increasing the thickness of the films ($\approx$100 nm) but comes with its own complications. With the two components in the system so intimately mixed, the electrons and holes generated within the OPV have no driving force guiding their direction other than concentration gradient of the donor and the acceptor material. Without any outside influence, the electrons would be localized on the acceptor material and the holes on the donor material and may not be diffusing to their appropriate electrodes. The bilayer device did not have this issue because it had a clearly defined donor and acceptor region for holes and electrons to transport to, respectively. In order to counteract this, electrodes with different work-functions are used to provide a symmetry breaking condition to influence the preferred direction for the charge carriers to travel.[18] In

addition to the use of the different electrodes providing a symmetry breaking condition, there

still must be a continuous pathway for the hole and electron transporting phases that reach the

electrodes, an issue that the bilayer configuration did not have due to its direct layering.[19] This

means that the nanoscale morphology in the BHJ has a substantial impact on the efficiency of

OPV devices. Regions that do not have a pathway to the electrodes are referred to as traps.

Fortunately, the benefits of the BHJ greatly outweigh the limitations compared to the bilayer

configuration and the BHJ is the donor-acceptor configuration used for the majority of OPV

fabrication.
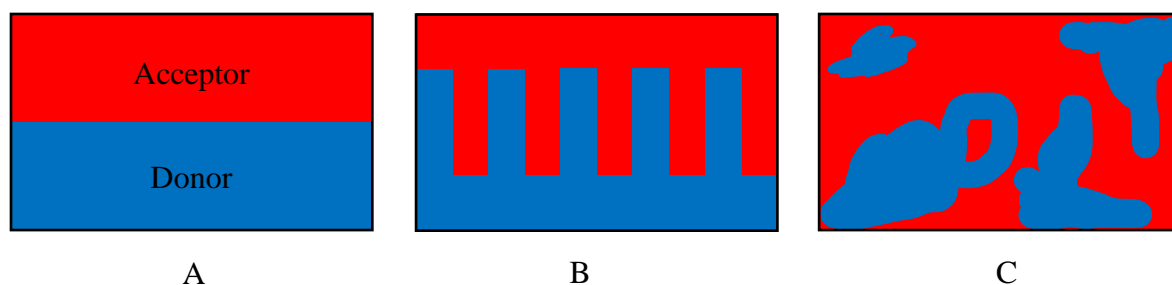
Figure 5.3. Different models for the active phase of an OPV. A) the simplest is a layer of donor with a layer of acceptor material on top of it. B) The structured interlinking of the two phases allows for the most opportunity for charge separation. C) The most common method of BHJ.

A standard sandwich architecture is used in the fabrication of BHJ OPVs (Figure 5.4).

The substrate consists of a transparent, conducting electrode, usually indium tin oxide (ITO), on

glass. The ITO is then treated, usually with a blend of poly(3,4-ethylenedioxythiophene) and

poly(styrene sulfonate (PEDOT:PSS), to improve its surface quality and facilitate hole transfer.

PEDOT:PSS coats the ITO from an aqueous solution. The layer consisting of the donor and

acceptor material is than deposited on top of the PEDOT:PSS. This layer is referred to as the

active layer. This active layer can be deposited a number of a different ways but is most

commonly done through solution spin coating or vacuum deposition. Lithium fluoride (LiF) is

commonly vacuum deposited onto the active layer to act as a buffer layer between the cathode

materials and the organic layer. This serves a number of different purposes. When the cathode is deposited onto the device it is common for the metal to diffuse into the polymeric layers which causes electrical shorting and limits the lifetime of the device.[20-22] The LiF layer has been shown to protect the active layer from this diffusion. This interfacial layer can also increase the rate of charge transfer and prevent recombination from occurring at the electrodes.[23-25] The final layer is the electrode, where Al is primarily used. It can be deposited a number of different means, such as spray-coating of Al nanoparticles, Al pastes and nanowire meshes, and sputtering.[26,27] Upon the electrode being layered, it is necessary to protect the entire system from atmospheric conditions or it will suffer loss of efficiency and reduced lifetime.[28] This can be done by placing the device in an inert container or encapsulated with a glass covering. It is important that contact can still be made with the electrodes so the characteristics of the OPV can be measured.
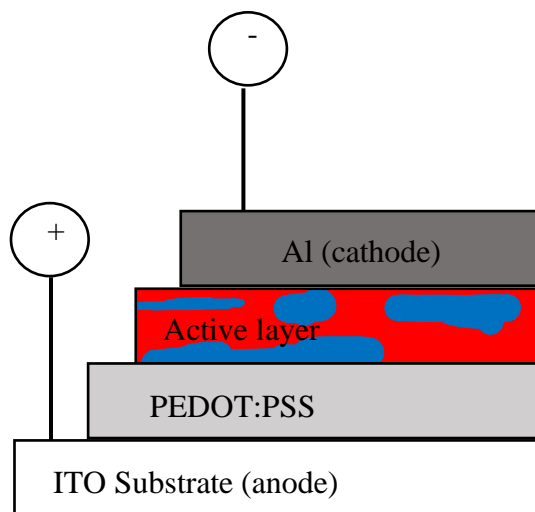
Figure 5.4. The standard structure of an OPV device.

Once fabricated, the OPV device must be characterized in order to determine the efficiency of the solar cell, as well as other characteristics. A measurement of the current density vs. voltage is plotted while the solar cell generates power under illumination (Figure 5.5). The power conversion efficiency (PCE) of a cell is the amount of power it generates vs. the power

applied to the solar cell through the light source. The power generated is equal to the product of the open circuit voltage (V_{OC}), the short circuit current density (J_{SC}), and the fill factor (FF). These three characteristics of solar cells are what is strived to be optimized to generate solar cells with higher PCEs.
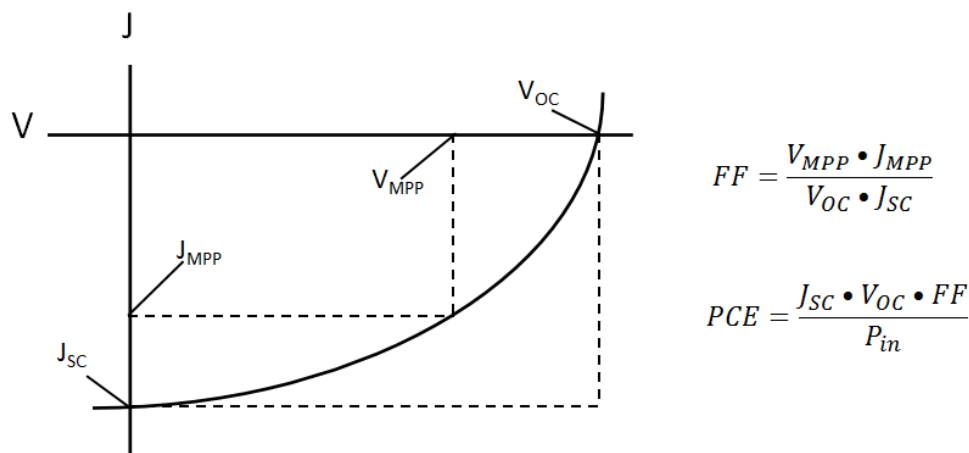
Figure 5.5. The voltage (V) vs. charge density (J) for an OPV. The equations for fill factor and power conversion efficiency are also shown for a given power input (P_{in}).

The V_{OC} is the voltage of the current density vs. voltage plot when the current density is zero. The energy difference between the HOMO of the donor material and the LUMO of the acceptor material has been found to have a linear relationship with the V_{OC}.[29,30] Charge carrier losses at electrodes can lower the V_{OC} and the morphology of the active layer of the BHJ film also affects the V_{OC}.[31,32] The J_{SC} is determined by the current density when the voltage is zero on the current density vs. voltage plot. The origin of the J_{SC} is the number of excitons that can be generated during solar illumination.[33] The donor material is the primary contributor to the J_{SC} and is strongly dependent of the E_g of the material. The smaller the E_g, the larger the J_{SC}. The FF of an OPV is how efficient the device generates and separates charges compared to the ideal scenario of all charge carriers being generated and separated upon illumination. This value is found by determining the voltage and current density that result in the greatest power (V_{MPP} and

123

J_{MPP}) and taking the product of those two numbers and dividing that by the product of V_{OC} and the J_{SC}. The FF is largely dependent on the morphology of the active layer, where a desirable morphology would be one in which there is optimal charge generation and separation.

With these three basic characteristics it would seem simple to fabricate an OPV that has a high PCE. However, there are a number of competing factors that limit the PCE. A large energy difference is desired between the HOMO of the donor and the LUMO of the acceptor in order obtain a large V_{OC} while a small energy difference between the HOMO and LUMO of the donor produces a large J_{SC}. In addition, it is believed the LUMO of the donor needs to be about 0.3 eV higher than the LUMO of the acceptor in order for efficient charge dissociation and minimal recombination.[33] The competition here results in either an increase to the V_{OC} and a decrease to the J_{SC} or the opposite.

While the majority of work focuses on the active layer of the solar cells, there are a large number of fabrication optimizations that can be employed to generate a higher PCE. One of the most fundamental means of altering the method of solar cell fabrication is the choice of solvent used for the spin coating. Shaheen et al. investigated the impact of solvent choice with a BHJ layer consisting of poly(2-methoxy- 5-(3',7'-dimethyloctyloxy)-1,4-phenylene vinylene) (MDMO-PPV) and $PC_{60}BM$.[34] The films were cast with one having chlorobenzene as the solvent while the other used toluene. The chlorobenzene cast solar cell had a nearly threefold increase in PCE compared to the toluene cast solar cell (2.5% vs. 0.9%). This is attributed to a difference in the morphology of the BHJ. There was a substantial increase in fullerene concentration in the active layer when chlorobenzene was used as the solvent which was attributed to the increased solubility of $PC_{60}BM$ in chlorobenzene compared to toluene. An additional example was an active layer consisting of the donor poly[*N*-heptadecanylcarbazole-2,7-diyl-*alt*-(4,7-bis(2-

thienyl)benzo[*c*][1,2,5]thiadiazole)] with [6,6]-phenyl C_{71}-butyric acid methyl ester ($PC_{70}BM$).[35] Solvents were screened for this solar cell and it was found that dichlorobenzene outperformed chloroform and chlorobenzene, although the difference in PCE was not reported.

Another method used to improve the PCE of solar cells is with the introduction of additives to the BHJ structure. The logic behind these additives is to optimize the nanomorphology of the film.[36] One of the most common additives is 1,8-diiodoctane (DIO). There is some uncertainty for what role DIO has that causes the improvement in the solar cells. There are some claims that DIO improves the solubility of the fullerene species, resulting in a reduction of the aggregate size.[37-39] However, there has also been findings that show the difference in solubility is not the driving factor for the changes in efficiency.[40] A more accepted explanation is that the presence of DIO assists with nanostructure evolution during film drying.[41,42] When DIO was added to an active layer of poly[(4,8-bis(alkyloxy)benzo[1,2-*b:4,5*-b'])dithiophene-2,6-diyl-*alt*-(alkylthieno[3,4-*b*]thiophene-2-carboxylate-4,6-diyl)] and $PC_{70}BM$.[43] The addition of only 3% of DIO by mass resulted in an increase of PCE from 3.8% to 4.2%, which is attributed to improved intermolecular packing as shown by transmission electron microscopy.

The ratio of the acceptor and donor within the blend has also been shown to have an impact on PCE. It is necessary that there is sufficient acceptor concentration to allow for efficient transport of charge carriers towards electrodes. However, too much acceptor material can result in a disruption of the crystallization of donor materials like poly(3-hexylthiophene) (P3HT) during the film formation.[44,45] The disruption of the P3HT crystallization results in an increase in the E_g, resulting in a reduction in the photons absorbed and charge generated. The ideal ratio has been found to vary based on solvent, polymer used, and even from laboratory to laboratory.[46,47]

125

There are also methods to optimize the solar cell after the active layer has been deposited. Initial studies on this aspect showed that a postproduction thermal annealing of 75 °C for 5 minutes produced devices with a higher PCE than other temperatures with an active layer of P3HT and $PC_{60}BM$.[48] The impact of thermal annealing is dependent on both the temperature of annealing and the duration of annealing. A more appropriate annealing temperature for a $P3HT:PC_{60}BM$ solar cell can result in a PCE increasing from 1.03% to 4.92% when annealed at 40 °C compared to 150 °C, respectively.[49] When annealed at 150 °C, the $P3HT:PC_{60}BM$ solar cell had a PCE of 4.70% after five minutes of annealing, but increased to 5.01% after 60 minutes.[49] It should be noted that these numbers will not be the same for all active layers, but it does provide the conceptual framework to demonstrate the potential that appropriate annealing conditions provide for a means of increasing the PCE.

An additional post-production method of improving the performance of BHJ OPVs is the use of solvent vapor annealing. This technique introduces a solvent in a closed container, allowing for the further phase separation of the donor and acceptor material in the active layer. Vapor annealing as shown to result in an increase in PCE of a $P3HT:PC_{60}BM$ blend from 3.3% to 4.4% using o-dichlorobenzene.[50] Solvent vapor annealing has also been used with solution-processed squarine and $PC_{60}BM$ that resulted in an increase in the PCE from 3.0% to 5.5%.[51] While the exact mechanism of this improvement has not been identified, the solvent used for the vapor annealing is dependent on its vapor pressure, the solubility of the donor material, the solubility or the acceptor material, and the duration of the exposure.[52]

All of these different methodologies have been attempts to increase the PCE by optimizing the fabrication of the solar cell and do not include the wide range of work that has gone into the synthesis of materials for the active layer. It has been shown that temperature and

annealing during the fabrication process have a large impact on the efficiency of the solar cell, but there has not been any known investigations in the temperature of the solution during the casting of the film despite the fact that elevated temperatures are commonly used during the casting of films. In this study the solvent temperature was varied upon casting of the films of a P3HT and $PC_{60}BM$ solution in dichlorobenzene. The impact of thermal annealing was also studied to determine if the impact of the solvent temperature replaced the PCE increase due to thermal annealing or if they would work in combination. This work was presented in a published paper.[53]
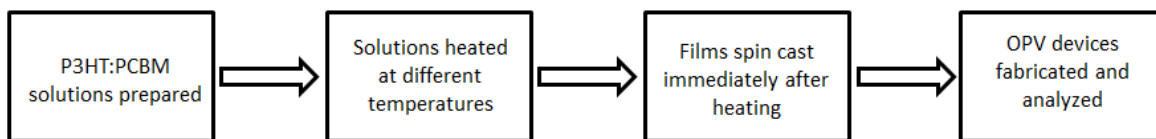
Scheme 5.1. Flowchart for the experiment design used to evaluate the impact of solvent temperature on organic solar cells.

Experimental

Organic solar cells were fabricated on patterned ITO glass with a sheet resistance of 20 Ω/in^2. The ITO glass was cleaned by sequential ultrasonic treatment in detergent, deionized water, acetone, and isopropanol and then treated in a bench-top plasma cleaner (PE-50 bench top cleaner, The Plasma Etch, Inc., USA) for 2 minutes. A PEDOT:PSS solution (Clevious P VP AI 4083 H. C. Stark, Germany) was filtered through a 0.45 µm filter and then spin coated at 4000 rpm for 60 seconds on the ITO glass. The PEDOT:PSS layer was then heated at 100 °C for 40 min in ambient conditions to remove any residual moisture present in the film. The PEDOT:PSS-coated substrates were then transferred to a N_2-filled glovebox. A blend solution of P3HT (Rieke Metals, Inc., MW = 17kDa) and $PC_{60}BM$ (Nano-C) at a concentration of 25 mg/mL (1:1 w/w) in 0.25 mL of o-dichlorobenzene was prepared in a vial. The solution was heated in an aluminum

block and agitated at different temperatures for three hours to ensure a consistent temperature throughout before spin coating on top of PEDOT:PSS layer at 475 rpm for 45 seconds.

After 1 hour of aging, half of the P3HT:PC$_{60}$BM blend films were thermally annealed at 105 °C for 5 minutes. The solar cell was capped with a cathode consisting of LiF (~1 nm) and Al (~100 nm) which was thermally evaporated on the active layer under a shadow mask in a base pressure of 1 x 10^{-6} mbar. The device's active area was ~7.9 mm^2 for all the solar cells discussed in this work. The J-V measurement of the devices was conducted on a computer controlled Keithley 2400 source meter. The J-V measurement system uses a solar simulator with a Class-A match to the AM1.5 Global Reference Spectrum. It is calibrated with KG5-filtered silicon reference cell with calibration traceable to NREL and NIST. Film thicknesses of the blend films were measured by atomic force microscopy.

Results and Discussion

Before discussion of the impact of the solvent temperature on the PCE of the solar cells it is important to characterize the differences that the solvent temperature had on some of the physical properties of the film. The different temperatures will result in solutions with different viscosities, different solubilities of the P3HT and PC$_{60}$BM, and different rates of evaporation despite being the same solvent and contents, all of which will influence the formation of the active layer. Films of three different temperatures were studied with an atomic force microscope (AFM):35 °C, 65°C, and 105 °C (Figure 5.6). The temperatures were chosen based on the PCE of the resulting solar cell. The imaging shows there is a distinct difference between the morphology of the solar cells. The 65 °C film appears to be the smoothest of the three, exhibiting a film thickness of 90 nm. The 35 °C and 105 °C films both have locations of irregularity, resulting in a bumpy surface, albeit different in their own way. The 35 °C film appears to be

consistently irregular while the 105 °C film has localized regions of more intense surface irregularity. It should also be noted that the 35 °C film maintained a thickness of 90 nm while the 105 °C film was only 80 nm.
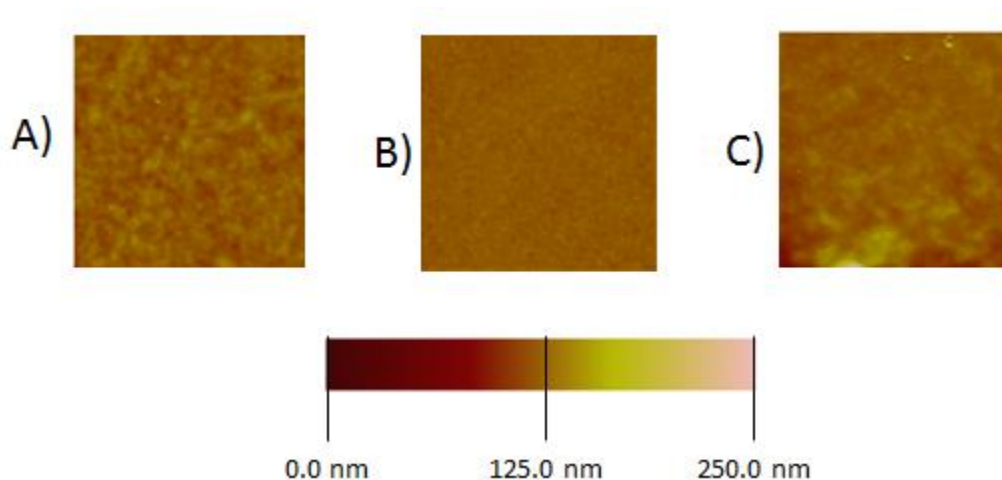
Figure 5.6. 5 nm x 5 nm square of annealed P3HT:PC$_{60}$BM films that were cast at the following temperatures: (A) 35 °C, (B) 65 °C, and (C) 105 °C.

The UV-vis absorption spectra for the three films (Figure 5.7) shows little shift in the absorption between the three films. The 35 °C and 65 °C have nearly identical absorption spectra, but the 105 °C film has a substantial drop in absorption. The decrease in absorption can be slightly contributed to the change in film thickness as the temperature increased (80 nm vs. 90 nm), but it is unclear if that is a function of only the film thickness or if the active layer is undergoing decomposition. There is a weak trend in the absorption decreasing as temperature is increased, with the 65 °C having a slightly reduced absorption compared to the 35 °C sample. It is possible that there is a critical temperature for each solvent or polymer that results in a substantial decrease in absorption either due to the change in viscosity of the solution resulting in it being less processable or decomposition of the blend, but that was not the focus of this study.

129
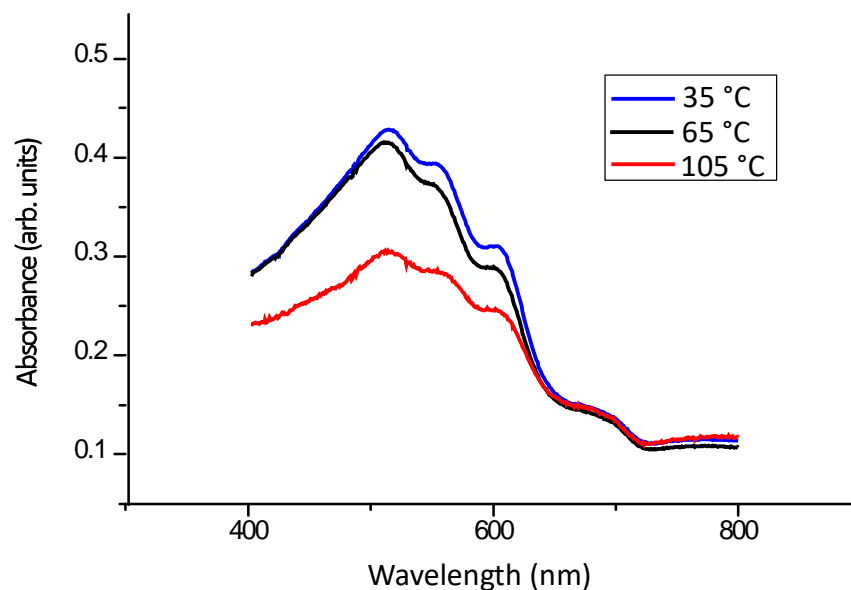
Figure 5.7. Absorption of the P3HT:PC$_{60}$BM films that were cast at different temperatures after annealing for 5 minutes at the labeled temperatures.

The compilation of the photovoltaic properties of the solar cells is shown in Table 5.1 and 5.2 of the non-annealed and annealed samples, respectively. The values come from the average and standard deviation of over 20 operating solar cells. The extent of thoroughness with these results is not present in any of the previously reported studies, or at least it is not explicitly stated in the methodology. Figure 5.8 presents the plots of the different properties of the solar cells at different solvent temperature, both with and without post-production annealing.

Table 5.1. The compilation of the solar cell properties of the non-annealed samples, including standard deviations. Each data compilation consists of at over 20 sample cells.

Solution Temp. (°C)	Fill Factor (%)		J_{SC} (mA/cm^2)		V_{OC} (V)		PCE (%)	
35	59.4	±3.5	3.75	±0.50	0.623	±0.021	1.36	±0.09
45	60.3	±0.8	5.77	±0.31	0.594	±0.021	1.91	±0.08
55	51.3	±3.7	5.43	±0.25	0.591	±0.004	1.85	±0.08
65	53.4	±2.2	6.72	±0.92	0.642	±0.006	2.06	±0.09
75	51.2	±4.2	7.25	±0.55	0.611	±0.008	1.95	±0.07
85	52.1	±2.3	5.74	±0.44	0.615	±0.002	1.48	±0.09
95	45.4	±2.4	6.25	±0.95	0.589	±0.008	1.36	±0.08
105	60.4	±1.9	4.20	±0.42	0.625	±0.005	1.31	±0.06

Table 5.2. The compilation of the solar cell properties of the annealed samples, including standard deviations. Each data compilation consists of at least 20 sample cells.

Solution Temp. (°C)	Fill Factor (%)		J_{SC} (mA/cm^2)		V_{OC} (V)		PCE (%)	
35	62.4	±0.8	5.22	±0.18	0.584	±0.008	1.90	±0.07
45	62.3	±1.0	6.41	±0.48	0.587	±0.005	2.29	±0.07
55	58.6	±0.6	7.72	±0.65	0.576	±0.003	2.56	±0.06
65	57.4	±0.3	7.22	±0.55	0.631	±0.051	2.50	±0.08
75	56.9	±2.7	7.13	±0.43	0.642	±0.007	2.41	±0.09
85	54.1	±3.4	5.82	±0.28	0.625	±0.029	1.88	±0.08
95	48.2	±2.9	6.45	±0.32	0.600	±0.007	1.60	±0.09
105	57.8	±3.4	5.21	±0.68	0.621	±0.013	1.54	±0.07

The changes in PCE as a function of temperature (Figure 5.8 A) shows the impact of the temperature of solvent casting and the PCE of the resulting OPV. The lowest controlled temperature, which was used as a replacement for the room temperature sample while still controlling the temperature (35 °C), resulted in a PCE of 1.36% and will be used as the control for analysis. With solely altering the solvent temperature it was possible to obtain a maximum PCE value of 2.06% at 65 °C. However, after the 65 °C maximum PCE there is a rapid drop of PCE, showing that there is eventually a point at which additional heat has a negative impact on the efficiency of the OPV.
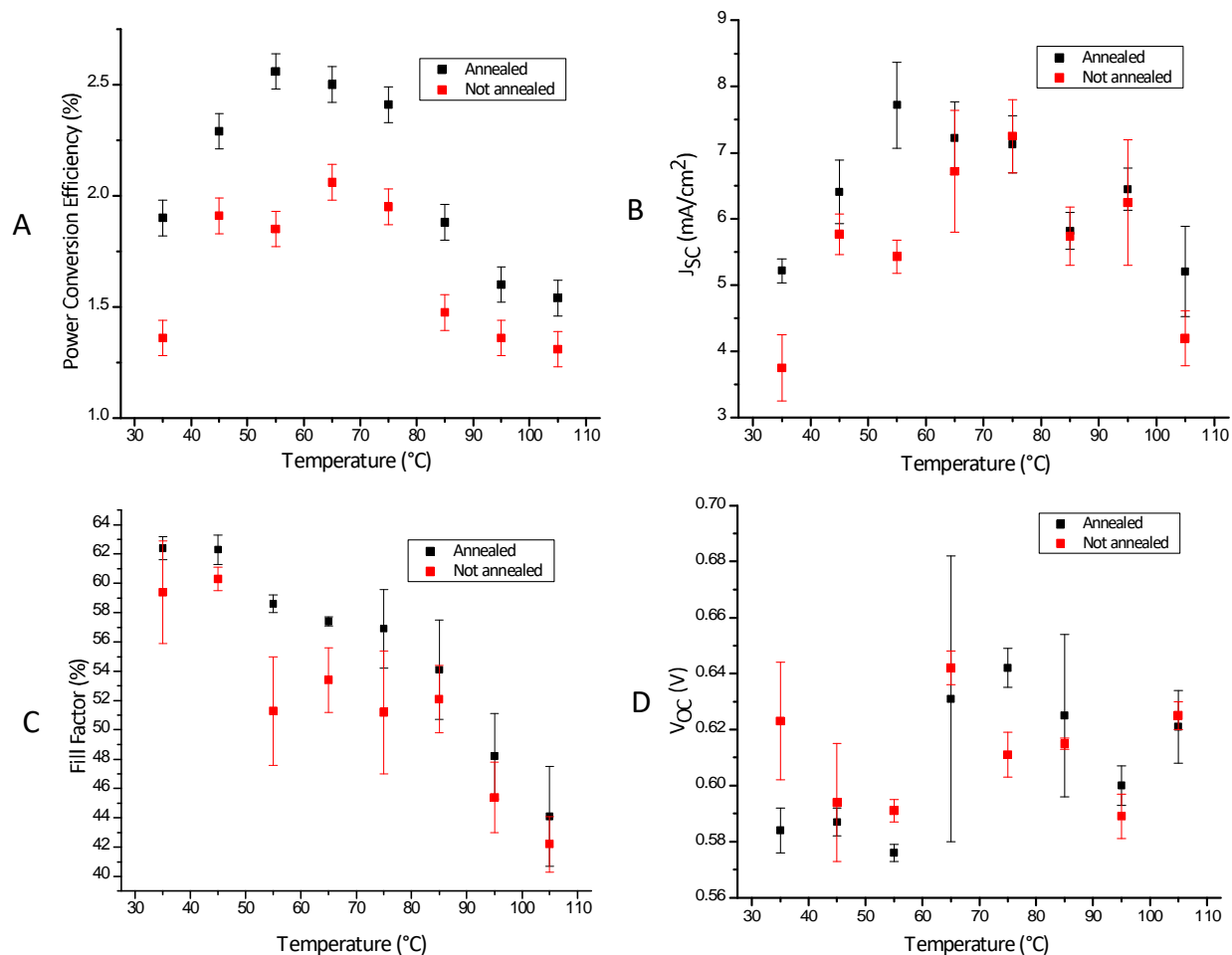
Figure 5.8. The graphical representation of the data compiled from the different OPV devices whose films were spun at different temperatures. The different plots consist of the power conversion efficiency (A), the short circuit current (B), the fill factor (C), and the open circuit voltage (D).

With the methodology chosen, this also allowed for the impact of thermal annealing to be compared both against and synergistically with solvent temperature control. The post-production thermal annealing resulted in an additional increase in the PCE at all temperatures. This result shows that the solvent temperature does not serve as a replacement to the already established thermal annealing but works synergistically with it to allow for a more efficient OPV with only a minor change in the fabrication method.

While this demonstrates that optimization of thermal annealing and solvent temperature casting both contribute positively to the PCE of OPVs, it is useful to understand which one has a

larger impact. The best way to do this would be to compare a standard to the exposure of each. The 35 °C non-annealed would be considered the unadulterated standard to compare the impact of the two methods. The annealing of the 35 °C sample resulted in a PCE increase of 0.54% while changing the solvent casting temperature to 65 °C resulted in a 0.70% increase. It is worth noting that the annealing process was not optimized, but this does show that the control of the solvent temperature has a comparable impact to the PCE increase as thermal annealing does.

The devices with the highest PCE were cast at different temperatures for the annealed and the non-annealed devices. The highest PCE for the annealed devices had a solvent casting temperature of 55 °C while the non-annealed sample had a maximum PCE at a solvent casting temperature of 65 °C. This shows that there is a diminishing return to the impact on the thermal annealing as higher solvent temperatures are used. This is consistent with the rest of the data as the difference between the annealed and non-annealed sample reduces as the solvent temperature increases.

The changes in solvent temperature did not appear to have a noticeable impact on the V_{OC} of the devices, as would be expected because the V_{OC} is closely related to the difference in energy between the HOMO of the donor and the LUMO of the acceptor, neither of which changed during the experiment. The J_{SC} appeared to have a strong dependence on the solvent temperature, obtaining a maximum J_{SC} at 75 °C and then having a decreasing value after that point. This increase in J_{sc} is likely due to improved ordering and stacking of the P3HT, resulting in an increase in the charge generation. The 75 °C did not have the highest PCE though and this is due to the impact that the solvent temperature had on the fill factor. As temperature increased there was an increase in FF until a maximum was reached followed by a steady decline in the FF

of the OPVs. The interplay between maximizing the J_{SC} and the FF will provide the ideal temperature for the solvent casting.

Conclusion

The work presented shows the impact that changing the casting temperature of the solvent has on the photovoltaic characteristics of organic solar cells with an active layer of P3HT:PC$_{60}$BM. The optimal solvent temperature when spin casting resulted in an increase in PCE of 0.70% compared to the room temperature cast device (2.06% vs 1.36%). This compares to an increase in PCE of only 0.54% by post-production thermal annealing, which is considered a standard part of the organic solar cell production process (1.90% vs 1.36%). Fortunately, the post-production thermal annealing increases the PCE of the solar cell in conjunction with the improvements from changing solvent temperature. The optimizing of the solvent temperature upon casting provides a simple means of increasing the PCE of the solar cell without any substantial additional work in the fabrication process.

While this work does reveal a significant improvement to the fabrication process, it also brings up many more questions to be answered. All of the solar cells fabricated used *o*-dichlorobenzene as the casting solvent. These results provide the basis to investigate the impact that using alternative solvents have while varying the solvent temperature. It is well established that different solvents result in different PCEs, so it is a logical progression that they would also behave differently when the solvents are cast at different temperatures.[5]

An additional set of studies would be to use a system other than the P3HT:PC$_{60}$BM active layer. Synthesizing thiophene polymers with different alkyl chain lengths would provide an opportunity to investigate how alkyl chain lengths have an impact on the solvent temperature upon film casting. It would also be worthwhile to investigate polycyclic systems and determine

134

their dependence on solvent temperature as well. Eventually it would be worthwhile to expand

the type of polymers that are investigated outside of that of thiophene polymers to determine if

and to what extent the solvent temperature still has on the PCE of the resulting organic solar cell.

Ma *et al.* did a study of post-production methods dealing with the polymer poly[(5,6-difluoro-

2,1,3-benzothiadiazol-4,7-diyl)-*alt*-(3,3'''-di(2-octyldodecyl)2,2';5',2'';5'',2'''-quaterthiophen-

5,5'''-diyl)] and PC$_{70}$BM and obtained a maximum PCE at 100 °C, although the work was

adjusting spin speed and solvent temperatures simultaneously rather than altering temperature

and having a consistent procedure.[54]

One unanswered question that arose from this study is what is the actual physical change

caused by the changing of the solvent temperature during the casting. This could be determined

by looking at the difference in the concentration of the donor and acceptor material in the active

phase. It is possible that the changing of the solvent temperature allows for more optimal

distribution of regions of donor and acceptor material, both in location and domain size, which

allow for better charge separation. Understanding of what the physical effects of the solvent

temperature would allow for the use of the temperature to be better controlled for desired results.

References

1.   Lu, L.; Zheng, T.; Wu, Q.; Schneider, A. M.; Zhao, D.; Yu, L. *Chem. Rev.* **2015**, *115*, 12666.

2.   Scharber, M. C.; Mühlbacher, D.; Koppe, M.; Denk, P.; Waldauf, C.; Heeger, A. J.; Brabec, C. J. *Adv. Mater.* **2006**, *18*, 789.

3.   Kirchartz, T.; Taretto, K.; Rau, U. *J. Phys. Chem. C* **2009**, *113*, 17958.

4**.**   Zhang, G.; Zhao, J.; Chow, P. C. Y.; Jiang, K.; Zhang, J.; Zhu, Z.; Zhang, J.; Huang, F.; Yan, H. *Chem. Rev.* **2018,** *118,* 3447.

5.   Spangaard, H.; Krebs, F. *Sol. Energy Mater. Sol. Cells* **2004,** *83*, 125.

6.   Dastoor, P. C.; Belcher, W. J. *Substantia* **2019,** *3*, 99.

7. Zhao, W.; Li, S.; Yao, H.; Zhang, S.; Zhang, Y.; Yang, B.; Hou, J. *J. Am. Chem. Soc.* **2017**, *139*, 7148.

8. Nunzi, J. M. C. *R. Physique* **2002**, *3*, 523.

9. Tang, C. W. *Appl. Phys. Lett.* **1986**, *48*, 183.

10. Tsuzuki, T. T.; Shirota, J.; Rostalski, J.; Meissner, D. *Sol. Energy Mater. Sol. Cells* **2000**, *61*, 1.

11. Uchida, J. X.; Rand, B. P.; Forrest, S. R. *Appl. Phys. Lett.* **2004**, *84*, 4218.

12. Zhou, X.; Blochwitz, J.; Pfeiffer, M.; Nollau, A.; Fritz, T.; Leo, K. *Adv. Funct. Mater.* **2001**, *11*, 310.

13. Wöhrle, D.; Meissner, D. *Adv. Mater.* **1991**, *3*, 129.

14. Jenekhe, S. A.; Yi, S. *Appl. Phys. Lett.* **2000**, *77*, 2635.

15. Breeze, A. J.; Salomon, A.; Ginley, D. S.; Gregg, B. A.; Tillmann, H.; Hoerhold, H. H. *Appl. Phys. Lett.* **2002**, *81*, 3085.

16. Sariciftci, N. S.; Braun, D.; Zhang, C.; Srdanov, V. I.; Heeger, A. J.; Stucky, G.; Wudl, F. *Appl. Phys. Lett.* **1993**, *62*, 585.

17. Halls, J. J. M.; Walsh, C. A.; Greenham, N. C.; Marseglia, E. A.; Friends, R. H.; Moratti, S. C.; Holmes, A. B. *Nature* **1995**, *78*, 451.

18. Hoppe, H.; Sariciftci, N. S. *J. Mater. Chem.* **2004**, *19*, 1924.

19. Hoppe, J. Ph. D. Thesis, Linz, 2004.

20. Suemori, K.; Yokoyama, M.; Hiramoto, M. *J. Appl. Phys.*, **2006**, *99*, 036109.

21. Reese, M. O.; Morfa, A. J.; White, M. S.; Kopidakis, N.; Shaheen, S. E.; Rumbles, G.; Ginley, D. S. *Sol. Energy Mater. Sol. Cells* **2008**, *92*, 746.

22. Lee, S. T.; Gao, Z. Q.; Hung, L. S. *Appl. Phys. Lett.* **1999**, *75*, 10.

23. Irwin, M. D.; Buchholz, B.; Hains, A. W.; Change, R. P. H.; Marks, T. J. *Proc. A Natl. Acad. Sci. U. S. A.* **2008**, *105*, 2783.

24. Schlatmann, A. R., Wilms Floet, D.; Hilberer, A.; Garten, F.; Smulders, P. J. M., Klapwijk, J. M.; Hadziioannou, G. *Appl. Phys. Lett.* **1996**, *69*, 1764.

25. Peumans, P.; Forrest, S. R. *Appl. Phys. Lett.* **2001**, *79*, 126.

26. Hau, S. K.; Yip, H. L.; Leong, K.; Jen, A. K. Y. *Org Electron.* **2009**, *10*, 719.

27. Lee, J. Y.; Connor, S. T.; Cui, Y.; Peumans, P. *Nano Lett.* **2008**, *8*, 689.

28. Cheng, P.; Zhan, X. *Chem. Soc. Rev.* **2016**, *45*, 2544.

29. Brabec, C. J.; Cravino, A.; Meissner, D.; Sariciftci, N. S.; Fromherz, T.; Minse, M.; Sanchez, L.; Hummelen, J. C. *Adv. Funct. Mater.* **2001**, *11*, 374.

30. Scharber, M.; Mühlbacher, D.; Koppe, M.; Denk, P.; Waldauf, C.; Heeger, A. J.; Brabec, C. *Adv. Mater.* **2006**, *18*, 789.

31. Mallairas, G. G.; Salem, J. R.; Brock, P. J.; Scott, J. C. *J. Appl. Phys.* **1998**, *84*, 1583.

32. Liu, L.; Shi, Y.; Yang, Y. *Adv. Funct. Mater.* **2001**, *11*, 420.

33. Zhou, H.; Yang, L.; You, W. *Macromolecules* **2012**, *45*, 607.

34. Shaheen, S. E.; Brabec, C. J.; Sariciftci, N. S.; Padinger, F.; Fromherz, T.; Hummelen, J. C. *Appl. Phys. Lett.* **2001**, *78*, 841.

35. Park, S. H.; Roy, A.; Beaupré, S.; Cho, S.; Coates, N.; Moon, J. S.; Moses, D.; Leclerc,M.;Lee, K.; Heeger, A. J. *Nat. Photonics* **2009**, *3*, 297.

36. Li, A.; Miao, X.; Deng, X. *Synth. Met.* **2013**, *168*, 43.

37. Kim, W.; Kim, J. K.; Kim, E.; Ahn, T. K.; Wang, D. H.; Park, J. H. *J. Phys. Chem. C* **2015,** *119,* 5954.

38. Kang, H.; Kim, G.; Kim, J.; Kwon, S.; Kim, H.; Lee, K. *Adv. Mater.* **2016,** *28,* 7821.

39. Lou, S. J.; Szarko, J. M.; Xu, T.; Yu, L.; Marks, T. J.; Chen, L. X. *J. Am. Chem. Soc.* **2011,** *133,* 20661.

40. Fontana, M. T.; Kang, H.; Yee, P. Y.; Zongwu, F.; Hawks, S. A.; Schelhas, L. T.; Subramaniyan, S.; Hwang, Y. J.; Jenekhe, S. A.; Tolbert, S. H.; Schwartz, B. J. *J. Phys. Chem. C* **2018,** *122,* 16574.

41. Zhang, Y.; Parnell, A. J.; Pontecchiani, F.; Cooper, J. F. K.; Thompson, R. L.; Jones, R. A. L.; King, S. M.; Lidzey, D. G.; Bernardo, G. *Sci. Rep.* **2017,** *7,* 44269.

42. Bokel, F. A.; Engmann, S.; Herzing, A. A.; Collins, B. A.; Ro, H. W.; DeLongchamp, D. M.; Richter, L. J.; Schaible, E.; Hexemer, A. *Chem. Mater.* **2017,** *29,* 2283.

43. Yao, E.-P.; Chen, C.-C.; Gao, J.; Liu, Y.; Chen, Q.; Cai, M.; Hsu, W.-C.; Hong, Z.; Li, G.; Yang, Y. *Sol. Energy Mater. Sol. Cells* **2014**, *130*, 20.

44. Chiu, M.-Y.; Jeng, U.-S.; Su, M.-S.; Wei, K.-H. *Macromolecules* **2010**, *43*, 428.

45. Kim, J. Y.; Frisbie, C. D. *J. Phys. Chem. C* **2008**, *112*, 17726.

46.   Nakamura, J.; Murata, K.; Takahashi, K. *Appl. Phys. Lett.* **2005**, *87*, 132105.

47.   Jin, S.-H.; Vijaya Kumar Naidu, B.; Jeon, H.-S.; Park, S.-M.; Park, J.-S.; Chul Kim, S.; Wook Lee, J.; Gal, Y.-S. *Sol. Energy Mater. Sol. Cells* **2007**, *91*, 1187.

48.   Padinger, R. S. Rittberger, N. S. Sariciftci, *Adv. Funct. Mater*. **2003**, *13*, 85.

49.   Ma, W.; Yang, C.; Gong, X.; Lee, K.; Heeger, A. J. *Adv. Funct. Mater.* **2005**, *15*, 1617.

50.   McDowell, C.; Abdelsamie, M.; Toney, M. F.; Bazan, G. C. *Adv. Mater.,* **2018**, *30,* 1707114.

51.   Wei, G.; Sun, S. W. K.; Thompson, M. E.; Forrest, S. R. *Adv. Energy Mater.* **2011,** *1,* 184.

52.   Kuan, S.; Xiao, Z.; Hanssen, E.; Klein, M. F. G.; Dam, H. H.; Pfaff, M.; Gerthsen, D.; Wong, W. W. H.; Jones, D. J. *J. Mater. Chem. A* **2014,** *2,* 9048.

53.   Anderson, T. E.; Köse, M. E. *J. Photochem. Photobiol. A* **2016,** *318*, 51.

54.   Ma, W.; Yang, G.; Jiang, K.; Carpenter, J. H.; Wu, Y.; Meng, X.; McAfee, T.; Zhao, J.; Zhu, C.; Wang, C.; Ade, H.; Yan, H. *Adv. Energy Mater.* **2015,** *5,* 1501400.

CHAPTER 6. SUMMARY

Conclusion

The donor-acceptor framework was explored and its understanding improved upon be generating a family of homo- and hetero-dimers consisting of the ambipolar unit 2,3-dihexylthieno[3,4-*b*]pyrazine (TP), the acceptor unit benzo[*c*][1,2,5]thiadiazole (BTD), and the donor 3,4-ethylenedioxythiophene (EDOT) was synthesized. The findings from the dimers indicate that the ambipolar TP has substantial contribution to the HOMO and the LUMO of the resulting dimer regardless of whether it is paired with an acceptor or a donor unit. The HOMO-LUMO gap of the donor-acceptor dimer BTD-EDOT was 2.40 eV and the HOMO-LUMO gap of the ambipolar-acceptor BTD-TP was 2.43 eV. The similar value of the HOMO-LUMO gap between these two different dimers indicate that the design of the ambipolar-acceptor dimer results in similar HOMO-LUMO gaps as the donor-acceptor dimers. This provides evidence that a polymer synthesized with alternating ambipolar-acceptor units could have similar electronic properties as the donor-acceptor polymer, which is already widely used for polymer design.

The crystal structure of the BTD-EDOT dimer provided additional insight on the donor-acceptor framework. One of the explanations for the reduction of the HOMO-LUMO gap of donor-acceptor materials is that the enhanced contribution of the quinoidal resonance structure of the material cause by the electron rich donor unit and the electron deficient acceptor unit results in a reduction in the bond-length alternation.[1-3] This would result in there being a double bond between the two units and a shortening of the interannular bond. However, the bond was found to not be shortened, indicating that there is not substantial contribution of the quinoidal resonance form of the dimer. This finding will hopefully encourage a more critical discussion of

139

the reasoning behind the characteristics of donor-acceptor materials rather than simply contributing the characteristics to the reduction in bond-length alternation.

The design of the ambipolar-acceptor dimer was expanded to ambipolar-acceptor polymers. The polymer with alternating ambipolar TP units and acceptor BTD units (poly(2,3-dihexylthieno[3,4-*b*]pyrazine-*alt*-benzo[*c*][1,2,5]thiadiazole)) resulted in a low band gap polymer that had a band gap (E_g) of 0.94 eV. The acceptor unit 2,3-dihexylquinoxaline (Qx) was also paired with TP to generate the ambipolar-acceptor polymer poly(2,3-dihexylthieno[3,4-*b*]pyrazine-*alt*-2,3-dihexylquinoxaline). This was also a low E_g polymer with an E_g of 1.33 eV. The third ambipolar-acceptor polymer consisted of alternating ambipolar 2,3-bis(hexyloxy)thieno[3,4-*b*]pyrazine and acceptor Qx units. The polymer poly(2,3-bis(hexyloxy)thieno[3,4-*b*]pyrazine-*alt*-2,3-dihexylquinoxaline) did not result in a low E_g polymer, but it did have a E_g 1.56 eV which is close to the low E_g threshold of 1.5 eV. This new ambipolar-acceptor polymer design proved to be a viable means of generating low E_g materials and could provide a new avenue for polymer design. All three of these polymers were generated by direct arylation polymerization (DArP) which is a newer polymerization method that does not have the toxic byproducts of other polymerization methods and requires less steps to functionalize the monomers for polymerization.[4-8] One surprising aspect of the polymers generated is the polymerization conditions worked well for all of the polymers, although a common drawback of DArP is the need to optimize conditions for each specific polymer.[9] Additionally, the two low E_g polymers are two of only a few low E_g polymers generated using DArP. This is one of the first uses of Qx with alkyl functionalizations instead of aryl functional groups. Alky groups result in an increase in interactions between the solvent to help with

solubility for polymers. Increased solubility assists in generating a higher molecular weight polymer, which usually results in more desirable characteristics of the resulting polymer.[10]

Progress was made towards the synthesis of 2,3-dialkylthieno[2,3-b]pyrazine. The hope was to utilize this as an end-capping unit for conjugated small molecules and utilize the extensive work that has been done with thieno[3,4-b]pyrazine based molecules and apply it to the isomer. Using a similar synthetic scheme as is used for the synthesis of 2,3-dialkythieno[3,4-b]pyrazine worked well until the reduction of 2,3-dibromo-4,5-dinitrothiophene. Multiple reduction methods were used but the desired product could not be isolated from any of the methods. Either an alternative reduction method will need to be implemented to finish the proposed synthetic pathway or a different synthetic route will need to be used. Earlier synthesis of thieno[2,3-b]pyrazine based molecules focused on building the thiophene onto the pyrazine and this could be re-evaluated with the mindset of also desiring a means to functionalize the thieno[2,3-b]pyrazine.

One of the applications of these conjugated polymers is as materials in organic photovoltaics. The final project explored the impact that solvent temperature during casting has on the overall efficiency of the resulting photovoltaic device. The donor material poly(3-hexylthiophene) and the acceptor material phenyl-C_{61}-butyric acid methyl ester ($PC_{60}BM$) make up the active layer and o-dichlorobenzene was the solvent for the film casting. It was found that the optimal temperature for this donor-acceptor combination at a 1:1 mass ratio was between 55 and 65 °C. One additional finding was that the changing of the solvent temperature does not negate the benefits of thermal annealing and in fact behaves synergistically with thermal annealing. The increase in the power conversion efficiency due to adjusting the solvent

temperature was comparable to the increase in power conversion efficiency of thermal annealing, something that is considered a standard practice in the fabrication of photovoltaic devices.

Future Directions

The work presented provides a basis to further explore and improve the donor-acceptor framework. Some pathways this expansion of the framework can take could focus on expanding upon the ambipolar unit or further exploring the ambipolar-acceptor polymer design.

The characteristics of thieno[3,4-*b*]pyrazine show that it is deserving of a classification outside of either simply an acceptor or a donor within the donor-acceptor framework.[11-15] Additional molecules have also been shown to share characteristics of thieno[3,4-*b*]pyrazine that would justify them also being categorized as ambipolar units.[13,16,17] The continual development of more ambipolar units would greatly assist utilizing the donor-acceptor framework for polymer design. One proposed additional ambipolar unit is thieno[3,4-*c*][1,2,5]thiadiazole (TT, Figure 6.1). This is a monomer unit that has already been used in conjugated materials and is classified as an acceptor unit, similar to TP.[18,19] In fact, in one paper it was compared alongside TP with both of them filling the role of the acceptor unit and TT was able to produce a trimer with a smaller HOMO-LUMO gap than TP. One of the major drawbacks to this compound is its lack of functionalization opportunities, which inhibits its tunability and could result in solubility issues as well.

Figure 6.1. Thieno[3,4-*c*][1,2,5]thiadiazole.

DArP proved an effective means for generating polymers the acceptor-ambipolar polymers but there is still room for optimization. One method that has been found to improve yields and increase the molecular weight of polymers is to have the synthesis be performed under high pressure.[20] Evan Culver performed the polymerization under high pressure of the acceptor-ambipolar polymers and it was found to have an increase in the molecular weights and an improvement in their electronic properties.[21,22] Additionally, the family of ambipolar-acceptor polymers can be increased by generating new polymers, which the Rasmussen group is actively pursuing. If the TT monomer unit does behave as an ambipolar unit, the pairing of the TT unit with the Qx unit would serve as a good expansion of the ambipolar-acceptor polymers with the solubilizing chains of the Qx unit helping to overcome the lack of solubilizing chains on the TT unit.

The impact of the solvent temperature for *o*-dichlorobenzene when casting polymer films is likely not unique to *o*-dichlorobenzene. The study could be reproduced with other common solvents for organic photovoltaic device fabrication, such as chloroform, acetone, toluene, or xylene.[23] The temperature screening would determine the ideal temperature for each of these solvents as well as investigate if the annealing continues to be synergistic with solvent temperature for the overall power conversion efficiency. If enough solvents are characterized then a potential relationship between the solvent, such as the boiling point of the solvent, and the temperature for maximum efficiency could be determined.

In addition to investigating different solvents, it would be worthwhile to investigate using different active phases. This would help establish whether the ideal temperature is solely dependent on the solvent or whether the active phase also influences the temperature. One method would be to fabricate a series of organic photovoltaic devices using *o*-dichlorobenzene as

the solvent and the active phase consists of $PC_{60}BM$ and a common donor material of poly(2-methoxy-5-(2-ethylhexyloxy)-1,4-phenylenevinylene). The change in the power conversion efficiency as temperature of the solvent changes could be compared to the work present with the poly-3-hexylthiophene data to see if there are any similarities. Additionally, the alkyl group on the thiophene monomer can be changed to a longer, shorter, or branched chain and that then polymerized. This would provide additional insight on the role that the alkyl group has with respect to film casting and efficiency as the temperature changes.

It was shown that the ambipolar-acceptor polymer with alternating TP and BTD units has potential to work as an acceptor material in organic photovoltaic devices.[22] The energy level of the LUMOs of the ambipolar-acceptor polymers were measured to be -4.1 and -3.9 eV, which is close to the values for the LUMOs of $PC_{60}BM$ (-3.7 eV) and phenyl-C_{71}-butyric acid methyl ester (-3.9 eV) and these are the two most commonly used acceptor materials. However, there has been a large focus for alternatives to fullerene-based acceptors and the ambipolar-acceptor polymers could be a synthetically facile option.[24-26] The ability to have a similar polymerization setup that results in a polymer with a tunable LUMO by using acceptors of different strengths would make it a great candidate for photovoltaic devices. One major issue with polymer/polymer blends is the intimate mixing that results in limited phase separation of the polymers.[29-30] This results in poor charge transport due to the lack of a continuous pathway and loss of crystallinity of the material. This could be overcome by varying the solubilizing chains in hopes introducing enough of a solubility difference between the two polymers that the appropriate domains will still be able to be formed. If having the donor and acceptor material mixed does not work, an alternative method would be to implement a multi-layer blade coating method in which the ambipolar-acceptor polymer would be deposited first and followed by the deposition of the

144

donor polymer.[31] There is already a need to transition to large scale device fabrication methods already instead of the commonly used research method of spin coating devices.[32] The combination of developing a methodology for fabricating photovoltaics devices on a large scale with a tunable acceptor material would be a significant step forward to justifying the production of organic photovoltaics using these ambipolar-acceptor polymers as an acceptor material.

References

1.   Bundgaard, E.; Krebs, F. *Sol. Energy Mater. Sol. Cells* **2007**, *91*, 954.

2.   Chochos, C. L.; Choulis, S. A. *Prog. Polym. Sci.* **2011**, *36*, 1326.

3.   van Mullekom, H. A. M.; Vekemans, J. A. J. M.; Havinga, E. E.; Meijer, E. W. *Mat. Sci. Eng. R* **2001**, *32*, 1.

4.   Po, R.; Bernardi, A.; Calabrese, A.; Carbonera, C.; Corso, G.; Pellegrino, A. *Energy Environ. Sci.* **2014**, *7*, 925.

5.   Pouliot, J.-R.; Grenier, F.; Blaskovits, J. T.; Beaupré, S.; Leclerc, M. *Chem. Rev.* **2016**, *116*, 14225.

6.   Bura, T.; Blaskovits, J. T.; Leclerc, M. *J. Am. Chem. Soc.* **2016**, *138*, 10056.

7.   Leclerc, M.; Brassard, S.; Beaupré, S. *Polymer Journal* **2020**, *52*, 13.

8.   Bohra, H.; Wang, M. *J. Mater. Chem. A* **2017**, *5*, 11550.

9.   Mercier, L. G.; Leclerc, M. *Acc. Chem. Res.* **2013**, *46*, 1597.

10.   Rasmussen, S. C. In *Encyclopedia of Polymeric Nanomaterials*; Kobayashi, S., Mullen, K., Eds.; Springer, Berlin, Heidelberg, 2013; Chapter 57.

11.   Mulholland, M. E.; Konkol, K. L.; Anderson, T. E.; Schwiderski, R. L.; Rasmussen, S. C. *Aust. J. Chem.* **2015**, *68*, 1759.

12.   Wen, L.; Heth, C. L.; Rasmussen, S. C. *Phys. Chem. Chem. Phys.* **2014**, *16*, 7231.

13.   Konkol, K. L.; Schwiderski, R. L.; Rasmussen, S. C. *Materials* **2016**, *9*, 404.

14.   Kenning, D. D.; Funfar, M. R.; Rasmussen, S. C. *Polymer Preprints* **2001**, *42*, 506.

15.   Kenning, D. D.; Mitchell, K. A.; Calhoun, T. R.; Funfar, M. R.; Sattler, D. J.; Rasmussen, S. C. *J. Org. Chem.* **2002**, *67*, 9073.

16.   Nietfeld, J. P.; Schwiderski, R. L.; Gonnella, T. P.; Rasmussen, S. C. *J. Org. Chem.* **2011,** *76,* 6383

17.   Nakanishi, T.; Shirai, Y.; Han, L. *J. Mater. Chem. A* **2015,** *3,* 4229.

18.   Tanaka, S.; Yamashita, Y. *Synth. Met.* **1995**, *69*, 599.

19.   Cimrová, V.; Kmínek, I.; Pavlaćková, P.; Vỳprachtickỳ, D. *Polym. Sci. Part A: Polym. Chem.* **2011**, *49*, 3426.

20.   Bura, T.; Beaupré, S.; Légaré, M. A.; Quinn, J.; Rochette, E.; Blaskovits, J. T.; Fontaine, F. G.; Pron, A.; Li, Y.; Leclerc, M. *Chem. Sci.* **2017**, *8*, 3913.

21.   Anderson, T. E.; Culver, E. W.; Almyahi, F. A.; Dastoor, P. C.; Rasmussen, S. C. *Synlett* **2018**, *29*, 2542.

22.   Culver, E. W.; Anderson, T. E.; Navarrete, J. T. L.; Delgado, M. C. R.; Rasmussen, S. C. *ACS Macro Lett.* **2018**, *7*, 1215.

23.   Zhang, S.; Ye, L.; Zhang, H.; Hou, J. *Mater. Today* **2016**, *19*, 533.

24.   Yan, C.; Barlow, S.; Wang, Z.; Yan, H.; Jen, A. K.-Y.; Marder, S. R.; Zhan, X. *Nature Rev. Mater.* **2018**, *3*, 18003.

25.   Cheng, P.; Li, G.; Zhan, X.; Yang, Y. *Nat. Photonics* **2018**, *12*, 131.

26.   Meng, L.; Zhang, Y.; Wan, X.; Li, C.; Zhang, X.; Wang, Y.; Ke, X.; Xiao, Z.; Ding, L.; Xia, R.; Yip, H.-L.; Cao, Y.; Chen, Y. *Science* **2018**, *361*, 1094.

27.   Benten, H.; Mori, D.; Ohkita, H.; Ito, S. *J. Mater. Chem. A* **2016**, *4*, 5340.

28.   Osaka, M.; Benten, H.; Ohkita, H.; Ito, S. *Macromolecules* **2017**, *50*, 1618.

29.   Osaka, M.; Mori, D.; Benten, H.; Ogawa, H.; Ohkita, H.; Ito, S. *ACS Appl. Mater. Interfaces* **2017**, *9*, 15615.

30.   Liu, X.; Huettner, S.; Rong, Z.; Sommer, M.; Friend, R. H. *Adv. Mater.* **2012**, *24*, 669.

31.   Chen, C.-Y.; Change, H.-W.; Change, Y.-F.; Change, B.-J.; Lin, Y.-S.; Jian, P.-S.; Yeh, H.-C.; Chien, H.-T.; Chen, E.-C. Chao, Y.-C.; Meng, H.-F.; Zan, H.-W.; Lin, H.-W.; Horng, S.-F.; Cheng, Y.-J.; Yen, F.-W.; Lin, I.-F.; Yang, H.-Y.; Huang, Y.-J.; Tseng, M.-R. *J. Appl. Phys.* **2011**, *110*, 094501.

32.   Aïch, B. R.; Lu, J.; Moisa, S.; Movileanu, R.; Estwick, E.; Tao, Y. *Synth. Met.* **2020**, *269*, 116513.

APPENDIX. CRYSTALLOGRAPHIC INFORMATION

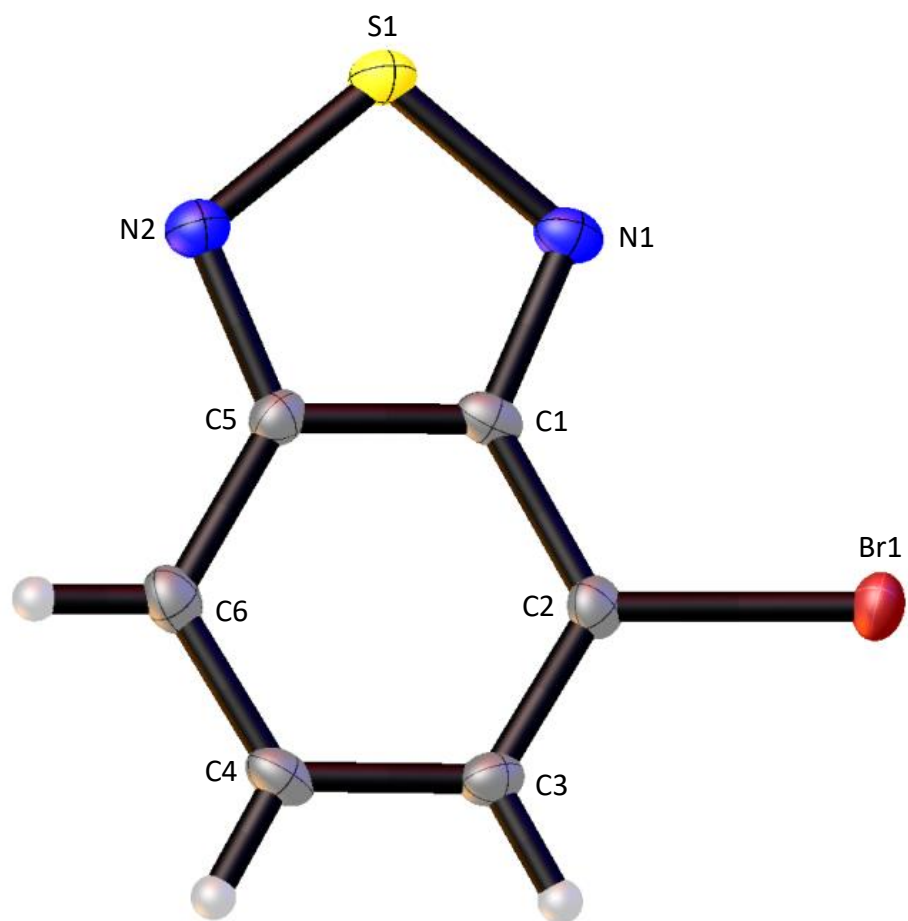## 4-Bromobenzo[*c*][1,2,5]thiadiazole (Chapter 2, 10)

Figure A.1. Thermal ellipsoid plot of **2.10** at the 50% probability level.
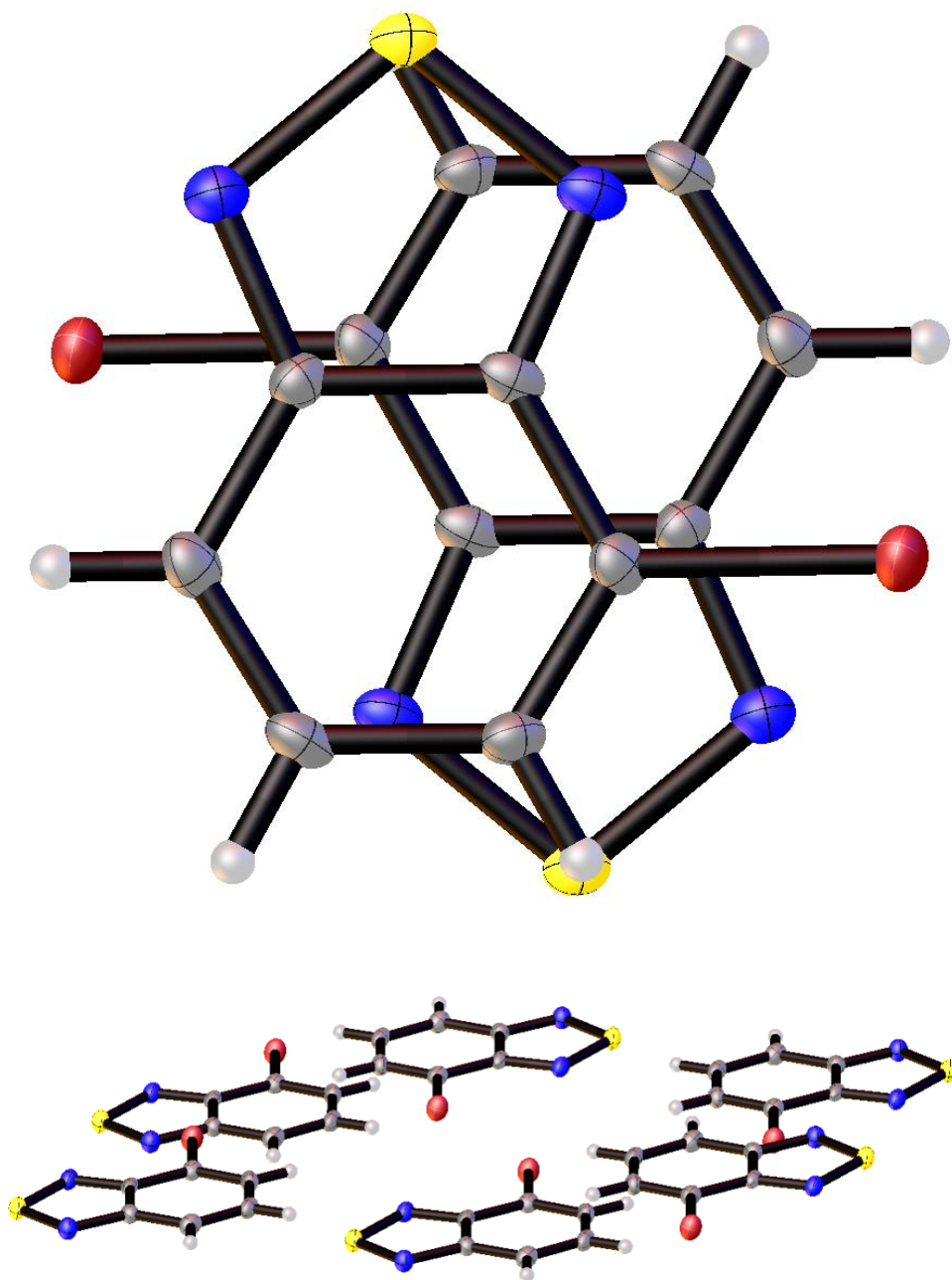
Figure A.2. Crystal packing of **2.10**.

Table A.1. Crystal data for **2.10**

Empirical Formula	$C_6H_3BrN_2S$
Formula weight	215.07
Temperature	293.15 K
Wavelength	1.54184
Crystal system	Triclinic
Space Group	P-1
Unit cell dimensions	a=7.1075 (10) Å α=68.754 (7)°
	b=7.1970 (12) Å β=76.414 (7)°
	c=7.6350 (10) Å γ=69.876 (8)°
Volume	339.06 (9) Å^3
Z	2
Density (calculated)	2.107 g/cm^3
Absorption coefficient	10.415 mm^{-1}
F(000)	208.0
Crystal size	0.191 x 0.11 x 0.064 mm^3
Theta range for data collection	6.269 to 66.672°
Reflections collected	6734
Independent reflections [I>2s]	1192 [R_{int} = 0.0414, R_{sigma} = 0.0273]
Reflections (I>2s)	1192
Goodness of fit on F^2	1.133
Final R indices [I>2s]	R_1 = 0.0265, wR_2 = 0.0694
R indices (all data)	R_1 = 0.0277, wR_2 = 0.0769

Table A.2. Fractional atomic coordinates (x10^4) and equivalent isotropic displacement parameters (Å^2 x 10^3) for **2.10**.

Atom	X	Y	Z
Br1	1757.3(5)	1412.4(5)	8841.4(4)
S1	3797.2(12)	3066.9(13)	2142.2(11)
N1	3058(4)	2244(4)	4389(4)
N2	3593(4)	5465(4)	1856(4)
C1	2640(5)	3879(5)	5022(5)
C2	1999(5)	3906(5)	6932(5)
C3	1668(5)	5695(5)	7329(5)
C4	1932(5)	7536(5)	5892(5)
C5	2926(5)	5725(5)	3595(4)
C6	2562(5)	7577(5)	4046(5)

Table A.3. Bond lengths (Å) for **2.10**.

Bond	Length	Bond	Length
Br1 – C2	1.891(3)	C1 – C5	1.423(5)
S1 – N1	1.620(3)	C2 – C3	1.358(5)
S1 – N2	1.618(3)	C3 – C4	1.419(5)
N1 – C1	1.346(4)	C4 – C6	1.367(5)
N2 – C5	1.358(4)	C5 – C6	1.420(5)
C1 – C2	1.427(5)		

Table A.4. Bond angles (°) for **2.10**.

Bonds	Angle	Bonds	Angle
N2 – S1 – N1	101.33(14)	C3 – C2 – C1	119.0(3)
C1 – N1 – S1	105.5(2)	C2 – C3 – C4	121.7(3)
C5 – N2 – S1	106.0(2)	C6 – C4 – C3	121.4(3)
N1 – C1 – C2	126.7(3)	N2 – C5 – C1	112.8(3)
N1 – C1 – C5	114.4(3)	N2 – C5 – C1	126.3(3)
C5 – C1 – C2	118.9(3)	C6 – C5 – C1	121.0(3)
C1 – C2 – Br1	118.7(2)	C4 – C6 – C5	118.1(3)
C3 – C2 – Br1	122.2(3)		

4-(2-3,4-Ethylenedioxythienyl)benzo[*c*][1,2,5]thiadiazole (Chapter 2, 5)

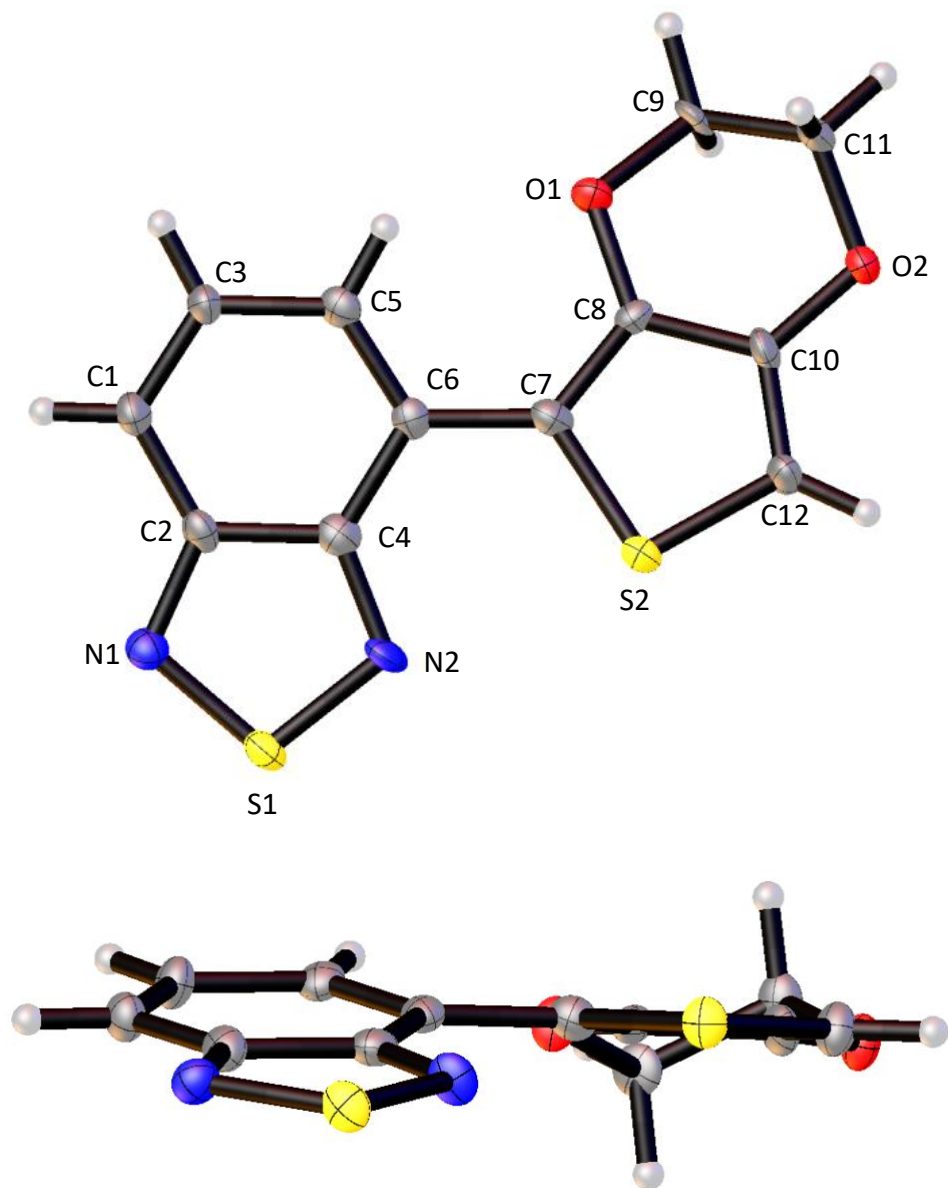Figure A.3. Thermal ellipsoid plot of **2.5** at the 50% probability. Also demonstrating the twist of the EDOT alkyl chain.
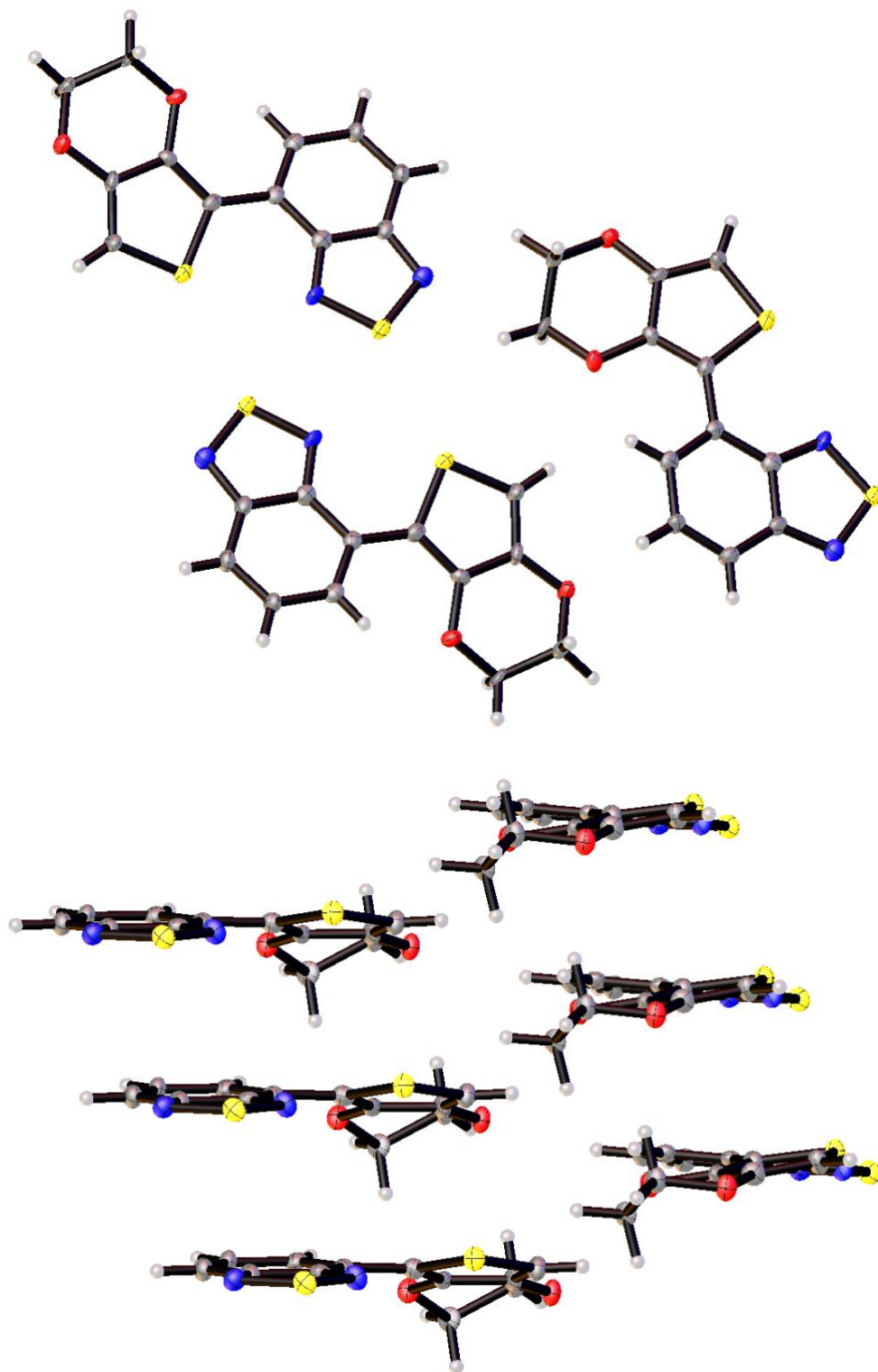
Figure A.4. Crystal packing of **2.5**.

Table A.5. Crystal data for **2.5**.

Empirical Formula	$C_{12}H_8N_2O_2S_2$
Formula weight	276.32
Temperature	100.01 K
Wavelength	1.54184
Crystal system	Monoclinic
Space Group	$P2_{1/c}$
Unit cell dimensions	a=3.8786 (6) Å $\quad\quad$ α=90 °
	b=21.357 (2) Å $\quad\quad$ β=96.283 (10)°
	c=13.401 (2) Å $\quad\quad$ γ=90°
Volume	1103.4 (3) Å^3
Z	4
Density (calculated)	1.663 g/cm^3
Absorption coefficient	4.342 mm^{-1}
F(000)	568.0
Theta range for data collection	3.911 to 66.771°
Reflections collected	6106
Independent reflections [I>2s]	1929 [R_{int} = 0.1397, R_{sigma} = 0.1361]
Reflections (I>2s)	1929
Goodness of fit on F^2	1.019
Final R indices [I>2s]	R_1 = 0.0817, wR_2 = 0.1948
R indices (all data)	R_1 = 0.1251, wR_2 = 0.2239

Table A.6. Fractional atomic coordinates (x10^4) and equivalent isotropic displacement parameters (Å^2 x 10^3) for **2.5**.

Atom	X	Y	Z
C1	5542(17)	4513(3)	1637(5)
C2	4197(17)	4721(3)	2512(5)
C3	6048(17)	3886(3)	1539(5)
C4	3324(16)	4281(3)	3269(5)
C5	5194(16)	3452(3)	2278(4)
C6	3804(16)	3625(3)	3138(4)
C7	2796(17)	3163(3)	3865(5)
C8	2274(16)	2530(3)	3727(4)
C9	1128(18)	1608(2)	2792(5)
C10	1241(18)	2221(3)	4577(5)
C11	1914(18)	1273(3)	3783(4)
C12	942(18)	2609(3)	5362(5)
N1	3606(14)	5323(2)	2752(4)
N2	2100(15)	4564(2)	4057(4)
O1	2745(12)	2225.1(18)	2845(3)
O2	458(12)	1591.4(17)	4585(3)
S1	2103(4)	5306.5(6)	3836.3(12)
S2	1902(4)	3365.7(6)	5063.4(11)

Table A.7. Bond lengths (Å) for **2.5**.

Bond	Length	Bond	Length
S2 - C7	1.735(6)	C8 - C7	1.376(8)
S2 - C12	1.716(6)	C4 - C6	1.425(8)
S1 - N2	1.614(5)	C4 - C2	1.451(8)
S1 - N1	1.624(6)	C10 - C12	1.354(8)
O2 - C10	1.379(6)	C6 - C5	1.376(8)
O2 - C11	1.440(7)	C6 - C7	1.469(8)
O1 - C8	1.380(7)	C9 - C11	1.510(8)
O1 - C9	1.457(6)	C5 - C3	1.421(8)
N2 - C4	1.347(8)	C1 - C3	1.363(8)
N1 - C2	1.351(7)	C1 - C2	1.406(9)
C8 - C10	1.411(8)		

Table A.8. Bond angles (°) for **2.5**.

Bonds	Angle	Bonds	Angle
C12 - S2 - C7	92.9(3)	C4 - C6 - C7	122.1(6)
N2 - S1 - N1	101.2(3)	C5 - C6 - C4	115.8(5)
C10 - O2 - C11	110.5(5)	C5 - C6 - C7	122.1(5)
C8 - O1 - C9	111.8(5)	O1 - C9 - C11	110.0(5)
C4 - N2 - S1	106.8(4)	O2 - C11 - C9	112.0(5)
C2 - N1 - S1	106.2(4)	C6 - C5 - C3	123.4(5)
O1 - C8 - C10	123.1(5)	C8 - C7 - S2	109.1(5)
C7 - C8 - O1	123.2(6)	C8 - C7 - C6	128.1(6)
C7 - C8 - C10	113.7(6)	C6 - C7 - S2	122.7(4)
N2 - C4 - C6	126.7(6)	C3 - C1 - C2	117.5(6)
N2 - C4 - C2	112.8(5)	C10 - C12 - S2	110.9(5)
C6 - C4 - C2	120.5(6)	C1 - C3 - C5	121.8(6)
O2 - C10 - C8	123.0(6)	N1 - C2 - C4	113.0(6)
C12 - C10 - O2	123.5(6)	N1 - C2 - C1	126.0(6)
C12 - C10 - C8	113.4(5)	C1 - C2 - C4	121.0(5)